Complex Social Systems: Emergent Phenomena, Social Contagions, and Opinion Consensus

by

Corbit R. Sampson

B.S., Western Washington University, 2019

M.S., University of Colorado, Boulder, 2022

A thesis submitted to the

Faculty of the Graduate School of the

University of Colorado in partial fulfillment

of the requirements for the degree of

Doctor of Philosophy

Department of Applied Mathematics

2025

Committee Members:

Juan G. Restrepo, Chair

Zachary Kilpatrick

Mason A. Porter

James D. Meiss

Nancy Rodriguez

Sampson, Corbit R. (Ph.D., Applied Mathematics)

Complex Social Systems: Emergent Phenomena, Social Contagions, and Opinion Consensus

Thesis directed by Prof. Juan G. Restrepo

The study of opinion dynamics provides useful insights into large-scale trends in the formation and evolution of opinions in social networks and acts as a platform for rich dynamical behavior. The increased use of online social media, which allows for the rapid dissemination of information throughout a social network, makes the field more important than ever today. In particular, topics such as the propagation of false information and the formation of echo chambers and radicalized communities are relevant in today's social climate. In this Thesis I will present my research in the fields of opinion dynamics and social contagion theory. First, I discuss my work on a binary opinion model on hypergraphs where both individual agents and groups of 3 agents have opinions that evolve both through dyadic (i.e., pairwise) interactions and group memberships. This model contains parameter regimes with oscillatory and excitable dynamics that are highly sensitive to the structure of the underlying hypergraph. Second, I discuss my work on the spread of two competing beliefs in a social network where individuals have an internal opinion models their cognitive biases and modulates their likelihood of adopting one of the two beliefs. The addition of cognitive biases in the spreading process enriches its transient dynamics, facilitating behavior such as the revival of a dying belief and the overturning of an initially widespread opinion. The model is also studied with the presence of external recruitment of spreaders to examine how the intentional spread of information can lead to the eventual dominance of one of the two beliefs. Lastly, I discuss my ongoing work on the social compass model, a model of opinion depolarization. Particularly, I apply the Ott-Antonsen ansatz to successfully produce a low-dimensional description of the dynamics and study the onset of consensus for a large class of distributions of initial opinions. I also study a generalization of the model that includes community structure and external forcing.

Dedication

This dissertation is dedicated to my wife, Ashley Sampson, who has never stopped believing in me and has endlessly supported me throughout our time together. Also to my parents, Ron and Kathleen Sampson, who have always supported me and taught me to marvel at the world and to never stop learning.

Acknowledgements

I would like to acknowledge and thank my advisor Juan Gabriel Restrepo, without whom I would have been lost. My thesis committee, Zachary Kilpatrick, Mason A. Porter, James D. Meiss, and Nancy Rodriguez for helpful comments and feedback. Ekaterina Landgren for helpful insight in social systems. Nicholas Landry and the rest of the development team for the compleX Group Interactions (XGI) package for Python for making such a useful and versatile toolkit. The faculty, staff, and my many cohort members in the Department of Applied Mathematics. Lastly, my friend and colleague Sabina Adhikari for many useful comments, input, and conversations, and who has been an indispensable part of keeping my sanity for the past 6 years. Thank you all.

Contents

Figures

Figure

Chapter 1

Introduction

"If all those around you believe some particular thing, you will soon be tempted to share in that belief."

- Frank Herbert, Children of Dune

The purpose of this thesis is to present my research as part of the requirements of the graduate school at University of Colorado at Boulder and the Department of Applied Mathematics for the completion of the Degree of Doctor of Philosophy. My research can loosely be placed under the heading of complex systems, with my contributions focusing on the fields of opinion dynamics and social contagion theory. The research presented in this dissertation comes from a collection of completed and ongoing projects in these fields. In addition to my research, this dissertation includes a discussion of related research in the fields of opinion dynamics, social contagion theory, and coupled oscillator systems, to help provide context and highlight the relevance of my contributions.

The remainder of this dissertation follows the following layout. Chapter 2 contains a literature review of relevant topics such as voter models (Sec. 2.2.1), models of clustering and alignment (Secs. 2.2.2 & 2.2.3), social contagions and compartmental models (Sec. 2.3), phase oscillator models (Sec. 2.4), and the social compass model (Sec. 2.4.2). The remaining chapters are based on research, both complete and ongoing, during my time at the University of Colorado at Boulder. Chapter 3 is based on a work titled "Oscillatory and Excitable Dynamics in an Opinion Model with Group Opinions" in collaboration with Prof. Juan G. Restrepo (the University of Colorado at Boulder) and Prof. Mason A. Porter (the University of California, Los Angeles), which studies the role of

group opinions in a discrete opinion model reminiscent of non-linear voter models. We observe a number of novel behaviors, including the formation of oscillatory and excitable dynamics similar to the formation of excitable and oscillatory dynamics observed in neural systems [2]. This work is currently available as a preprint via arXiv (arXiv identifier 2408.13336) and is under revision in Physical Review E. Chapter 4 is based on a work titled "Competing Social Contagions with Opinion Dependent Infectivity" in collaboration with Prof. Juan G. Restrepo. This work studies an agent-based model of two competing beliefs, modeled as social contagions, where individuals have an internal opinion that modulates their likelihood of adopting one of the two beliefs, modeling the role of cognitive biases such as confirmation bias and the illusory truth effect. We observe that including opinion-dependent infection and recovery rates results in novel transient dynamics that depend non-trivially on the initial state of the system, with potential consequences for the spread of misinformation and disinformation [3]. This work was published by Physical Review E (111, 024313) on Feb. 24, 2025. Chapter 5 is based on an ongoing project with Prof. Juan G. Restrepo examining generalizations and alternative approaches to study the social compass model, a model for opinion depolarization proposed by Ojer et al. (Sec. 2.4.2) [1, 4]. In particular, we are examining the application of the Ott-Antonson ansatz (Sec. 2.4) to the social compass model and extending the model to include features such as external sources and community structure.

Chapter 2

Background

2.1 Complex systems

The natural world is full of systems comprised of a large number of aggregate parts. The fundamental building blocks of matter, the atoms, combine and interact to form molecules, cells, and organisms. These organisms themselves interact creating social groups, observed both in humans and animals, and particularly among humans we create many artificial interacting systems such as transportation systems, autonomous multi-agent systems, and many others. Such systems, along with many others, are examples of *complex systems*. The constituent parts of a complex system, often called "agents", typically interact following a set of relatively simple microscopic rules. Despite the relative simplicity of the interactions among the agents in a complex system, they can produce remarkably complicated macroscopic phenomena which are often non-trivial extensions of their microscopic interactions. These macroscopic phenomena are known as *collective behavior* or *emergent behavior* and have become a defining feature of complex systems [5, 6]. Some basic examples include the ability of complex systems to successfully spread information, reach spontaneous synchronization, and many others [5, 7, 8, 9].

In recent decades, the study of complex systems has gained substantial attention in a diverse array of fields such as biology, social sciences, mathematics, and physics [5, 6]. The field of complex systems is itself comprised of the study of many other fields typically involving self-organization and collective behavior, dynamical systems, network science, game theory, and many others [5]. For the purposes of this dissertation, we focus on the role of network science in the study of

complex systems. Network science provides a natural language to describe interactions among many individual components, with some examples including social interactions (social networks), the power-grid and logistics networks (transportation networks), and even interspecies interactions (ecological networks)[10]. Due to the important role of network science in the study of complex systems to encode the details of agent interactions, this is where we begin, with a short introduction to networked systems and some associated terminology.

2.1.1 Networked systems

Networked systems are ubiquitous in both the natural and human-made world and represent a major paradigm in the field of complex systems [5]. Networks naturally appear in a diverse collection of fields, ranging from food webs in biology and ecology, to the distribution networks such as those that make up supply chains and the power grid that we depend on [10]. Even the structures that make up societal interactions can be understood as networked systems, typically referred to as *social networks* [10]. These networks are closely related to the spread of information, ideas, and beliefs within society and are the primary type of network that is relevant to this dissertation. Understanding some of the ideas, terminology, techniques, and canonical examples in network science is a necessary prerequisite to the study of complex systems and dynamical systems on networks, parent fields to the primary topic of this dissertation, opinion dynamics. The following subsections provide a brief introduction to the relevant concepts and terminology from network science that pertain to the remainder of this dissertation.

2.1.2 Mathematical formalism of networks

A *network*, sometimes called a graph, is a collection of nodes and the edges that connect them. Mathematically, a network is typically represented as $\mathcal{G} = (\mathcal{V}, \mathcal{E})$, where $\mathcal{V}$ is the set nodes and $\mathcal{E}$ is the set of edges, each of which is a pair of nodes, representing pairwise interactions among the nodes. There are numerous possible examples of network structures in the real world, but since we are focusing on the topic of social systems we will focus on examples relevant to this area. One

set of examples is online social networks. In this context, the nodes could represent user accounts, while the edges may represent two accounts following each other. However, even in the context of online social media other choices may be appropriate, such as online social networks where the edges represent liking, sharing, or commenting on posts of one user by other users. Networks can be *directed* or *undirected*. In a directed network edges are ordered pairs representing a one-way interaction. For example, on online social media platforms where one individual "follows" the other, a directed network would be an appropriate model to encode such interactions. In undirected networks, interactions are symmetric. For example, friendship in some online social networks (e.g., Facebook) is mutual and such friendship networks can be represented via an undirected network. In some networked systems it is appropriate to have self-edges, in which a node is connected to itself (any system where individuals have self-interactions), or multi-edges, in which an edge occurs multiple times (e.g., repeated interactions in social contact networks). Networks that contain multi-edges are refereed to as *multigraphs*, while networks that contain neither self-edges nor multi-edges are known as *simple graphs* or *simple networks* [10].

There are many ways to encode the structure of a network. A convenient way is by using the network's *adjacency matrix* (denoted A). Let $\mathcal{G}$ be a simple directed network with nodes $\mathcal{V} = \{1, 2, 3, \ldots, N\}$ and $\mathcal{E}$ the set of edges of $\mathcal{G}$. Then the adjacency matrix A of $\mathcal{G} = (\mathcal{V}, \mathcal{E})$ is an $N \times N$ matrix with entries defined as

$$A_{ij} = \begin{cases} 1 & \text{if edge } (i,j) \in \mathcal{E}, \\ 0 & \text{otherwise,} \end{cases} \tag{2.1}$$

indicating there is an edge pointing from node j to node i. When $\mathcal{G}$ is an undirected network, $(i,j) \in \mathcal{E}$ whenever $(j,i) \in \mathcal{E}$ and the resulting adjacency matrix is symmetric, $A = A^T$. An alternative method for encoding the structure of a network is the *incidence matrix* (denoted M). The incidence matrix encodes the relation between the nodes and edges, instead of directly encoding the relations between nodes. For a simple network $\mathcal{G}$ with nodes $\mathcal{V} = \{1, 2, 3, \ldots, N\}$ and an edge

set $\mathcal{E}$ of size K, the incidence matrix M of $\mathcal{G}$ is the $N \times K$ matrix M with entries defined as

$$M_{ie} = \begin{cases} 1 & \text{if node } i \text{ belongs to edge } e, \\ 0 & \text{otherwise.} \end{cases} \tag{2.2}$$

For networks that contain multi-edges, one can generalize the definition of a network to allow the edge set $\mathcal{E}$ to be a multiset, allowing for multiple instances of each element to occur. With this adjustment, the entries of the adjacency and incidence matrices of a multigraph are instead defined as the number of times an edge occurs between nodes i and j, for the adjacency matrix, and the number of times node i appears in edge e, for the incidence matrix. When networks contain self-edges then the diagonal entries of the adjacency matrix are non-zero and represent the number of self-edges (i.e., the number of edges in which the node appears more than once) that the nodes have.

In some situations, it is appropriate to allow the nodes or edges to carry weights or dynamic variables [10, 11, 12, 13, 2]. Weighted nodes and edges are often used to model heterogeneity in the structure of the interactions. Within the context of dynamical systems on networks, it is common to use nodes to represent dynamical systems that interact through coupling along the network structure, in which case one or more dynamical variables are defined on each node [10]. Additionally, it has been a recent extension to allow the edges to also carry dynamical variables such as the work in [11, 12, 13] on coupled oscillators. Variables defined on edges can also be included in models of opinion dynamics. One such model is the topic of Chapter 3 [2].

Each node in a network has an associated *degree* k, defined as the number of edges that the node participates in. In terms of the adjacency matrix, for undirected, unweighted networks, the degree of node i is $k_i = \sum_{j=1}^{N} A_{ij} = \sum_{j=1}^{N} A_{ji}$. Note that this expression includes self-edges and multi-edges, if they are present. For a directed network, one has to distinguish between the number of links that point to a given node i, its *in-degree* $k_i^{(\text{in})}$, from the number of links that point away from node i, its *out-degree* $k_i^{(\text{out})}$. In terms of the adjacency matrix, these are given by $k_i^{(\text{in})} = \sum_{j=1}^{N} A_{ij}$ and $k_i^{(\text{out})} = \sum_{j=1}^{N} A_{ji}$, respectively. The average degree of a network $\langle k \rangle$ is given

by

$$\langle k \rangle = \langle k^{(\text{in})} \rangle = \langle k^{(\text{out})} \rangle = \frac{1}{N} \sum_{i=1}^{N} \sum_{j=1}^{N} A_{ij}. \tag{2.3}$$

Note that one gets the same result averaging over the in- and out-degrees, so when studying directed networks one needs only consider the average degree of the network, and not the average in-degree and average out-degree. Networks in which all nodes have the same degree are known as *regular networks* and are often labeled with the degree. For example, in a network where all nodes have degree k then one says that the network is k-regular. Lastly, it is often helpful to define the *degree distribution* $P(k)$ of a network, which is the distribution describing the probability that a node chosen uniformly at random will have degree k. The degree distribution of a network is often used together with a random graph generative model to construct null models. These null models are useful to understand the role of nodal degrees in dynamical systems on networks versus the role of other network features.

One of the most important random graph generative model is the *configuration model* [10]. The configuration model allows the creation of a random graph with a specific degree sequence (i.e., a prespecified list of the degree held by each node). Fig. 2.1 contains a schematic of the creation of a single instance of a random network generated by the configuration model, which is discussed now. Consider a collection of nodes $\mathcal{V} = \{1, 2, 3, \ldots, N\}$ with a specified degree sequence $[k_1, k_2, k_3, \ldots k_N]$ [see Fig. 2.1a]. The degree k_i specifies the number of "stubs" (or "half-edges") that node i contributes to the network. Then, pairs of stubs are selected uniformly at random to be paired together into an edge [see Fig. 2.1b and c] until all stubs have been combined, resulting in a random network with the specified degree sequence [see Fig. 2.1d] [10]. However, the configuration model suffers from two minor issues. First, the stub matching procedure described above requires that the total number of stubs is even, as pairs of stubs are selected. Thus the degree sequence must have the property that

$$\frac{1}{2} \sum_{i=1}^{N} k_i = m \in \mathbb{N}, \tag{2.4}$$

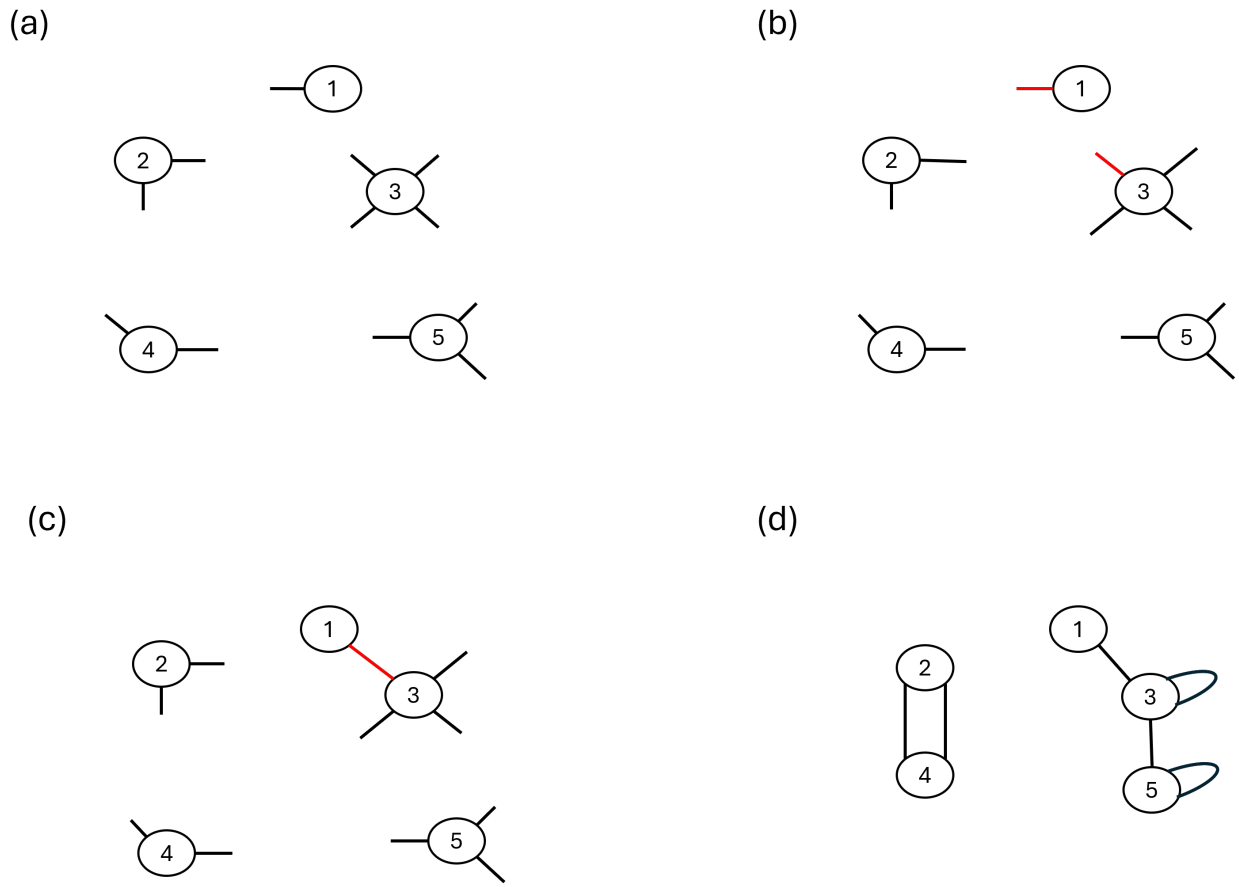

Figure 2.1: A schematic of the configuration model for $N = 5$. (a) Each node i has a specified degree indicating the number of stubs it contributes. (b) Pairs of stubs are selected uniformly at random (shown as red stubs). (c) Selected stubs are connected into an edge (shown as a red edge). (d) Stub selection is repeated until all stubs have formed into edges.

where m is the total number of edges that will form [10]. More generally, the degree sequence must be *graphical*, which means a network with the specified degree distribution can be realized [14]. Second, selecting stubs uniformly at random introduces the possibility that self-edges and multi-edges are produced, which is undesirable in some applications. However, it can be shown that the fraction of self-edges and multi-edges tends towards zero as the size of the network becomes large if the prescribed degree distribution is not too heterogeneous [10]. This allows one to remove self- and multi-edges from the resulting network while introducing only a small deviation from the desired degree sequence. The formation of edges by uniform random selection of stubs allows one to easily determine the probability that an edge between nodes with degree k_i and k_j will form. Particularly, consider a stub of node i. From Eq. (2.4), the total number of stubs is $2m$. Adjusting for the selected stub there are $2m-1$ remaining stubs. Then, the probability that a stub of node j is selected from the remaining stubs is thus $k_j/(2m-1)$ and, since there are k_i ways that a stub of node i could have been selected, this results in a probability that an edge is formed between nodes i and j given by

$$p_{ij} = \frac{k_i k_j}{2m-1}. \tag{2.5}$$

More accurately, this is the expected number of edges between nodes i and j, although this distinction becomes irrelevant in the limit of large m [10]. The -1 that appears in the denominator also becomes negligible in the limit as m becomes large, leading to the more common expression for the probability that an edge will form between nodes i and j [10],

$$p_{ij} = \frac{k_i k_j}{2m}. \tag{2.6}$$

The probability given in Eq. (2.6) has also been used to formulate an alternative generative model where nodes have a specified expected (or target) degree, known as the Chung-Lu model [10, 15, 16, 17].

The inclusion of network structures into dynamical systems can result in significant changes to the qualitative behavior of these systems. One example of this can be found in models that exhibit

a continuous bifurcation as they transition from one regime to another, such as contagion spreading, synchronization of coupled oscillators, and polarization and consensus [18, 19, 20, 21, 22, 4]. The bifurcation threshold of these models often vanishes in the limit $N \to \infty$ when studied on scale-free networks [i.e., those with a limiting degree distribution of the form $P(k) \sim k^{\gamma}$] [18, 19, 20, 21, 22, 4]. This indicates that on large scale-free networks epidemics may form more easily for a given rate of infection [18, 19, 20], synchronization of coupled oscillators can be reached for weaker coupling strength [21, 22], and consensus can be more readily reached from a polarized state [4]. Another example is how the stability of complete synchronization of coupled identical oscillators is highly dependent on the network structure of the coupling [23]. It has also been observed that the successful diffusion of information and innovation in social networks are highly affected by network structure as well. Some studies have shown that diffusion is most successful on networks that exhibit the small world structure [24, 25].

2.1.3 Systems with polyadic interactions

Pairwise networks, such as those discussed above, are a paradigmatic model of interactions in complex systems. However, pairwise interactions are insufficient to capture the complexity of many real-world systems [26]. For example, the formation and spreading of opinions within a population often occurs through social interactions among many individuals simultaneously, in addition to one-on-one interactions. These group interactions, such as group discussions, participation in online forums, and interactions in a classroom setting, are often known as polyadic interactions [27, 28]. Polyadic interactions also occur frequently in systems outside of social science, such as in multi-species interactions in biology [29, 30], metabolic and genetic systems in medicine [31], and coupling in neural systems [32, 33, 34]. (Some studies suggest, however, that polyadic interactions in neural systems may be redundant and could be described by pairwise interactions [35, 36].) In many cases such polyadic interactions cannot be decomposed into linear combinations of pairwise (dyadic) coupling [26]. For example, the spread of complex opinions and beliefs often needs multiple sources of exposure or additional social reinforcement, thus requiring group interactions to spread [37, 38,

39, 40, 41, 42], or spread differently when mediated by group interactions than when mediated by pairwise interactions [41, 40, 43, 44, 45, 46, 47, 48].

Polyadic interactions can lead to changes in the qualitative dynamics of networked dynamical systems, producing phenomena not observed otherwise in the corresponding pairwise network system. Some examples include the opinion jumping phenomenon in polyadic bounded-confidence models [28] and the formation of bistable regions in epidemic models and Kuramoto models with polyadic interactions [49, 45, 50, 51, 52].

There are a number of different mathematical structures that can be used to model polyadic interactions. The most common are bipartite (more generally n-partite) networks, simplicial complexes, and hypergraphs. In this thesis we will use hypergraphs to encode polyadic interactions. The remainder of this section covers the relevant mathematical formalism of hypergraphs which is necessary for Chapter 3.

2.1.4 Mathematical formalism of hypergraphs

A *hypergraph* is a generalization of a network that allows for edges of sizes larger than 2. Mathematically, a hypergraph $\mathcal{H}_{\mathcal{G}}$ can be defined as a pair $(\mathcal{V}, \mathcal{E})$, where $\mathcal{V}$ is the set of nodes and $\mathcal{E}$ is the set of *hyperedges*, each of which is a nonempty subset of $\mathcal{V}$ of size at least 2 [27, 53, 10].

A hypergraph is said to be d-uniform if it contains only hyperedges comprised of exactly d nodes. When working with a hypergraph, $\mathcal{H}_{\mathcal{G}} = (\mathcal{V}, \mathcal{E})$, it is often useful to decompose it into a collection of d-uniform hypergraphs, $\mathcal{H}_{\mathcal{G}_d} = (\mathcal{V}, \mathcal{E}_d)$, such that $\mathcal{E} = \cup_d \mathcal{E}_d$, where $\mathcal{E}_d$ is the set of hyperedges of size d. In a pairwise graph, each node $i \in \mathcal{V}$ has an associated degree, k_i, which represents the number of edges that i participates in. For hypergraphs it is useful to consider the degree of node i within each of the d-uniform sub-hypergraphs. That is, node i has degree $k_i^{(d)}$ if it belongs to $k_i^{(d)}$ hyperedges of size d. The *hyperdegree* of node i is then the vector $\mathbf{k}_i = [k_i^{(2)}, k_i^{(3)}, \ldots, k_i^{(N)}]$. As with pairwise networks, each hypergraph has a hyperdegree distribution, $\mathcal{P}(\mathbf{k})$, which is a probability distribution describing the probability that a node chosen uniformly at random has hyperdegree $\mathbf{k}$.

One can define an incidence matrix similar to the one defined for a pairwise network. The incidence matrix M of a hypergraph $\mathcal{H}_\mathcal{G}$ is an $|\mathcal{V}|$-by-$|\mathcal{E}|$ matrix with entries defined as

$$M_{ij} = \begin{cases} 1 & \text{if node } i \text{ belongs to hyperedge } j, \\ 0 & \text{otherwise.} \end{cases} \tag{2.7}$$

The incidence matrix defined above assumes the hypergraph contains no multi-edges, is undirected, and is unweighted. Details on generalizations for directed and weighted hypergraphs can be found in [54, 55].

2.2 Opinion dynamics

Within social systems the formation of *consensus* (i.e., a state of agreement among all individuals) is an important component for societal function and acts as a foundation for many concepts that we rely on every day, such as money, language, decorum, and notions of equality [56, 57, 58]. As such, in today's social climate of political polarization and tribalism [59], misinformation [60], and increased interactions via social networks [61, 62], developing an understanding of how consensus can form, if and when it will occur, and how it may change in time has become an important question that has drawn the interest of sociologist [63], physicists and mathematicians [64, 65, 66, 67, 28], and many others [68, 64, 69]. The mathematical study of the formation, spread, and evolution of opinions and beliefs within a population is known as *opinion dynamics*. Although opinion dynamics depends on many simplifying assumptions about the nature of individual interactions, it helps provide insight into how the opinions of individuals in a population can change over time and how this process is affected by the structure of underlying social networks and the role of cognitive and social biases [70].

In the study of opinion dynamics, one typically considers a population of individuals (or agents), often represented as nodes in a network or hypergraph. Each agent is assigned one or more dynamical quantities that represent their opinions, stances, or beliefs on a collection of topics. These opinions can be discrete quantities representing, for example, an individual's vote in an election

or whether or not they have adopted a certain belief or social practice, or continuous quantities representing one's stance on a topic along a spectrum. The collection of opinions carried by each agent allows an individual to be represented in an *opinion space*, for example, $\{0, 1\}$ for binary opinions or $[0, 1]$ for continuous opinions on a single topic. Consensus can then be understood as a state where all individuals in a population have the same state in opinion space. It is also common to consider a state where all individuals are clustered together in opinion space, representing a state of partial consensus in the population. In some models of opinion dynamics, it is also possible for a population to split into multiple opinion clusters (i.e., groups of individuals that have almost the same opinion), a state sometimes referred to as opinion fragmentation [71]. In some cases, opinion fragmentation can lead to the formation of opinion clusters that are well separated, a state sometimes referred to as *opinion polarization* [72].

In addition to social systems, there are examples of consensus-like behaviors in many animals. Examples of these behaviors are flocking of birds, schooling of fish, herding of foragers, and swarming of insects [73, 74, 75, 76, 77, 78, 79, 80, 81, 82, 83]. In these cases opinion spaces are replaced by state spaces of position, velocity, or angle. In such cases, consensus-like behaviors are referred to simply as clustering or sometimes as alignment. The latter terminology is used since many models use vector quantities, such as velocity, which are directional. As in social systems, consensus-like behaviors within animal populations are important for species survival and are important for food acquisition, protection from predators, and mating. Models that exhibit consensus or alignment also have many applications to engineering, particularly in relation to the management of autonomous systems such as unmanned air vehicles, formation control, distributed sensor networks, and attitude alignment for satellite clusters [84]. There are also applications of consensus models in the topic of decentralized training of machine-learning algorithms [85].

2.2.1 Voter models

One particularly simple class of models from opinion dynamics are the *voter models*, first proposed by Clifford and Sudbury as a model of species competition [76, 86, 87]. In the standard

voter model one considers a network of N individuals (voters), each with an opinion that is 0 or 1. At each time step one selects a voter, uniformly at random, to update their opinion. The voter then copies the state of one of its neighbors selected uniformly at random. The standard voter model and its variants have been a topic of great interest in mathematics and statistical physics. In this section we provide a survey of several variants and the behavior that they exhibit.

A collection of early work studied the conditions under which consensus, a state where all individuals have the same opinion, is reached for the standard voter model on infinite $d-$dimensional lattices in the limit as time tends to infinity [76, 86, 88]. Clifford and Sudbury showed that the voter model reaches stable coexistence, a stationary distribution such that there are infinitely many 0's and 1's, when $d \geq 3$ and produces clustering, in the sense that the probability of adjacent individuals disagreeing becomes vanishingly small in the long-time limit, in $d = 1$ and $d = 2$ [76, 88].

Although the standard voter model is a vast simplification of a complex system, there have been a number of studies demonstrating interesting behavior and generalizations that help provide insight into the behavior of real-world systems. One example is the standard voter model on heterogeneous networks [89, 90]. Sood and Redner showed that for the standard voter model on configuration model random networks, the average time to consensus scales as $N\langle k\rangle^2/\langle k^2\rangle$, where $\langle k\rangle$ and $\langle k^2\rangle$ denote the first and second moments of the network's degree distribution, implying that consensus is reached more rapidly when the degree distribution is more broad. Furthermore, Sood and Redner showed that when the network is scale-free [i.e., has a limiting degree distribution of the form $P(k) \sim k^{-\gamma}$] then the average time to consensus scales as $O(N)$ for $\gamma > 3$ and scales sub-linearly for $\gamma \leq 3$ [89, 90]. Fernandez-Garcia et al. also provided an interesting example of a spatial compartmental variation of a noisy voter model (imperfect copying of a neighbor's state) that was able to capture a number of statistical features of U.S. presidential elections [64].

A different direction in the generalization of voter models is the creation of non-linear voter models, which we will use in Chapter 3. In the standard construction, the probability that a selected voter changes its opinion is simply the fraction of their disagreeing neighbors. In *non-linear voter models* the probability that a node changes their state is a non-linear function of the number or

fraction of disagreeing neighbors. One such example of a non-linear voter model was proposed by Lambiotte and Redner and is known as the *vacillating voter model* [91]. In this model a voter will examine the opinions of two neighbors and change its opinion if it disagrees with either of them, resulting in a higher probability that a voter will change its opinion. This mechanism inhibits the formation of consensus. Later, Lambiotte and Redner considered a one-dimensional version of the model [92]. Particularly, they noted that in one dimension a voter can only have 0, 1, or 2 disagreeing neighbors. Under the assumption that the probably of changing opinions with no disagreeing neighbors should be zero, then their model has one natural parameter, the conviction parameter $\alpha = p_2/p_1$, where p_i is the probability that a voter will change state with i disagreeing neighbors [92]. In this model they found that for $\alpha > 2$, which corresponds to having stronger conviction, the system reached consensus faster than in the standard voter model, and for $\alpha < 2$ the system reached consensus much slower. They also showed that the probability of reaching consensus has a non-trivial dependence on the initial conditions of the system.

Another example of non-linear voter models are the *threshold voter models*, in which a voter surveys the opinions of its neighbors, within T hops on the network, and changes opinions if the number of disagreeing neighbors is greater than some threshold θ [93, 94, 95]. This model was studied on the infinite $d-$dimensional lattice, and Cox and Durrett conjectured that when $\theta = 1$ the model results in stable coexistence of the two opinions for all cases except $T = d = 1$. A rigorous proof of this was later provided by Liggett [93, 94]. In the case that $d = 1$, Andjel et al. provided a proof that clustering, defined in the same way as for the linear voter models, occurs for all $\theta = T \geq 1$ [95]. These threshold voter models are similar to the later *Watts' threshold model* proposed by Duncan J. Watts to study the formation of infrequent opinion cascades observed in such phenomena as cultural fads, collective action, and the diffusion of norms and innovation [96].

A similar, although distinct, model of species competition is the majority rule model proposed by Galam to describe public debates [97]. In this model a collection of N interacting voters each have an opinion that can be either 0 or 1. At each time step, a subset of these voters is selected uniformly at random to participate in a vote. Then all the voters in the subset simultaneously

adopt the majority state in that group. To expand on this work, Lanchier and Neufer introduced a spatial variation of this model, known as the spatial majority rule model [98]. In this variation, instead of selecting groups of voters uniformly at random, a spatial structure is encoded using a hypergraph and the voter groups are hyperedges. Lanchier and Neufer studied a case that is analogous to the infinite $d-$dimensional lattice of early voter models, particularly considering n^d-regular hypergraphs. They found that for $d = 1, 2$ the model had similar clustering behavior to the standard voter model when n is odd and to a biased voter model (i.e., where individuals with a particular state update their opinion at a faster rate) when n is even. However, unlike the standard voter model, they found that clustering, and later consensus, was possible for any dimension when n was odd.

2.2.2 Clustering and alignment models

We now turn our discussion to models of alignment and clustering. These types of models have a wide range of applications, including problems in social systems [76, 94, 8, 66, 99], applications to the movement and flocking of animals [9, 76, 77, 78, 79], and even several applications to consensus and alignment problems within the fields of robotics and automation [84, 100, 101, 102]. Some examples include examining conditions of flocking (formation control problems) such that connectedness of the underlying interaction network is ensured [100], the use of potential fields to maintain the connectivity in networks of mobile agents [102], and consensus models on switching network topologies [84]. The models discussed in this section, both in the context of animal behavior and opinion dynamics, often consider the role of localized interactions. Localized interactions are commonly observed in social interactions and animal behavior via physical distance (i.e., nearby in space) or topologically defined distance (e.g., nearest network neighbors). A prominent example of the importance of topologically defined distances in biology was a study by Ballerini et al. that made comparisons between observation data of flocks of starlings and numerical models. Ballerini et al. found that the starlings seem to interact on average with 6 to 7 neighboring birds, as opposed to all neighbors within a fixed distance, suggesting that, in some cases, a topological distance between

members of a flock may be more important than a physical distance [79].

Models of clustering and consensus (i.e., the formation of a single cluster) are important in the study of social systems. We begin with a foundational class of models of opinion dynamics, the discrete-time models similar to the DeGroot model of consensus [8, 99]. In DeGroot's original model, each individual has an initial real-valued opinion $x_i(0)$ at time $t = 0$. Then, at every time t, every agent i revises their opinion as a weighted average of the opinions of all other agents of the form $x_i(t+1) = \sum_{j=1}^{N} A_{ij} x_j(t)$, where A is a row-stochastic matrix (where $A_{ij} \geq 0$ and $\sum_{j=1}^{N} A_{ij} = 1$). The necessary and sufficient conditions for convergence of the DeGroot model were then formulated by Berger [103]. Friedkin and Johnsen later proposed a separate model of opinion dynamics focusing on details of the opinion-forming process [104]. This model acts as a variant of DeGroot's original model where individuals remember their initial opinion, which affects their opinion at each subsequent time step. More recent studies by Ding et al. and Dong et al. studied an extension of the DeGroot model that includes self-confidence, network structure, and leaders [105, 106]. Lastly, DeGroot's model later influenced the bounded-confidence models, which will be discussed below, such as the Hegselmann-Krause (HK) and the Deffuant-Weisbuch (DW) models [66, 99]. In fact, the Hegselmann-Krause model is a direct adaptation of the DeGroot model where interactions can only occur locally in opinion space. Since these bounded-confidence models comprise such a large collection of work on their own, they warrant a separate section and are the topic of Sec. 2.2.3.

2.2.3 Bounded-confidence models

A particularly important and well-studied class of models in opinion dynamics are the *bounded-confidence models*. The two main variants of which are the Deffuant-Weisbuch (DW) [66, 107, 108, 109, 110, 111, 112, 113, 28] model and the Hegselmann-Krause (HK) [99, 114, 115, 110, 116] model. Although these two models are different, both are based on interactions that only occur between agents with sufficiently close opinions. First, in the DW model one considers a population of N interacting agents each with a continuous opinion x_i, traditionally in the interval

$[0, 1]$. At each time step two nodes, say j and i, are selected uniformly at random to interact and adjust their opinions according to the rule

$$x_i^{new} = x_i^{old} + m(x_j^{old} - x_i^{old}) ,$$
$$x_j^{new} = x_j^{old} + m(x_i^{old} - x_j^{old}) ,$$

if and only if $|x_j^{old} - x_i^{old}| < c$, where $m \in [0, 1/2]$ is a convergence parameter and $c \in [0, 1]$ is the confidence bound [66]. In the HK model, again, one considers a population of N interacting agents where at each time t each agent, say agent i, has a continuous opinion $x_i(t)$. At each time step, each agent i's opinion is updated as the average opinion of all nodes within node i's confidence bound, i.e.,

$$x_i(t + 1) = \frac{1}{|I(i)|} \sum_{j \in I(i)} x_j(t) ,$$

where $I(i) = \{1 \leq j \leq n : |x_i(t) - x_j| \leq c\}$, c is the confidence bound, and $|I(\cdot)|$ denotes the number of elements in the set [99]. The basic behavior of both models is the formation of one or more opinion clusters depending on the value of the confidence bound c. In Deffuant's original paper, it was found from numerical simulation that the number of clusters in the final distribution of opinions seemed to scale as $1/2c$, referred to as the $1/2c-$rule [66, 111]. In addition to this, Deffuant et al. considered two primary variations. The first variation was a bounded-confidence model with network topologies, and the second was a bounded-confidence model with vector opinions, such as the later work by Huet et al. [108].

Deffuant incorporated network structure into the DW model by considering interactions on a $2-$dimensional grid. This was found to lead to similar behavior to that for the fully mixed case, with two main exceptions. For larger values of the confidence bound ($c > 0.3$) the majority of the agents would reach the same opinion, but some "extremists" with opinions near the maximum and minimum values would remain separate. For $c < 0.3$, a number of opinion clusters would form, but it was noted that consensus can only be reached on connected clusters in the network [66]. Since then there have been many studies in this direction. Some initial work to study the DW

model on scale-free network topologies showed the networks to have only a minimal effect on the behavior of the model [111]. However, a 2018 paper by Meng et al. provided a comprehensive examination of the DW model on a large variety of networks and found that the network topology affected the average time to consensus and the number of clusters for a specific confidence bound, showing that the $1/2c-$rule was inaccurate for many networks [112]. Some more recent works have studied the effect of additional network structures such as non-static networks and hypergraphs [113, 28]. Kan et al. considered a generalization of the DW model in which the network re-wires to promote homophily within the network, and found that this led to more difficulty forming a consensus and the possibility of a pseudo-consensus, a state where two non-interacting clusters form which have opinions that only differ by a small amount. Hickok et al. considered the DW model on networks with polyadic interactions (simultaneous interactions among multiple agents). They found that the inclusion of polyadic interactions allows "opinion jumping", the change in an agent's opinion by an amount larger than the confidence bound [28]. In a different direction, a later work by Deffuant and Weisbuch discussed a variant known as the *smooth bounded-confidence model* to study the phenomenon of extreme opinion shifting reported in social psychology [107]. In this model, agents have both a time-dependent opinion, $x_i(t)$, and confidence bound, $u_i(t)$. Both opinions and confidence bounds update via a Gaussian influence function. In this variant the opinions with small confidence bounds become more influential, leading to more frequent formation of clusters at extreme opinions.

For the HK model many initial results looked at the effect of static asymmetry in the confidence bound, i.e., defining $I(i)$ as $I(i) = \{1 \leq j \leq n : -c_l \leq x_j - x_i \leq c_r\}$, and opinion dependent asymmetry, $I(i) = \{1 \leq j \leq n : -c_l(x_i(t)) \leq x_j - x_i \leq c_r(x_i(t))\}$. The static asymmetry leads to a bias towards extreme opinions (i.e., opinions near the boundary of the opinion space), causing consensus to form at a more extreme opinion, while the opinion-dependent asymmetry promotes the formation of two opinion clusters at opposite extremes (i.e., near opposite boundaries of the opinion space) [114]. A study by Schawe et al. examined the behavior of the HK model on a variety of network topologies. Particularly, they found that for some network topologies consensus

is possible for confidence bounds below the threshold corresponding to well-mixed populations. Furthermore, it was found that for random networks the threshold for consensus approaches zero in the thermodynamic limit, regardless of the network's degree distribution. This implies that for random networks in the limit $N \to \infty$, as opposed to the two-dimensional lattice, consensus is possible for any confidence bound given a sufficiently long time [117].

2.3 Social contagions

A social contagion can be defined as the spread of a piece of information, such as a behavior, belief, or emotion, in a spreading process analogous to the spread of biological contagions [118]. One of the earliest known uses of the term "social contagion" was made by Le Bon in 1895 (or 1903 by some records) to describe the onset of collective behaviors in large groups, such as the formation of panic groups rushing towards an exit [119, 120]. It has been observed that behaviors such as smoking, sexual behavior, and the use of drugs and alcohol can spread through social networks as contagions [121]. Many recent works have expanded the scope of social contagions to include the spread of social fads, online trends, and crime waves [118]. Today, with the widespread use of online social media, social contagions are ubiquitous with common examples including the creation and spreading of memes [122, 123, 124], the practice of online "challenges" [125, 126], and the spreading of rumors [127, 128]. The spread of rumors and beliefs as social contagions has even been shown to be closely related to the spread of infectious disease and vaccination practices, which has major implications for public health [129, 130, 131, 60]. Social contagions have also been studied in marketing with the development of "viral marketing" strategies based on the concept of electronic word of mouth [132, 133, 134, 125]. Finally, the role of spreading rumors and beliefs can be closely tied with the spread of misinformation (the unintentional spread of false information) and disinformation (the malicious spread of false information), which makes it an important topic concerning political stability and national security [60, 135], and which this thesis will study in Chapter 4.

In many ways, there is considerable overlap between the study of social contagions and

opinion dynamics. Models such as voter models and threshold models rely on individuals adopting the opinions, beliefs, or behaviors of the individuals with whom they interact (Sec. 2.2.1) and threshold voter models are conceptually similar to the soon-to-be discussed "complex contagions". Even models of opinion dynamics with continuous opinions, such as bounded-confidence models and variants, are driven by the passage of information from one individual to another through a social network (Sec. 2.2.3). To help make a distinction, we will consider models of social contagions in the context of the mathematical techniques that are used. For the remainder of this section we will be considering models of social contagion spreading that follow the techniques and terminology of mathematical epidemiology, particularly the framework of compartmental models.

2.3.1 Compartmental models

Compartmental models of mathematical epidemiology first appeared in the early twentieth century, with the earliest examples being what we now refer to as SIR (Susceptible-Infected-Removed) models [136]. In the SIR model, individuals are grouped by the status of their infection. Susceptible individuals (S) are those that are not currently infected and can become infected, infected (I) individuals are those that carry the contagion of interest and can infect other individuals in the system, and, finally, removed (R) individuals are those that cannot infect other individuals; this includes individuals that have recovered and gained immunity from their exposure or succumbed to the infection. Fig. 2.2 shows a schematic of the standard SIR model. Susceptible individuals transition to infected with rate $\bar{\beta}$ upon interaction with an infected individual. Infected individuals become removed from the system with rate γ and remain infected otherwise. The rate $\overline{\beta}$ is known as the infection rate or infectivity of the contagion and represents the probability per unit time that an individual becomes infected from a single exposure to the contagion. The rate of removal γ is related to the time an individual spends infected. In particular, the average infection time is $1/\gamma$. Mathematically, the traditional SIR model is typically treated using the assumption of a "well-mixed" population of N individuals (all-to-all interactions) resulting in a system of ordinary

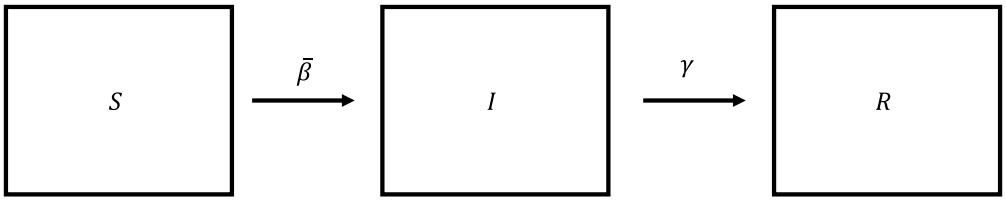

Figure 2.2: A schematic representation of the basic SIR compartmental model. Upon interaction with an infected individual, a susceptible individual S transitions to the infected compartment I with probability per unit time $\bar{\beta}$. Infected individuals spontaneously transition to the removed compartment R with probability per unit time γ.

differential equations

$$\frac{dS}{dt} = -\beta SI, \tag{2.8}$$

$$\frac{dI}{dt} = \beta SI - \gamma I, \tag{2.9}$$

$$\frac{dR}{dt} = \gamma I, \tag{2.10}$$

where S, I, and R are the fraction of the population in each compartment and $\beta = N\bar{\beta}$. Additionally, by definition these variables satisfy $S + I + R = 1$. Additional compartments can be added to describe more complex situations, such as if individuals can become exposed but are unable to spread the infection until an average incubation period has passed, if individuals can be vaccinated, if reinfection is possible after an average refractory period, and many more [137]. Additional heterogeneity can be included by relaxing the assumption of a well-mixed population and including an underlying network structure describing a contact network of individuals or large-scale transition pathways such as transportation networks between countries, states, or counties [138, 139].

When discussing contagions (both social and otherwise), it is often helpful to examine the transition to epidemic (or endemic, depending on the model) behavior, known as the epidemic threshold. A key quantity that determines this transition is the basic reproduction number R_0 of the contagion. The basic reproduction number is the expected number of infected individuals generated by a single infected individual in a population of otherwise all susceptible individuals [140]. The basic reproduction number provides a measure of how effective a contagion is in a population and can be used to determine if the contagion is capable of spreading throughout a

system. Particularly, $R_0 = 1$ marks the epidemic threshold and represents when the disease-free state becomes unstable and the contagion begins to spread through the system. For the SIR model, the basic reproduction number is $R_0 = \beta/\gamma$, so that the epidemic occurs when $\beta > \gamma$. A common technique for determining the basic reproduction number of a more general compartmental model is the "next generation matrix method" introduced in [141].

An in-depth discussion of mathematical epidemiology is beyond the scope and context of this dissertation. For a more complete discussion on compartmental models in the context of infectious diseases see [142]. We now turn to compartmental models in the context of social contagions.

2.3.2 Developments in complex and interacting social contagions

We begin our discussion of current research on social contagions with the seminal paper by Granovetter, "The strength of weak ties" [143]. Granovetter showed that so-called "weak ties", such as those that exist between colleagues and acquaintances, help to facilitate the spread of contagions throughout a social network more than "strong ties", those that exist between close friends [143, 140]. This work was later built on by Watts and Strogatz, who showed that these "weak ties" act as bridges between otherwise distantly connected clusters of individuals in a social network [144, 140]. Together, these works started a great interest in the role of network structures in dynamical systems [140]. While "weak ties" promote the spread of simple contagions (those that can spread through single exposures), social contagions are often influenced by many social and cognitive biases such as repeated exposure bias, illusory truth effect, and conformist and anti-conformist behaviors [37, 38, 39, 40]. In particular, the spread of some behaviors or beliefs require multiple or repeated exposures to spread throughout a social system, especially when adoption of these behaviors or beliefs may be perceived as risky or costly to the individual [41, 42]. To model this, Centola and Macy proposed that some social contagions spread as "complex" contagions, which require additional social affirmation or reinforcement to spread, motivated by earlier research by McAdam and Paulsen [41, 42]. Studying the spread of these complex contagions, Centola and Macy's work showed that while networks with many weak ties promote the spread of simple

contagions, they inhibit the spread of complex contagions [41, 140]. As put by Guileault et al. (Ref. [136], page 4),

> The primary consequence of the distinction between simple and complex contagions for diffusion through social networks is that as "worlds" become very small, the speed of simple contagions increases, while complex contagions become harder to spread.

With the work of Centola and Macy, and the sociological research that inspired their work, it has become apparent that social contagions can spread under the influence of many additional factors, such as multiple repeated exposures (as in Centola and Macy's work) [41, 40, 43, 44, 45, 46, 47, 48] or interacting contagion systems (i.e., systems of multiple contagions that may compete for resources or interact to promote or discourage infection) [129, 130, 131, 145, 146, 147, 148]. In the following we discuss various models of complex contagion.

The first generalization of a complex contagion that is discussed here in the context of the work by Centola and Macy, was proposed by Iacopini et al. and named "simplicial contagion" [43]. In this work, Iacopini et al. formulated an SIS-type model of a complex contagion on simplicial complexes. In this model, the contagion can spread via both pairwise links and higher-order simplices (i.e., groupings of multiple individuals similar to a hyperedge, see Sec. 2.1.4), where all simplices of a given order have their own infection rate, allowing the contagion to spread at different rates in interactions of different sizes. These simplicial contagions show qualitatively different dynamics than simple contagions, such as the formation of hysteresis around the epidemic threshold, creating a discontinuous transition under some parameter regimes [43]. Building on this idea, Ferraz de Arruda et al. developed a generalization to hypergraphs, following the same basic structure but no longer requiring the interaction network to strictly be that of a simplicial complex [149]. Their model displayed qualitatively similar behavior to the previous simplicial contagions, but with a larger parameter space and more varied dynamics. More importantly, the project outlines an in-depth framework for studying dynamical processes on hypergraphs [149]. Later, Landry and Restrepo further built on the model of Ferraz de Arruda et al. to allow for hyperdegree heterogeneity and hyperdegree correlation (i.e., correlation between the number of interactions

of each size in which an individual participates), and the effects of higher-order healing (i.e., an increased rate of healing for individuals that participate in group interactions with infected nodes) [45]. It was found that increasing the heterogeneity of the pairwise degrees suppressed the formation of a discontinuous transition, while increasing heterogeneity in the higher-order degree distribution promoted it. Landry and Restrepo also studied this model on hypergraphs with hyperdegree correlation [46]. More recently, Landry and Restrepo studied the effect of community structure for a hypergraph social contagion model, showing that, with the presence of polyadic interactions, only the existence of sufficiently disconnected communities is needed to create opinion disparity (the formation of different average opinions in different social groups) [47]. Recently, Serrano et al. studied a variation of Iacopini et al.'s simplicial contagion model that allowed for stochastic variation in the infection rates [48].

Another direction in the study of social contagions has looked at the role of interacting contagions, a concept which exists in the study of biological contagions as well [150, 151, 152, 153, 154, 155]. Some such studies have focused on the co-evolution of a biological contagion (simple contagion) with a social practice (typically a complex contagion) [129, 130, 131], while others have focused on multiple competing rumors [145, 146, 148, 147]. One of the earliest studies looking at social behaviors spreading as a complex contagion, which then affects the spread of a simple (biological) contagion, was by Campbell and Salathé [129]. In their model, Campbell and Salathé consider the spread of a social contagion, representing the spread of a negative vaccination sentiment and subsequent refusal to be vaccinated. This is followed by the spread of a biological contagion in the remaining susceptible populations (i.e., those that adopted the anti-vaccination stance) [129]. Campbell and Salathé found that when the social contagion spread as a complex contagion (requiring repeated exposures) the outbreaks of the biological contagion were both larger and occurred more frequently. A later work by Fu et al. proposed and studied a model of co-spreading contagions, representing the simultaneous spread of a biological and a social contagion, each spreading on separate network structures [130]. Fu et al. were able to make a direct comparison of their model with real-world vaccination, health, and social network data collected from students at Har-

vard College during the 2009 H1N1 epidemic. Fu et al.'s results suggest that many epidemiological models for biological contagions may provide dramatic underestimates of the basic reproduction numbers and that the rate of spread of vaccination behavior may be more important than the rate of spread of the biological contagion when assessing the outlook of a potential epidemic [130]. A more recent study that looked at allowing the social contagion and biological contagion to spread simultaneously, and one seemingly unaware of Fu et al.'s work, examined a similar concept but allowed the social contagion to be a simplicial contagion as described earlier by Iacopini et al. In this work, by Lucas et al., it was found that the spread of a social (complex) contagion that acts as a driver to the biological (simple) contagion can create a discontinuous epidemic threshold in the simple contagion [131]. This shows that simple contagions can display qualitative dynamics of complex contagions (such simplicial or hypergraph contagions) when driven by an underlying complex contagion, even if one of these contagion is otherwise unobserved [131].

Another direction of work that considers the effects of interacting contagions in the context of social systems are those that look at multiple social contagions spreading simultaneously in a system, inspired by the simultaneous spread of multiple rumors in a social network. In these cases, there are three possible types of interactions: competition, cooperation, and non-interaction. For the modeling of competition and cooperation, there are a number of potentially meaningful approaches, for example, contagions could compete in the sense of consumption of resources (susceptible agents), or the contagions could compete in the sense that an agent can carry multiple contagions at once, but the contagions inhibit each other's infection rates. For cooperation a natural possibility is that individuals can carry multiple contagions, but some contagions increase the infection rate of other contagions (modeling, for example, a rumor which becomes more believable when you already believe a different rumor). We begin a brief survey with a fully competitive two-contagion SIS type model proposed by Trpevski et al. [145]. In this work, Trpevski et al. consider the asymmetric spread of two resource-competing contagions. This model was considered on several different network topologies and it was found that the relative success of each contagion was highly dependent on the underlying network [145]. A later work by Beutel et al. considered

a variation on this previous type of model, but with symmetric spreading of the two contagions and partial competition [146]. Recently there have also been models of competing contagions constructed using a variation of an SIR-type model that included resource competitive or cooperative spreading and "stiflers", which are "recovered" individuals that enter into a refractory period before once again becoming susceptible [147]. Lastly, Myers and Leskovec developed an interesting statistical model of multiple interacting rumors spreading through an online social network [148]. Myers and Leskovec's model treats cooperation and competition in the variable infectivity approach mentioned above, whereby an individual becomes more (or less) receptive to a piece of information based on what previous information they have been exposed to.

2.4 Kuramoto models

Another important emergent behavior is spontaneous synchronization in systems of coupled oscillators. Some examples include clapping synchronization of members of an audience [156], synchronization of flashing fireflies [157, 158], coupled metronomes [159], and pedestrians walking on suspension bridges [160, 161, 162]. More importantly, the onset of synchronization, as well as the more general study of coupled oscillator systems, is highly important to a number of fields with many applications in biology, engineering, and physics [163, 164, 165, 166, 167, 168, 157, 158, 169, 170]. In biology and medical science, synchronization is of interest due to its role in a number of systems [166, 167, 168, 157, 158, 169, 170, 160, 161, 162]. For example, the synchronization of a number of neural structures is closely tied to the onset of epilepsy [166]; investigations into cardiorespiratory synchronization are used to study the existence of hidden synchronization regimes in the human body [167]; and the synchronization of pacemaker cells in the heart plays an important role in triggering heart contractions [168]. Within physics and engineering there are examples such as synchronization of quantum dipoles and decentralized power grids [163, 164, 165]. Synchronization also plays an important role in human interactions, for example, brain patterns have been observed to synchronize during non-verbal interactions [169, 171, 172, 173], and a number of animal studies have displayed evidence of synchronized circadian rhythms at various scales (chemical, social, and

cellular) [170]. There is also interest in controlling these systems. Examples include applications to stabilization in micro- and smart-grid technologies [174, 175], control applications to cardiac pacemaker cells and neural synchrony [176], and even wearable robotic systems to improve human athletic performance [177]. Synchronization has also been used to model opinion dynamics. Some prominent examples include the work by Hong and Strogatz on conformists and contrarians [178], Ojer et al.'s social compass model [1, 4], Pluchino et al.'s work on naturally changing opinions [179], and Zhang et al.'s recent generalization for opinions on the unit sphere [180].

The purpose of this section is to provide a brief summary of the Kuramoto model of coupled phase oscillators and the use of the Ott-Antonsen ansatz [181] before introducing the social compass model developed by Ojer et al. [1]. The social compass model is a model of opinion consensus and polarization that uses the structure of the Kuramoto model. As such, many of the techniques and generalizations of the Kuramoto model are applicable to the study of the social compass model, motivating this section. Then in Chapter 5 we will return to studying some of these generalizations of the social compass model by applying the Ott-Antonsen ansatz.

The Kuramoto model is one of the most important models of synchronization of oscillators with wide-reaching applications and generalizations. Kuramoto showed that an ensemble of N weakly coupled oscillators could be described approximately in terms only of phase angles θ_i, $i = 1, 2, \ldots, N$, by following a so-called phase-reduction procedure [182]. The simplest description of such coupled phase oscillators is known as the Kuramoto model and is given by the system of ODEs

$$\dot{\theta}_i = \omega_i + \frac{K}{N} \sum_{j=1}^{N} \sin(\theta_j - \theta_i), \quad i = 1, \ldots, N. \tag{2.11}$$

Here ω_i is the intrinsic frequency of oscillator i, K is the coupling constant, and $\sin(\theta_j - \theta_i)$ represents an attractive coupling between oscillators. For small values of the coupling strength K, the system will exist in an incoherent state in which the oscillators each oscillate approximately independently with their intrinsic frequency. However, when the coupling strength exceeds a certain critical value, the system will spontaneously synchronize [183].

To study the onset of synchronization, it is helpful to define the order parameter

$$z = re^{i\psi} = \frac{1}{N}\sum_{j=1}^{N} e^{i\theta_j}, \tag{2.12}$$

where ψ is the phase of the order parameter and r is its magnitude. To understand Eq. (2.12), we represent each oscillator as a complex number in the complex unit circle with phase θ_j, then take the average of these complex numbers, resulting in Eq. (2.12). The magnitude of the order parameter, r, represents the degree of synchronization in the system. When r is close to 1, most oscillators have a phase close to ψ; when r is near to 0, the system is in an incoherent state. Although the form of the Kuramoto model of Eq. (2.11) involves coupling between each pair of oscillators, with the order parameter in Eq. (2.12) one can rewrite the Kuramoto model as

$$\dot{\theta}_i = \omega_i + rK\sin\left(\psi - \theta_i\right), \quad i = 1, \ldots, N, \tag{2.13}$$

or

$$\dot{\theta}_i = \omega_i + \mathrm{Im}\{(Kz)e^{-i\theta_i}\}, \quad i = 1, \ldots, N. \tag{2.14}$$

In Eqs. (2.13) and (2.14) the dynamics of each oscillator are governed by coupling to the global order parameter z.

2.4.1 The Ott-Antonsen ansatz

In this subsection we summarize a technique to study the dynamics of the Kuramoto model and its variations proposed by Edward Ott and Thomas M. Antonsen [181]. This approach is now known as the Ott-Antonsen ansatz. An outline of the Ott-Antonsen ansatz is described below for the all-to-all Kuramoto model.

First, taking the continuum limit as the number of oscillators goes towards infinity, the order parameter z [see Eq. (2.12)] becomes

$$z = \int_{-\infty}^{\infty}\int_{0}^{2\pi} f(t,\theta,\omega)e^{i\theta}d\theta d\omega, \tag{2.15}$$

where $f(t, \theta, \omega)$ is the density of oscillators with intrinsic frequency ω and phase θ at time t. Then we require that the density f satisfies the continuity equation

$$\frac{\partial f}{\partial t} + \frac{\partial}{\partial \theta}\left[\left(\omega + \mathrm{Im}\{Kze^{-i\theta}\}\right) f\right] = 0, \tag{2.16}$$

as no oscillators are created or destroyed. In Eq. (2.16), the factor $\omega + \mathrm{Im}\{Kze^{-i\theta}\}$ is the right hand side of Eq. (2.14). Next, we make a Fourier series expansion of f in θ to get

$$f(t, \theta, \omega) = \frac{g(\omega)}{2\pi}\left[1 + \sum_{n=1}^{\infty} \alpha_n(t, \omega)e^{-in\theta} + \text{C.C.}\right], \tag{2.17}$$

where C.C. stands for the complex conjugate and $g(\omega)$ is the distribution of natural frequencies. Substituting Eq. 2.17 into Eq. (2.16) would result in an infinite number of equations indexed by n for each coefficient in the expansion in Eq. (2.17). However, Ott and Antonsen proposed making the ansatz that the expansion coefficients α_n are all powers of a *single* coefficient α, i.e., $\alpha_n = \alpha^n$. With this ansatz, Eq. (2.15) reduces to

$$z = \int_{-\infty}^{\infty} \overline{\alpha}(t, \omega)g(\omega)d\omega \tag{2.18}$$

and Eq. (2.16) reduces to an ordinary differential equation for α,

$$\frac{\partial \alpha}{\partial t} + \frac{K}{2}(z\alpha^2 - \overline{z}) + i\omega\alpha = 0, \tag{2.19}$$

thus reducing the original N dimension dynamical system to a single differential-integral equation. Furthermore, if the integral in Eq. (2.18) can be evaluated exactly, then the reduced equation can be expressed as a small number of coupled ordinary differential equations. In Ott and Antonsen's original paper they consider the case of $g(\omega)$ being a combination of one or more Lorentzian distributions, allowing the integral to be computed exactly using the method of residues. This allows the dynamical system to be reduced to a small number of coupled non-linear differential equations that capture the original dynamics of the N dimensional system (in the limit as $N \to \infty$) and can be used to study the onset of synchronization for more complex systems.

The introduction of the Ott-Antonsen ansatz allowed for further study of a large variety of generalizations of the Kuramoto model. For example, Childs and Strogatz were able to develop

the stability diagram of the periodically forced Kuramoto model using the ansatz demonstrating a number of bifurcations [184]. Skardal and Arenas used the technique to show the creation of discontinuous transitions and multistability of a Kuramoto-type model on simplicial complexes [185]. Martens et al. showed that bimodal frequency distributions can create standing wave solutions, where two counter-rotating groups of phase-locked oscillators coexist [186].

2.4.2 The social compass model

Recently, Ojer et al. proposed a model of opinion consensus, concentrating on the effect of initial opinions, within populations of agents each with continuous opinions on two topics, X and Y. Denoting the continuous opinions of agent i as x_i and y_i, relative opinions on topics X and Y are represented as a phase in polar coordinates $\theta = \text{atan2}(y_i, x_i)$, which we call an opinion orientation, while the magnitude $\rho_i = \sqrt{x_i^2 + y_i^2}$ of their opinions represents the individuals' conviction, [here, $\text{atan2}(y, x)$ is defined as the argument of the complex number $x+iy$, taken in $[0, 2\pi)$]. The dynamics of each agent's opinion orientation θ_i is described by the system

$$\dot{\theta}_i = \rho_i \sin(\phi_i - \theta_i) + \frac{K}{N} \sum_{j=1}^{N} \sin(\theta_j - \theta_i), \quad i = 1, \ldots, N. \tag{2.20}$$

Here $\phi_i = \theta_i(0)$ is the initial opinion orientation of agent i, ρ_i is the conviction of agent i, and K is the coupling constant. In Eq. (2.20), the first term represents an individual's tendency to return to their initial opinion orientation ϕ_i, while the second term represents the interactions between node i and all other individuals, thus pulling node i towards the opinion orientations of all other nodes. The strong similarity between this model and the Kuramoto model allows for substantial overlap in the techniques that can be used to study the dynamics of the system. Similar to the Kuramoto model, Ojer et al. show that their model exhibits a transition from a polarized state (analogous to the incoherent state of the Kuramoto model) to a consensus state (analogous to the synchronized state) for sufficiently strong coupling. Furthermore, it was found that depending on the distribution of initial opinion orientations (ϕ_i, ρ_i) the transition to consensus can occur as a discontinuous transition for uncorrelated initial opinions [meaning that the distribution $P(\phi, \rho)$ is quadrimodal

in ϕ] to a continuous transition for correlated initial opinions [meaning $P(\phi, \rho)$ is bimodal in ϕ] [1]. In a follow-up work by Ojer et al. [4], they formulated a multi-dimensional generalization of their model (allowing opinions across more than 2 topics) and investigated the effects of including network heterogeneity on the formation of consensus when the distribution of initial opinions is correlated (bimodal). It was found that the depolarization threshold vanishes as the network size goes to infinity for uncorrelated random networks with power-law degree distributions.

The development of the social compass model is rather recent, and to date, these are the only two works that have been published on the model. The topic of possible generalizations to the social compass model and the application of the Ott-Antonsen ansatz will be the subject of chapter. 5.

Chapter 3

Oscillatory and Excitable Dynamics in an Opinion Model with Group Opinions

3.1 Introduction

The opinions of individuals in a social network often change when they are exposed to the opinions and actions of other individuals. The ensuing opinion dynamics of such individuals has received considerable attention from sociologists [63], economists [68], political scientists [64, 69], applied mathematicians and theoretical physicists [64, 65, 66, 67, 28], and many others. Researchers have studied models of opinion dynamics on social networks to gain insight into phenomena such as the propagation of false or misleading information [187, 188], the emergence of consensus opinions [189, 67, 190], and the formation of echo chambers [191, 192]. See [193, 194] for reviews of opinion models.

Models of opinion dynamics necessarily involve many assumptions about the nature of the opinions of individuals, the interactions between individuals, and how such interactions affect the opinions of other individuals [70]. Most opinion models assume that agent opinions change as a result of pairwise (i.e., dyadic) interactions. In opinion models, the agent opinions are typically either real-valued scalars or real-valued vectors (e.g., if one wants to simultaneously model opinions of multiple things). In some models, the opinions have discrete values; in others, they have continuous values, such as in an interval of the real line [194]. Researchers typically consider discrete-value opinions when examining phenomena in which entities make discrete choices, such as when people vote for a candidate for a political office. By contrast, researchers often consider continuous-valued opinions when they want to explicitly account for a wide spectrum of views, such as political out-

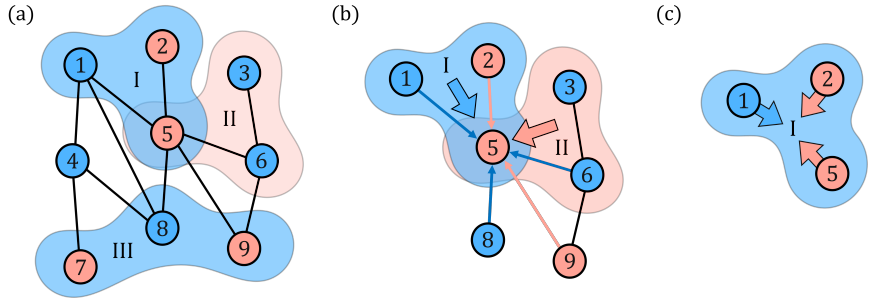

Figure 3.1: A schematic illustration of how the opinions of nodes and groups are influenced by the opinions of other nodes and groups in our model. (a) A hypergraph with 9 nodes and 3 groups. Nodes 1, 3, 4, 6, and 8 have opinion 1 (in blue), and nodes 2, 5, 7, and 9 have opinion 0 (in light red). Groups I and III have opinion 1 (in blue), and group II has opinion 0 (in light red). (b) Node 5's opinion is influenced by the opinion of its neighboring nodes 1, 2, 6, 8, and 9 (thin arrows) and by the opinions of groups I and II (thick arrows). (c) Group I's opinion is influenced by the opinions of its constituent nodes 1, 2, and 5 (thick arrows).

looks that range from very liberal to very conservative. There are a wealth of opinion models [195, 194], which researchers study on networks to examine how social structures affect opinion dynamics. As discussed in Chapter 2, examples of opinion models include the DeGroot consensus model [8], voter models [76, 86] and their generalizations [196], majority-rule models [197], and bounded-confidence models [198].

A basic assumption in most opinion models is that only the individual agents, which are represented by the nodes of a network, are endowed with an opinion. In the present chapter, we relax this assumption by allowing groups of nodes to hold a collective opinion. Social groups, which range in scope from family and friendship units to large political and corporate organizations, help shape the fabric of society [199, 200, 201]. In many situations, it is reasonable to posit that social groups themselves can possess opinions. For example, large corporate organizations sometimes take public stances on social issues [202]. Additionally, courts such as the United States Supreme Court hear cases and document collective opinions through their decisions on these cases [203]. Moreover, a mathematics department at a university may broadcast a collective opinion, such as through documentation on its website or through a hiring decision, that differs markedly from the opinions of its individual faculty. The opinion of a research group, such as the applied-mathematics

group, may also differ from the individual opinions of members of that group. In all of these examples, a group's opinion does not necessarily reflect a consensus among the members of that group, as individuals in the group can disagree (sometimes rather strongly) with the group opinion. Importantly, groups and individual members of a group can influence each other. Group opinions are influenced by the opinions of its constituent members, and the opinions of individuals are influenced by the collective opinions of the groups in which they participate [204, 205].

In the present chapter, we formulate and analyze a model of opinion dynamics in which both a network's nodes and its groups of nodes have binary opinions. The opinions of individual nodes are affected both by their neighbors in a network and by the opinions of the groups in which they participate. The opinions of groups are affected by the opinions of their constituent nodes. For simplicity, we neglect interactions between distinct groups. In Fig. 3.1, we give a schematic illustration of how the opinions of nodes and groups are influenced by the opinions of other nodes and groups in our model, which we describe in detail in Sec. 3.2. In our model, group opinions can lead to oscillatory dynamics or excitable dynamics. In the oscillatory regime, the mean opinion of a network develops self-sustained oscillations. In the excitable regime, it is possible for a situation in which most of the nodes have the same opinion to quickly and temporarily change to a situation in which most of the nodes have the other opinion. The emergence of oscillatory and excitable regimes depends strongly on the correlation between group structure and dyadic network adjacencies. We develop a mean-field approximation of our model's dynamics and use it to gain insight into its dynamics. We find that the onset of excitable dynamics occurs due to a bifurcation from a stable equilibrium to sustained oscillatory dynamics. This bifurcation resembles the onset of excitable dynamics in models of neuronal dynamics [206, 207]. There is some qualitative similarity between the excitable dynamics in our model and the formation of social fads, which is a collective behavior in which a topic, object, or behavior experiences an increase in popularity that forms suddenly, lasts a short amount of time, and declines rapidly [208, 209].

As discussed in Chapter 2, the role of group interactions, which are often called "higher-order interactions" or "polyadic interactions", in opinion dynamics and other dynamical processes on

networks has received much attention in the past few years [27, 210, 211, 212]. The renewed interest in polyadic interactions in complex systems has built on foundational work that dates back many decades [213, 214, 215, 216]. In social systems, a lot of recent research has extended existing models to incorporate polyadic interactions [189, 43, 67, 217, 65, 218, 190, 28, 219, 220, 221, 222, 223]. In these extensions, the opinions are associated with individual agents and they change due to both pairwise and group interactions. By contrast, in our model, we also assign opinions to the groups themselves. In this sense, our work is related to recent studies of the synchronization of quantities that are defined on the edges and higher-order simplices of a simplicial complex [224].

The incorporation of polyadic interactions into network dynamics can significantly affect qualitative behavior. For example, "opinion jumping" can occur in polyadic bounded-confidence models [28], bistable regions can arise in polyadic models of disease spread [43, 49, 45], and the qualitative nature of synchronization transitions of phase oscillators are affected by polyadic interactions [225, 50]. Our observation that group opinions can induce oscillatory and excitable dynamics provides another example of how polyadic interactions can fundamentally modify the dynamics of networked systems. For simplicity, we consider polyadic interactions only through groups of size 3 (i.e., the groups always have exactly 3 nodes). Although this choice prevents us from exploring the effects of group-size heterogeneity (which occurs in most social systems), it has the important advantage of allowing us to easily engage with our primary focus, which is to study the effects of group opinions. Even with this major assumption, our model has very rich dynamics that differ markedly from existing opinion models (which do not incorporate group opinions).

In our model, the individual nodes do not account for their own current opinions when they update their opinions. With this choice of opinion updating, we emphasize the role of (both dyadic and polyadic) social interactions in opinion evolution. Essentially, we are examining a regime in which the effects of self-influence are small in comparison to the effects of social interactions. In this respect, our opinion model is very different from many opinion models [194], but it follows the tradition of classical voter models [76, 86, 196]. In our model, groups can influence themselves, but distinct groups cannot influence each other. Because of group self-influence, we can use our model to

explore the effects of social phenomena, such as "pluralistic ignorance" [226, 227] and "groupthink" [228], that can decelerate changes in group opinions. In pluralistic ignorance, the members of a group believe incorrectly that they hold a minority opinion within a group [226, 227]. Pluralistic ignorance, which one can view as a "minority illusion" [229] in social dynamics, provides a potential mechanism to slow social change through a process of self-silencing, such that individuals appear to conform to a belief that they believe is held by the rest of a group [230]. Groupthink refers to the tendency of individuals in a group to seek social conformity and thereby disregard their own opinions. Our opinion model does not directly encode pluralistic ignorance or groupthink, but one can view its group self-influence term (which slows changes in group opinions) as incorporating them indirectly.

This chapter proceeds as follows. In Sec. 3.2, we introduce our stochastic model of opinion dynamics. In Sec. 3.3, we discuss the model of random hypergraphs on which we simulate these opinion dynamics. In Sec. 3.4, we derive a mean-field description of our stochastic opinion model, study its steady-state behavior, and compare that behavior to the steady-state behavior of the original opinion model. We also discuss the assumptions and approximations that we use to derive the mean-field description. In Sec. 3.5, we discuss the formation of group–node discordance states. In Sec 3.6, we examine the formation of excitable and oscillatory dynamics. Finally, in Sec. 3.7, we summarize and discuss our findings. Our code, figures, and data are available at `https://github.com/CorbitSampson/Oscillatory_Excitable_Opinion_Dynamics.git`.

3.2 Our stochastic opinion model

In this section, we describe our stochastic model of opinion dynamics with group opinions. We consider a set $\mathcal{V}$ of N nodes, which we index by $i \in \{1, 2, \ldots, N\}$. Each node holds a binary opinion, which is either 0 or 1. Our model uses discrete time, so the time $t \in \{0, 1, \ldots\}$. Let x_i^t denote the opinion of node i at time t. As in opinion models on ordinary graphs, which assume dyadic interactions between nodes, our nodes are adjacent to each other if there is an edge between them in a graph $\mathcal{G}$, which has an associated adjacency matrix A. We assume that $\mathcal{G}$ is undirected

and unweighted, so $A_{ij} = A_{ji} = 1$ if nodes i and j are adjacent to each other and $A_{ij} = A_{ji} = 0$ if they are not adjacent. We also suppose that there are S groups of nodes; each group is a subset of $\mathcal{V}$. For simplicity, we suppose that all groups have exactly 3 nodes. Each group has either opinion 0 or opinion 1. We label the groups with the index $j \in \{1, 2, \ldots, S\}$, and we denote the opinion of group j at time t by y_j^t. The $N \times S$ incidence matrix M has entries $M_{ij} = 1$ if node i participates in group j and $M_{ij} = 0$ if it does not. We henceforth refer to the groups in our networks as "triangles". The dyadic degree of each node i is its number of edges, and its triadic degree is its number of triangles. Node i's dyadic degree is thus $k_i = \sum_j A_{ij}$, and its triadic degree is $q_i = \sum_j M_{ij}$. The mean number of edges per node is $\langle k \rangle = \sum_i k_i/N$, and the mean number of triangles per node is $\langle q \rangle = \sum_i q_i/N$.

The opinion of a node is influenced both by the opinions of its adjacent nodes (i.e., dyadic influence) and by the opinions of the groups in which it participates (i.e., polyadic influence) [see Fig. 3.1b]. The opinion of a group is influenced by the opinions of its constituent nodes [see Fig. 3.1c]. Groups do not directly influence other groups.

We now describe our model in detail. The opinions of the nodes (i.e., individuals) and triangles (i.e., groups) evolve stochastically according to the update rule

$$x_i^{t+1} = \begin{cases} 1 & \text{with probability } p_i^N\left(\mathbf{x}^t, \mathbf{y}^t\right) \\ 0 & \text{otherwise}\,, \end{cases} \tag{3.1}$$

$$y_j^{t+1} = \begin{cases} 1 & \text{with probability } p_j^E\left(\mathbf{x}^t, \mathbf{y}^t\right) \\ 0 & \text{otherwise}\,, \end{cases} \tag{3.2}$$

where $\mathbf{x}^t = [x_1^t, x_2^t, \ldots, x_N^t]^{\mathrm{T}}$ is a node opinion vector at time t and $\mathbf{y}^t = [y_1^t, y_2^t, \ldots, y_S^t]^{\mathrm{T}}$ is a triangle opinion vector at time t.

Suppose that the probability that node i adopts opinion 1 is a nonlinear function of a linear combination of the opinions of its adjacent nodes (via its incident edges) and the opinions of the

triangles in which it participates. That is,

$$p_i^N\left(\mathbf{x}^t, \mathbf{y}^t\right) = f_N\left(a\bar{x}_i^t + b\bar{y}_i^t\right) , \tag{3.3}$$

where

$$\bar{x}_i^t = \sum_{j=1}^{N} A_{ij} x_j^t / \langle k \rangle , \tag{3.4}$$

$$\bar{y}_j^t = \sum_{k=1}^{S} M_{jk} y_k^t / \langle q \rangle , \tag{3.5}$$

the influence function f_N is a sigmoidal function [see Eq. (3.8) below], and a and b are real-valued constants [1] . The parameter a encodes the influence of node opinions on their neighbors, and the parameter b encodes the influence of triangle opinions on their constituent nodes, as we will discuss in more detail below. As we discussed in Sec. 3.1, nodes do not consider their own current opinions when they update their opinions (i.e., $A_{ii} = 0$ for all i).

We suppose that the probability that a triangle adopts opinion 1 is a sigmoidal function of a linear combination of its own current opinion and the opinions of its constituent nodes. That is,

$$p_j^E\left(\mathbf{x}^t, \mathbf{y}^t\right) = f_E\left(c\bar{z}_j^t + dy_j^t\right) , \tag{3.6}$$

where

$$\bar{z}_j^t = \frac{1}{3}\sum_{i=1}^{N} M_{ij} x_i^t , \tag{3.7}$$

the influence function f_E is a sigmoidal function [see Eq. (3.8) below], and c and d are real-valued constants. The parameter c encodes the influence of node opinions on the triangles to which they belong, and the parameter d encodes the tendency of a triangle to maintain its opinion. For simplicity, we use the same sigmoidal function for the influence function for all nodes and all triangles. We thus write

$$f(z) := f_N(z) = f_E(z) = \frac{1}{2}\left[1 + \tanh(m(z-\mu))\right] , \tag{3.8}$$

[1] One can absorb the quantities $\langle k \rangle$ and $\langle q \rangle$ in Eqs. (3.4) and (3.5) into the model parameters a, b, c, and d.

where μ is the inflection point of the sigmoid $f(z)$ and $1/m$ is proportional to the width of the sigmoid's transition region. We use a sigmoidal function because it is convenient for representing saturating interactions [231]. Researchers have used sigmoidal functions in models of many other scenarios, including echo chambers and polarization [191], smooth bounded-confidence dynamics [192], and many other saturating interactions, which occur in diverse fields that range from neuroscience to robotics [232].

In Table 3.1, we summarize the parameters and other key quantities of our model. These parameters include the influence parameters (a, b, c, and d), the influence function f and its parameters μ and $1/m$, and parameters and other descriptors of network structure.

It is important to highlight the parameters a, b, c, and d, which encode the amount of (positive or negative) opinion influence at each time step. We interpret positive values of a, b, c, and d as conforming to influence, and we interpret negative values of these parameters as rejecting influence. The parameters a and b encode how much nodes are influenced by their neighboring nodes (the parameter a) and by the groups in which they participate (the parameter b). In particular, $a > 0$ (respectively, $a < 0$) increases (respectively, decreases) the probability that a node transitions to or maintains opinion 1 when more of its neighbors have opinion 1. Analogously, $b > 0$ (respectively, $b < 0$) increases (respectively, decreases) the probability that a node transitions to or maintains opinion 1 as it participates in more groups with opinion 1. The parameter c plays an analogous role for group opinions as b does for node opinions. Specifically, $c > 0$ (respectively, $c < 0$) increases (respectively, decreases) the probability that a group transitions to or maintains opinion 1 when more of its participants have opinion 1. The parameter d encodes how much a group's current opinion affects its subsequent opinion. In particular, $d > 0$ (respectively, $d < 0$) increases (respectively, decreases) the probability that a group maintains opinion 1.

3.3 Random-hypergraph model

It is convenient to use hypergraphs to describe our networks, which consist of nodes, edges, and triangles. While hypergraphs were discussed already in Chapter 2, we repeat here some of

Table 3.1: The parameters and other key quantities of our opinion model.

Parameter	Description
a	Influence of individuals on other individuals
b	Influence of groups on individuals
c	Influence of individuals on groups
d	Influence of a group on itself
f	Sigmoidal influence function
μ	Inflection point of the sigmoid f
$1/m$	Width of the transition of the sigmoid f
r	Correlation coefficient between dyadic degree and triadic degree
$\mathcal{P}$	Hyperdegree distribution
P_1	Marginal dyadic degree distribution
P_2	Marginal triadic degree distribution
k_i	Dyadic degree (i.e., ordinary node degree) of node i
q_i	Triadic degree of node i

the definitions for convenience. A hypergraph is a generalization of a graph that includes both ordinary edges (i.e., dyadic adjacencies) and hyperedges with more than two nodes (i.e., polyadic adjacencies) [10, 211]. Following standard convention, we refer to any of these adjacencies as hyperedges. Mathematically, a hypergraph $\mathcal{H}_\mathcal{G} = (\mathcal{V}, \mathcal{E})$ consists of a set $\mathcal{V}$ of nodes and a set $\mathcal{E}$ of hyperedges. Each hyperedge is a nonempty subset of $\mathcal{V}$; the number of nodes in this subset is the "size" of the hyperedge.

In an ordinary graph, each node $i \in \mathcal{V}$ has an associated degree k_i, which indicates the number of edges that are attached (i.e., "incident") to it. In a hypergraph, the hyperdegree of node i is the vector $\mathbf{k}_i = [k_i^{(2)}, k_i^{(3)}, \ldots, k_i^{(L)}]$, where L is the size of its largest hyperedge and the lth-order degree $k_i^{(l)}$ is the number of size-l hyperedges that are incident to node i. Each hypergraph has a hyperdegree distribution $\mathcal{P}(\mathbf{k})$, which encodes the probabilities that a uniformly-randomly-chosen node has hyperdegree $\mathbf{k}$ for each $\mathbf{k}$. We consider hypergraphs with hyperedges of sizes 2 and 3; the hyperedges of size 2 encode dyadic adjacencies, and the hyperedges of size 3 encode the triadic (i.e., group) adjacencies. For such hypergraphs, the hyperdegree of a node is $\mathbf{k} = [k, q]$.

To study our opinion model, it is convenient to use random hypergraphs with specified

hyperdegree sequences. We use such configuration-model random hypergraphs because we are able to control their hyperdegree sequences. In Appendix A.1, we provide a detailed discussion of the random-hypergraph model that we employ. The formation of hyperedges in this random-hypergraph model depends only on the specified hyperdegree of each node, so one can employ hyperdegree-based compartmental models when studying dynamical processes on the hypergraphs that it generates. Such techniques have been used extensively in the study of disease spread on networks [233, 234].

To examine the effects of correlations between the dyadic degree k and the triadic degree q, we employ a convenient family of hyperdegree distributions to produce the degree sequences in our random hypergraphs. Given the marginal degree distributions $P_1(\cdot)$ and $P_2(\cdot)$ for the edges and triangles, respectively, there are two extremes for the joint distribution $\mathcal{P}(k, q)$. In one extreme, we let $k = q$, which implies that $\mathcal{P}(k, q) = P_1(k)\delta(k-q)$. In the other extreme, k and q are uncorrelated, which implies that $\mathcal{P}(k, q) = P_1(k)P_2(q)$. To systematically explore the effects of correlations between the dyadic and triadic degrees, we use a hyperdegree distribution that interpolates between these two extremes. This joint distribution is

$$\mathcal{P}(k, q) = P_1(k)P_2(q)(1 - r) + P_1(k)\delta(q - k)r\,, \tag{3.9}$$

where the Pearson correlation coefficient $r \in [0, 1]$ between the dyadic and triadic degrees parameterizes the amount of correlation between these degrees. When $r = 0$, the dyadic degree k and triadic degree q are uncorrelated; when $r = 1$, we have that $k = q$ for every node.

To examine the effects of degree heterogeneity, we suppose that the degree distributions $P_1(k)$ and $P_2(q)$ have the approximate power-law form

$$P_1(k) = P_2(k) = P(k) = \begin{cases} \left(\frac{\gamma-1}{k_{\min}^{1-\gamma}}\right) k^{-\gamma}\,, & k \geq k_{\min} \\ 0\,, & \text{otherwise}\,, \end{cases} \tag{3.10}$$

where $k_{\min}$ is the minimum degree. In a particular hypergraph that we construct using our random-hypergraph model, we generate the hyperdegree of each node using bivariate inverse sampling from

the distribution that is described by Eqs. (3.9) and (3.10). We then construct the hypergraph using a procedure that we describe in Appendix A.1.

3.4 Mean-field approximation, initial conditions, and steady-state solutions

3.4.1 Mean-field approximation of Eqs. (3.1)–(3.2)

We develop a mean-field description that approximates the dynamics of our stochastic opinion model (3.1)–(3.2). Our mean-field description tracks the dynamics of three order parameters:

(1) the expected fraction V^t of nodes with opinion 1 in a uniformly random selected edge at time t;

(2) the expected fraction U^t of nodes with opinion 1 in a uniformly random selected triangle at time t; and

(3) the expected fraction Y^t of triangles with opinion 1 at time t.

Alternatively, V^t represents the probability of moving to an opinion-1 node by following an edge that one chooses uniformly at random.

In this section, we present a simplified derivation of our mean-field approximation. In Appendix A.2, we show a detailed derivation of this approximation. Because we generate hypergraphs using a configuration model, the probability that there is a hyperedge that connects a group of nodes depends only on the hyperdegrees of those nodes. Therefore, we can use a hyperdegree-based compartmental model to obtain mean-field equations. First, we approximate the order parameters V^t and U^t in terms of the expected fraction $x_{\mathbf{k}}^t$ of nodes with hyperdegree $\mathbf{k} = [k, q]$ that have opinion 1 at time t. As we show in Appendix A.2, these approximations take the form

$$V^t = \sum_{\mathbf{k}} \frac{k\mathcal{P}(\mathbf{k})x_{\mathbf{k}}^t}{\langle k \rangle}\,, \tag{3.11}$$

$$U^t = \sum_{\mathbf{k}} \frac{q\mathcal{P}(\mathbf{k})x_{\mathbf{k}}^t}{\langle q \rangle}\,. \tag{3.12}$$

The variables V^t and U^t are both closely related to — but can differ from — the expected fraction $\sum_{\mathbf{k}} \mathcal{P}(\mathbf{k})x_{\mathbf{k}}^t$ of nodes with opinion 1 at time t.

To obtain a system of discrete-time evolution equations for the order parameters V^t, U^t, and Y^t, consider the probability [see Eq. (3.1)] that a node i with hyperdegree $\mathbf{k} = [k, q]$ has opinion 1 at time $t + 1$. Assuming that all nodes with the same hyperdegree behave in the same way, we seek to approximate the variables $\bar{x}_i^t$, $\bar{y}_i^t$, $\bar{z}_j^t$, and y_j^t that appear in the probabilities (3.3)–(3.7) in terms of the order parameters.

We approximate $\bar{x}_i^t$, which is the normalized number of neighbors of node i that have opinion 1, by

$$\bar{x}_i^t \approx kV^t/\langle k\rangle\,. \tag{3.13}$$

The term $\bar{y}_i^t$, which is the normalized number of triangles that are attached to node i and have opinion 1 [see Eq. (3.7)], is approximately

$$\bar{y}_i^t \approx qY^t/\langle q\rangle \tag{3.14}$$

because node i is attached to q triangles and Y^t is the expected fraction of triangles that have opinion 1.

We insert the approximations (3.13) and (3.14) into Eqs. (3.1)–(3.3) to obtain

$$x_{\mathbf{k}}^{t+1} \approx f\left(\frac{ak}{\langle k\rangle}V^t + \frac{bq}{\langle q\rangle}Y^t\right)\,. \tag{3.15}$$

Under the mean-field assumption that all triangles behave in the same way (i.e., $y_j^t = y^t$ and $\bar{z}_j^t = \bar{z}^{\,t}$ for all j), the time evolution of the expected fraction Y^t of triangles with opinion 1 satisfies

$$Y^{t+1} = f(c\bar{z}^{\,t} + d)Y^t + f(c\bar{z}^{\,t})(1 - Y^t)\,. \tag{3.16}$$

Similarly to our approximation of $\bar{y}_i^t$ in Eq. (3.14), we approximate $\bar{z}^{\,t}$ by

$$\bar{z}^{\,t} \approx U^t\,, \tag{3.17}$$

which is the expected fraction of nodes at time t with opinion 1 in a triangle that we select uniformly at random. Substituting Eq. (3.17) into Eq. (3.16) yields

$$Y^{\,t+1} = Y^t f\left(cU^t + d\right) + (1 - Y^t)f(cU^t)\,. \tag{3.18}$$

Inserting Eq. (3.15) into Eqs. (3.11)–(3.12) yields a closed map for the time evolution of the three order parameters:

$$\begin{aligned} V^{\,t+1} &= \sum_k \sum_q \frac{k\mathcal{P}(k,q)}{\langle k\rangle} f\left(\frac{a\,k}{\langle k\rangle}V^t + \frac{b\,q}{\langle q\rangle}Y^t\right) , \\ U^{\,t+1} &= \sum_k \sum_q \frac{q\mathcal{P}(k,q)}{\langle q\rangle} f\left(\frac{a\,k}{\langle k\rangle}V^t + \frac{b\,q}{\langle q\rangle}Y^t\right) , \\ Y^{\,t+1} &= Y^t f\left(cU^t + d\right) + (1-Y^t) f(cU^t)\,. \end{aligned} \tag{3.19}$$

The mean-field description (3.19) relies on various approximations, which we now summarize and discuss. First, our mean-field description is a hyperdegree-based compartmental model, so it assumes that the expected time evolution of all nodes with hyperdegree $\mathbf{k}$ is the same. (For example, the probability that each such node has opinion 1 at time t is $x_{\mathbf{k}}^t$.) This approximation relies on the fact that we assume that all nodes of hyperdegree $\mathbf{k}$ possess the same type and number of expected connections. Our mean-field description also assumes that the dyadic and triadic degrees of each node are both sufficiently large that we can replace the variables $\bar{x}_i^t$, $\bar{y}_i^t$, and $\bar{z}_i^t$ by their means [as we did in Eqs. (3.13), (3.14), and (3.17)]. In particular, we do not expect our mean-field approximation to give a good approximation for sparse hypergraphs. One can generalize our mean-field description to account for hypergraph models (e.g., degree-assortative random hypergraphs [235]) in which nodes have intrinsic variables and connect to each other with probabilities that depend on these variables. Such generalizations of configuration models have a long history of success in investigations of dynamical processes on graphs [236].

3.4.2 Selection of initial conditions

We now discuss our selection of initial conditions of our stochastic opinion model (3.1)–(3.2) and its mean-field approximation (3.19). The spaces of initial conditions for these two models differ drastically from each other, so we need to select initial conditions that allow us to compare these models as effectively as possible.

In our simulations of the stochastic opinion model (3.1)–(3.2), the initial opinion of each node and each triangle is either 0 or 1. To reduce the number of parameters that we need to describe

the initial conditions of the stochastic opinion model, we specify only the initial probabilities that nodes and triangles that have opinion 1. We specify the initial opinion of each node and each triangle independently. Each node initially has opinion 1 with probability u_1 and opinion 0 with probability $1-u_1$, and each triangle initially has opinion 1 with probability u_2 and opinion 0 with probability $1-u_2$. We then specify the initial conditions of the stochastic opinion model (3.1)–(3.2) as ordered pairs (u_1, u_2) of initial probabilities.

The mean-field map (3.19) describes the evolution of the three orders parameters V^t, U^t, and Y^t, so we directly specify the initial conditions V^0, U^0, and Y^0 of these order parameters. This specification contrasts with our selection of initial conditions in the stochastic opinion model (3.1)–(3.2), for which we can specify initial conditions using only two parameters. To mitigate this discrepancy, in our examples that compare simulations of (3.1)–(3.2) and (3.19), we let $V^0 = U^0 = u_1$ and $Y^0 = u_2$ to make the initial conditions for the two descriptions as similar as possible. We make this choice because the order parameters V^t and U^t are related (but not equal) to the fraction of nodes with opinion 1 [see Eqs. (3.11) and (3.12)] and Y^t is the expected fraction of triangles with opinion 1.

In several of our examples, we compare many possible choices of the initial conditions of the stochastic opinion model (3.1)–(3.2) and mean-field map (3.19). In Appendix A.3, we give a detailed description of how we select these initial conditions.

3.4.3 Steady-state solutions of the stochastic opinion model (3.1)–(3.2)

We now examine the steady-state solutions (i.e., states in which the order parameters V^t, U^t, and Y^t are constant) of the stochastic opinion model (3.1)–(3.2) by studying the fixed points of the mean-field equations (3.19). We obtain qualitatively similar steady-state solutions and bifurcations for any value of the hyperdegree correlation $r \in [0, 1]$. Therefore, for simplicity, we assume in the present discussion that $r = 1$, which implies that the dyadic degree and triadic degree are equal (i.e., $k = q$). We use this assumption for the remainder of this section and throughout Sec. 3.5. We will see in Sec. 3.6 that relaxing this assumption results in qualitatively different dynamics. Under

this assumption, $V^t = U^t$ and the mean-field equations (3.19) reduce to

$$\begin{aligned} V^{t+1} &= \sum_k \frac{kP(k)}{\langle k\rangle} f\left(\frac{k}{\langle k\rangle}\left(aV^t + bY^t\right)\right) , \\ Y^{t+1} &= Y^t f\left(cV^t + d\right) + (1 - Y^t) f\left(cV^t\right) . \end{aligned} \tag{3.20}$$

Any fixed point $[V^t, Y^t] = [V^*, Y^*]$ of the map (3.20) must satisfy

$$V^* = \sum_k \frac{kP(k)}{\langle k\rangle} f\left(\frac{k}{\langle k\rangle}\left(aV^* + bY^*\right)\right) , \tag{3.21}$$

$$Y^* = Y^* f\left(cV^* + d\right) + (1 - Y^*) f\left(cV^*\right) . \tag{3.22}$$

Solving (3.22) for Y^* and substituting the result into Eq. (3.21) shows that the fixed points of Eqs. (3.20) have the form $[V^*, Y^*] = [F(V^*), G(V^*)]$, where

$$\begin{aligned} F(V) &= \sum_k \frac{kP(k)}{\langle k\rangle} f\left(\frac{k}{\langle k\rangle}\left(aV + bG(V)\right)\right) , \\ G(V) &= \frac{f(cV)}{1 + f(cV) - f(cV + d)} . \end{aligned} \tag{3.23}$$

The equation $V^* = F(V^*)$ is a one-dimensional equation for V^* that one can solve using a root-finding algorithm. After determining V^*, we obtain Y^* using the equation $Y^* = G(V^*)$.

To illustrate the usefulness of Eqs. (3.21)–(3.22) to study steady-state solutions of the stochastic opinion model (3.1)–(3.2), we compare the fixed points that we obtain from the solution of Eqs. (3.21)–(3.22) with the results of simulations of Eqs. (3.1)–(3.2). In Fig. 3.2, we plot both the steady-state values V^* and Y^* that we obtain from simulations of Eqs. (3.1)–(3.2) (dots) and the fixed-point solutions of Eqs. (3.21)–(3.22) (solid and dashed curves) as a function of the sigmoid inverse-width parameter m for $a = b = c = d = \mu = 1/2$, power-law exponent $\gamma = 4$, and mean degrees $\langle k\rangle = \langle q\rangle = 20$. Because a, b, c, and d all have positive values, all nodes and groups experience only conforming influence. For each value of m, we iterate Eqs. (3.1)–(3.2) for 400 steps and plot the values of V^* and Y^* after the final step. We do 100 independent simulations of this process with evenly spaced initial conditions in the unit square (see Appendix A.3). For each value of m, we use the same hypergraph with $N = 700$ nodes. Both our simulations of the stochastic opinion model (3.1)–(3.2) and our analysis of the mean-field approximation (3.20) illustrate that

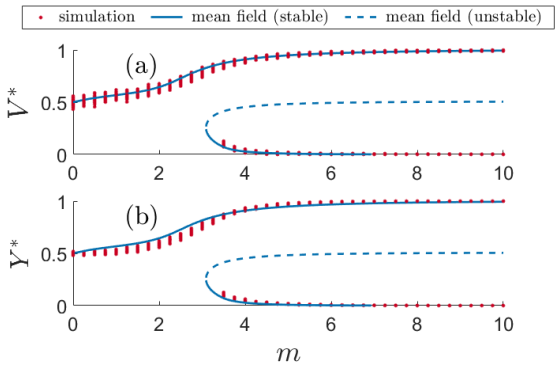

Figure 3.2: An example of a bifurcation of the steady-state solutions when the dyadic and triadic degrees are equal (i.e., $r = 1$) in simulations of our stochastic opinion model (3.1)–(3.2) and solutions of the mean-field equations (3.20) for the parameter values $a = b = c = d = \mu = 0.5$, power-law exponent $\gamma = 4$, and mean degrees $\langle k \rangle = \langle q \rangle = 20$. The bifurcation parameter is the inverse-width parameter m of the sigmoidal influence function (3.8). We show the values of (a) V^* and (b) Y^* that we obtain from the mean-field equations (solid and dashed curves) and from means of 100 simulations of our stochastic opinion model (dots).

the system transitions from a regime with a single steady state to a regime with two distinct steady states as we increase m. Although we observe some quantitative differences between our mean-field description and direct simulations of the original stochastic opinion model, the fixed points of the mean-field equations are reasonably successful at approximating the steady-state solutions of the stochastic model. The bifurcation in Fig. 3.2 gives an interesting example of the behavior of our opinion model. A similar bifurcation was also observed in another opinion model with sigmoidal interactions [232]. Therefore, we do not focus on such bifurcations of steady-state solutions in situations with equal dyadic and triadic degrees ($r = 1$). Instead, we investigate novel features that arise due to the presence of group opinions. In particular, we observe (1) states in which the mean node and mean group opinions are different and (2) excitable and oscillatory opinion dynamics. The oscillator dynamics (see Sec. 3.6) arise only when the dyadic degree and triadic degree are not fully correlated (i.e., when $r < 1$).

3.5 Group–node discordance

An important feature of our opinion model is that it admits solutions in which the mean opinion of the nodes differs significantly from the mean opinion of the groups. We refer to these solutions as *group–node discordance states*. These states can model situations in which a social organization (or other social group) has a different official stance than the individuals who comprise that organization. In our model, we measure the discordance of a solution by calculating

$$D(V^*, Y^*) = |V^* - Y^*| \,. \tag{3.24}$$

A group–node discordance state occurs when $D(V^*, Y^*) > 0$. The maximum possible discordance is $D(V^*, Y^*) = 1$.

We explore how group–node discordance states can arise for different strengths of group influence (i.e., for different values of the group-influence parameters c and d). We plot $D(V^*, Y^*)$ versus the node-opinion influence parameter a (with $a = b$) using the mean values of V^* and Y^* from 16 independent simulations of the stochastic opinion model (3.1)–(3.2), and we compare this plot to a numerical solution of the fixed-point equations (3.21)–(3.22) for the mean-field approximation (3.20). In this comparison, we use a single realization of a configuration-model hypergraph with $N = 2000$ nodes, inverse-width parameter $m = 4$, power-law exponent $\gamma = 4$, and mean degrees $\langle k \rangle = \langle q \rangle = 20$ for both $\mu = 0.5$ [see Fig. 3.3a] and $\mu = 0.25$ [see Fig. 3.3b]. The initial conditions of the 16 independent simulations are evenly spaced in the unit square (see Appendix A.3). For $\mu = 0.5$, we obtain more group–node discordance [i.e., larger values of $D(V^*, Y^*)$] when the node parameters a and b are very different from the hyperedge parameters c and d. We see this in Fig. 3.3a for $c = d = 0.1$ (red solid curve and open circles) and $c = d = 0.9$ (orange solid curve and open squares). In both Fig. 3.3a and Fig. 3.3b, the maximum discordance occurs when $a + b$ is on the opposite side of μ as $c + d$. When $c = 0.1$ and $d = 0.9$, we observe a more uniform discordance in the system, with a small decrease near $a = b = 0.5$. When $\mu = 0.25$ [see Fig. 3.3b] for $c = d = 0.1$ and $c = d = 0.9$, we observe the same general trend. The group–node discordance states arise most prominently when $c + d < \mu < a + b$ or $a + b < \mu < c + d$. For $\mu = 0.5$ [see Fig. 3.3a], the transition

to a group–node discordance state for $c = d = 0.1$ looks like it may be discontinuous; for $\mu = 0.25$ [see Fig. 3.3b], the transition to a group–node discordance state is continuous.

We also explore how the width (which is proportional to $1/m$) of the sigmoid transition region affects the onset of group–node discordance states by calculating $D(V^*, Y^*)$ versus m for several values of a, b, c, and d. We show the results of our numerical simulations in Fig. 3.4, which uses the same initial conditions, network parameters, and other conventions as Fig. 3.3. When $a = b = c = d = 0.5$ (blue curve and closed circles), the width parameter m has a minimal effect and $D(V^*, Y^*)$ remains close to 0, indicating that there is very little group–node discordance. For both $a = b = 0.2$, $c = d = 0.8$ (red curve and open circles) and $a = b = 0.8$, $c = d = 0.2$ (orange curve and open squares), the group–node discordance $D(V^*, Y^*)$ has a maximum at an intermediate value of m. We also observe an interesting difference between the cases $\mu = 0.5$ [see Fig. 3.4a] and $\mu = 0.25$ [see Fig. 3.4b]. When $a = b = 0.8$ and $c = d = 0.2$, there is a possibly discontinuous transition from discordance to non-discordance for $\mu = 0.5$; however, the transition is continuous for $\mu = 0.25$.

3.6 Excitable and oscillatory dynamics

Our opinion model also has excitable and oscillatory opinion dynamics. To illustrate these dynamics, we simulate both the stochastic opinion model (3.1)–(3.2) and the mean-field approximation (3.19) with the parameters $(a, b, c, d) = (1, -0.5, 0.25, 0.25)$ and $(m, \mu) = (8, 0.25)$. In this regime, the nodes are influenced considerably by the opinions of their neighboring nodes ($a = 1$), nodes reject the opinions of their groups ($b = -0.5$), groups are influenced equally by their constituent nodes and their own opinions ($c = d = 0.25$), and the sigmoidal influence function of the nodes and groups has a small inflection point ($\mu = 0.25$) and a very steep transition ($m = 8$).

We first suppose that the dyadic and triadic degrees are equal (so the correlation between them is $r = 1$). This situation yields excitable dynamics, in which a dynamical system is initially at a locally stable steady-state solution, but — for a sufficiently large perturbation (which is often called a "stimulus") — it experiences a large excursion through phase space before returning to the

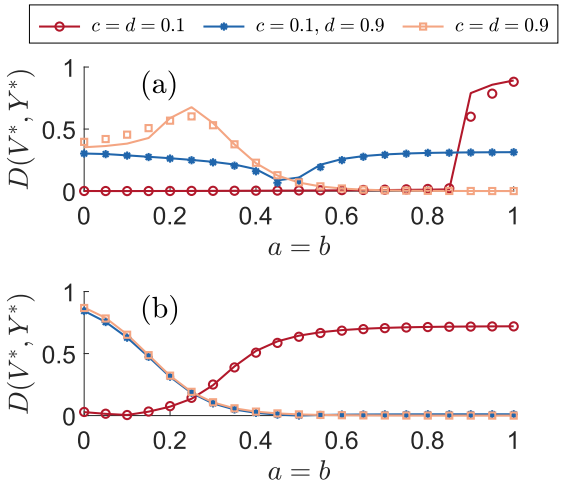

Figure 3.3: The group–node discordance $D(V^*, Y^*)$ versus the node-opinion influence parameter a, with $a = b$, for a single numerical solution $(V^*, Y^*) = (F(V^*), G(V^*))$ of Eqs. (3.23) (solid curves) and the mean of 16 independent simulations of the stochastic opinion model (3.1)–(3.2) for a single configuration-model hypergraph with $N = 2000$ nodes, inverse-width parameter $m = 4$, power-law exponent $\gamma = 4$, mean degrees $\langle k \rangle = \langle q \rangle = 20$, and several values of the group-influence parameters c and d. We consider (a) $\mu = 0.5$ and (b) $\mu = 0.25$. The initial conditions of the 16 simulations are evenly spaced in the unit square (see Appendix A.3).

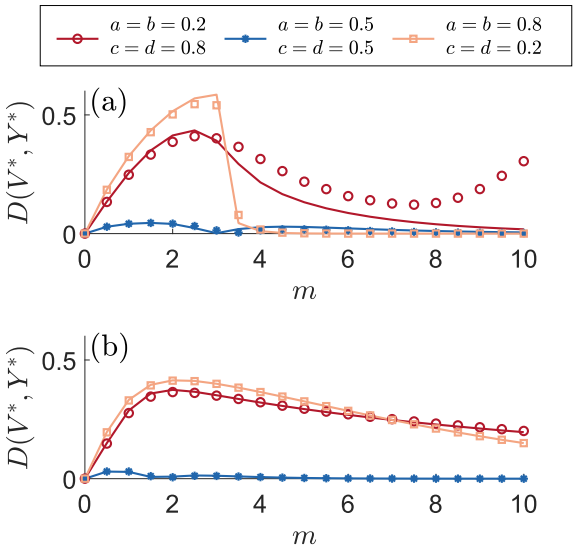

Figure 3.4: The group–node discordance $D(V^*, Y^*)$ versus the sigmoid inverse-width parameter m for a single numerical solution $(V^*, Y^*) = (F(V^*), G(V^*))$ of Eqs. (3.23) (solid curves) and the mean of 16 independent simulations of the stochastic opinion model (3.1)–(3.2) for a single realization of a configuration-model hypergraph with $N = 2000$ nodes, power-law exponent $\gamma = 4$, mean degrees $\langle k \rangle = \langle q \rangle = 20$, and several values of a, b, c, and d. We consider (a) $\mu = 0.5$ and (b) $\mu = 0.25$. The initial conditions of the 16 simulations are evenly spaced in the unit square (see Appendix A.3).

steady-state solution [206, 207]. Excitable dynamics are common in neuronal and cardiac systems, and they are often associated with a system being near a bifurcation from a resting state to sustained spiking or oscillatory behavior [206, 207, 237]. In Fig. 3.5a, we show the order parameters V^t (red) and Y^t (blue) from numerical simulations of Eqs. (3.1)–(3.2) for the aforementioned parameter values and a configuration-model hypergraph with $N = 1000$ nodes and an approximate power-law hyperdegree distribution with $\gamma = 4$. The dashed curves show the fixed-point solution that we obtain by solving Eqs. (3.21)–(3.22). In these simulations, the expected node fraction V^t remains close to the fixed-point solution for a short time before it increases sharply and then subsequently decreases and returns approximately to the fixed-point solution. The expected triangle fraction Y^t has the same behavior; its dynamics follow V^t with a short delay. We use the term *opinion pulses* for these spikes in V^t and Y^t.

In Fig. 3.5b, we show V^t as a function of time in simulations of the stochastic opinion model (3.1)–(3.2) (top) and the mean-field equations (3.19) (bottom). For the mean-field equations, we introduce a stimulus at time $t = 200$ by increasing both V^t and U^t by 0.2 (vertical arrow). The mean-field equations yield a single opinion pulse, which resembles the ones that we observe in simulations of our stochastic opinion model (3.1)–(3.2), in which finite-size fluctuations seemingly provide a stimulus.

As we decrease the correlation r between the dyadic and triadic degrees, the opinion pulses become more frequent until they eventually become self-sustained oscillations. In Fig. 3.5c, we show an example of such oscillations for $r = 0.15$. We again observe that the mean-field equations (3.19) successfully reproduce the qualitative behavior of the stochastic opinion model (3.1)–(3.2).

One can use the mean-field equations (3.19) to understand the transition from excitable to oscillatory dynamics as the correlation r decreases. When $r = 1$, the mean-field map (3.19) has three fixed points [see Fig. 3.6a]. We obtain these fixed points using root-finding methods and determine their linear stability by calculating the eigenvalues of the Jacobian matrix of (3.19). We compute the Jacobian matrix numerically using the "Adaptive Robust Numerical Differentiation" package for MATLAB [238]. One of the fixed points [see the closed blue circle in Fig. 3.6a–b] is

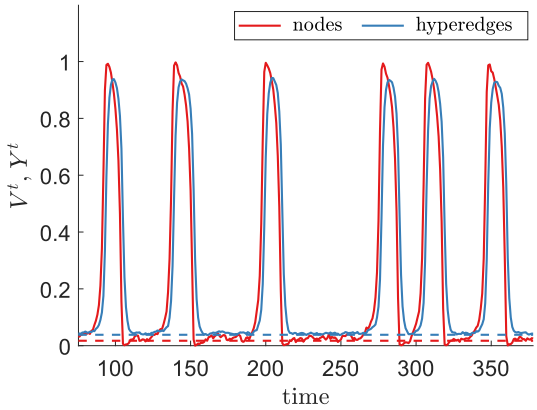

(a) An example of opinion pulses in a single simulation of our stochastic opinion model (3.1)–(3.2) with parameter values $a = 1$, $b = -0.5$, $c = d = 0.25$, $\mu = 0.25$, and $m = 8$ for a configuration-model hypergraph with equal dyadic and triadic degrees (i.e., $r = 1$) that we draw from an approximate power-law distribution with exponent $\gamma = 4$ and mean-degrees $\langle k \rangle = \langle q \rangle = 20$. We plot the expected node fraction V^t in red and the expected triangle fraction Y^t in blue. The dashed lines show the fixed points that we obtain by solving Eqs. (3.21)–(3.22).

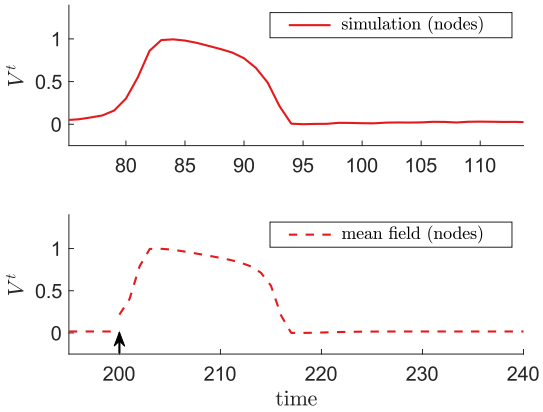

(b) Comparison of a single pulse of the expected node fraction V^t for (top) a single simulation of our stochastic opinion model (3.1)–(3.2) and (bottom) the mean-field equations (3.20) for the parameter values $a = 1$, $b = -0.5$, $c = d = 0.25$, $\mu = 0.25$, and $m = 8$ for a hypergraph with equal dyadic and triadic degrees (i.e., $r = 1$) that we draw from an approximate power-law distribution with exponent $\gamma = 4$ and mean-degrees $\langle k \rangle = \langle q \rangle = 20$. We apply a stimulus (which is indicated by the black arrow) of $(\delta V, \delta U, \delta Y) = (0.2, 0.2, 0)$ to the mean-field equations to induce an excitation at time $t = 200$.

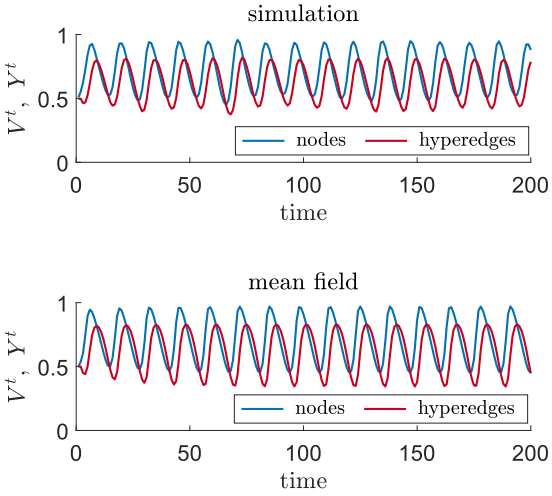

(c) An example of the oscillatory dynamics in (top) a single simulation of our stochastic opinion model (3.1)–(3.2) and (bottom) the mean-field equations (3.19) for parameter values $a = 1$, $b = -0.5$, $c = d = 0.25$, $\mu = 0.25$, $r = 0.15$, $m = 8$, $\gamma = 3.8$, and $\langle k \rangle = \langle q \rangle = 20$. We plot the expected node fraction V^t in blue and the expected triangle fraction Y^t in red. The initial conditions of the stochastic opinion model are $(u_1, u_2) = (0.5, 0.5)$, and the initial conditions of the mean-field equations are $(V^0, U^0, Y^0) = (0.5, 0.5, 0.5)$.

Figure 3.5

linearly stable. It is located near the origin, so we refer to it as the "near-0" fixed point. A nearby fixed point [see the open green circle in Fig. 3.6a–c] is a saddle. The third fixed point [see the red star in Fig. 3.6a–c] is an unstable spiral, and we refer to this spiral as the "away-from-0" fixed point. When the mean-field system (3.19) is close to the near-0 fixed point (which is linearly stable) and is perturbed so that it crosses the stable manifold of the saddle, it makes an excursion through phase space. It gets close to the unstable spiral and then returns to the stable fixed point, completing an opinion pulse. In Fig. 3.6a, we show an example of such a trajectory in phase space. As we decrease r, the stable and saddle fixed points approach each other [see Fig. 3.6b], and one can then create opinion pulses using smaller stimuli. Eventually, the linearly stable fixed point and the saddle collide in a SNIC (i.e., saddle–node on invariant circle) bifurcation, resulting in oscillatory behavior [see Fig. 3.6c]. See [207] for details about SNIC bifurcations.

We have seen that oscillatory dynamics arise via a SNIC bifurcation as the correlation coefficient r decreases. To obtain a broader perspective of the bifurcations and associated changes in qualitative dynamics that occur as the parameters change, we show a bifurcation diagram in (r, γ) space in Fig. 3.7a. Recall that γ is the exponent of the approximate power-law degree distributions of our configuration-model hypergraphs, so smaller values of γ correspond to more heterogeneous degree distributions. For small values of r and γ, the fixed points of the mean-field map (3.19) are linearly stable, which we indicate in the diagram by writing "steady state". Through the numerical linear stability analysis that we described above, we observe three bifurcations as γ and r increase (see Fig. 3.7a). We describe these three bifurcations in the order that they occur. First, there is a Hopf bifurcation of the away-from-0 fixed point (red curve), which transitions from a linearly stable spiral to a linearly unstable spiral. This bifurcation marks the onset of oscillatory dynamics. Second, there is a SNIC bifurcation of the near-0 fixed point (blue curve), which transitions from a saddle to a linearly stable fixed point. This bifurcation marks a change from oscillatory dynamics to excitable dynamics. Third, there is a "complex-to-real bifurcation" where the away-from-0 fixed point transitions from an unstable spiral to an unstable node. This bifurcation marks the return of steady-state behavior. The bifurcation diagram in Fig. 3.7a indicates where excitable and

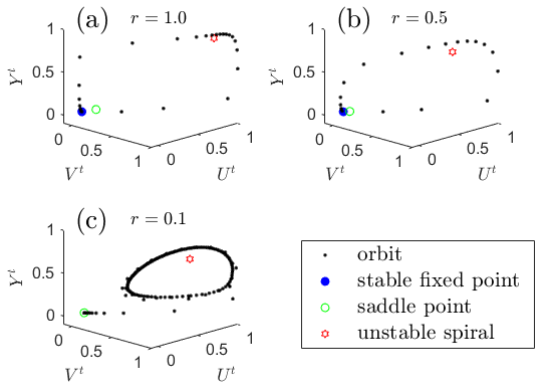

Figure 3.6: The phase-space trajectories of solutions of the mean-field equations (3.19) with a perturbation $(\delta V, \delta U, \delta Y) = (0.25, 0.25, 0)$ for hyperdegree distributions with correlations between the dyadic and triadic degrees of (a) $r = 1$, (b) $r = 0.5$, and (c) $r = 0.1$. The merging of stable and unstable fixed points near an unstable spiral leads to the transition from excitable to oscillatory dynamics. The other parameter values are $a = 1$, $b = -0.5$, $c = d = 0.25$, $\mu = 0.25$, $m = 8$, $\gamma = 4$, and $\langle k \rangle = \langle q \rangle = 20$.

oscillatory dynamics occur in the parameter range $(r, \gamma) \in [0, 1] \times [2.5, 6]$.

The mean-field map (3.19) is an approximation of the stochastic opinion model (3.1)–(3.2), so we expect similar bifurcations to occur in the stochastic opinion model. Therefore, we believe that the aforementioned bifurcations provide a good explanation of the onset of excitable and oscillatory dynamics in both the mean-field equations (3.19) and the stochastic opinion model (3.1)–(3.2) that they approximate. To numerically verify this conjecture, we study the qualitative dynamics of the stochastic model (3.1)–(3.2) for different values of both the correlation coefficient r and the exponent γ of the approximate power-law degree distribution. We compute the difference

$$\mathcal{H}(V^t, \mathcal{I}) := \max_{\mathcal{I}}(V^t) - \min_{\mathcal{I}}(V^t)\,, \tag{3.25}$$

between the maximum and minimum values of the expected node fraction V^t in an interval $\mathcal{I}$. A fixed-point solution of Eqs. (3.19) gives $\mathcal{H}(V^t, \mathcal{I}) \approx 0$ if we choose an interval $\mathcal{I}$ after the transient dynamics disappear. Oscillations and opinion pulses both yield $\mathcal{H}(V^t, \mathcal{I}) > 0$. In principle, one can also distinguish between pulses and oscillations by sliding and/or varying the length of the interval $\mathcal{I}$, but we do not employ these approaches (and we have not examined them thoroughly).

In Fig. 3.7b, we plot $\mathcal{H}(V^t, \mathcal{I})$ versus the power-law exponent γ from Eq. (3.10) and the

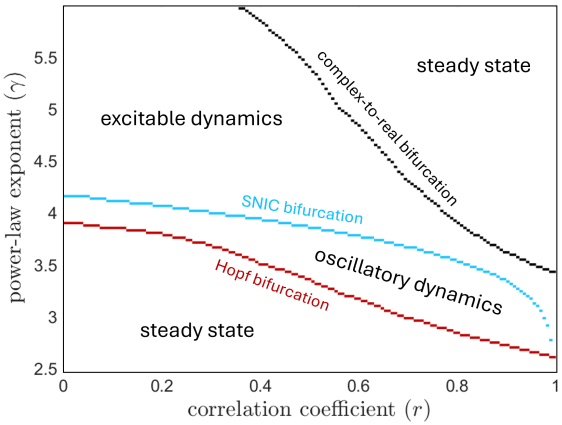

(a) A bifurcation diagram of the transitions between stationary, excitable, and oscillatory states of the mean-field equations (3.19). Each curve indicates a bifurcation in the linear stability of the near-0 fixed point or the away-from-0 fixed point. As one crosses the red curve, the away-from-0 fixed point undergoes a Hopf bifurcation. As one crosses the light blue curve, the near-0 fixed point undergoes a saddle–node bifurcation. As one crosses the black curve, the away-from-0 fixed point transitions from a linearly unstable spiral to a linearly unstable node.

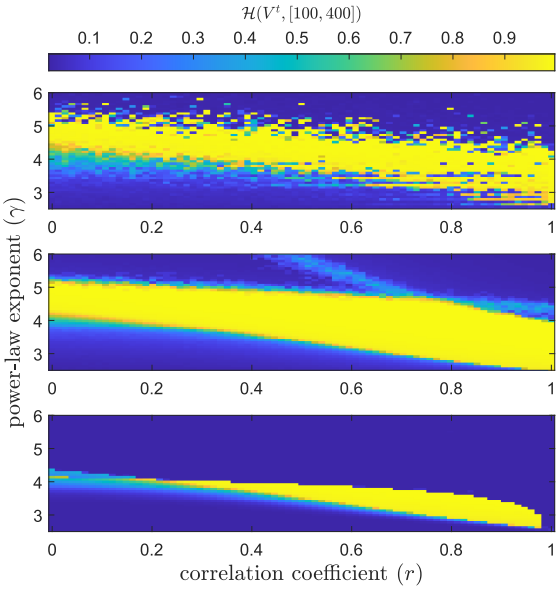

(b) A heat map of $\mathcal{H}(V^t, \mathcal{I}) = \max_{\mathcal{I}}(V^t) - \min_{\mathcal{I}}(V^t)$ [see Eq. (3.25)] for (top) a mean of 25 independent simulations of the stochastic opinion model (3.1)–(3.2); (middle) a mean of 25 independent simulations of the stochastically perturbed mean-field equations (3.26); and (bottom) a mean of 25 independent simulations of the original mean-field equations (3.19). The horizontal axis is the correlation coefficient r, and the vertical axis is the power-law exponent γ. In these simulations, we use a single realization of a configuration-model hypergraph and the parameter values $a = 1$, $b = -0.5$, $c = d = 0.25$, $\mu = 0.25$, $m = 8$, and $\langle k \rangle = \langle q \rangle = 20$. For both the stochastic opinion model and the mean-field equations (both with and without stochastic fluctuations), we select 25 evenly spaced initial conditions in the unit square (see Appendix A.3).

Figure 3.7

correlation coefficient r for dyadic and triadic degrees in the interval $\mathcal{I} = [100, 400]$, which seems to provide adequate time for the transient behavior to disappear. For each pair (r, γ), we simulate the stochastic opinion model (3.1)–(3.2) and the mean-field equations (3.19) to obtain $\mathcal{H}$ from Eq. (3.25). For both the stochastic opinion model and the mean-field equations, we select 25 evenly spaced initial conditions in the unit square (see Appendix A.3). In the top panel of Fig. 3.7b, we plot $\mathcal{H}$ from simulations of the stochastic opinion model (3.1)–(3.2). In the bottom panel, we plot $\mathcal{H}$ from the mean-field equations (3.19). For a given value of the correlation coefficient r, oscillatory or excitable dynamics occur only for a narrow range of power-law exponents, illustrating that these dynamics are very sensitive to network structure. A stronger correlation between dyadic and triadic degrees (i.e., a larger r) requires a smaller value of γ (i.e., a more heterogeneous network) for oscillatory or excitable dynamics to occur. Interestingly, perfectly correlated dyadic and triadic degrees (i.e., $r = 1$), which reduce the dimensionality of the mean-field equations (3.19) from 3 to 2, suppress the oscillatory dynamics. Observe that the yellow band [which indicates a large value of $\mathcal{H}(V^t, \mathcal{I})$] in the bottom panel of Fig. 3.7b does not extend to $r = 1$.

Despite the qualitative similarities between the dynamics of the stochastic opinion model (3.1)–(3.2) (see the top panel of Fig. 3.7b) and those of the mean-field equations (3.19) (see the bottom panel of Fig. 3.7b), there are key differences between the qualitative dynamics of these models. As we discussed above, although the mean-field equations support excitable dynamics, they require a stimulation to yield opinion pulses. To mimic the effect of the stochastic model's finite-size fluctuations, which are absent in the deterministic mean-field equations (3.19), we introduce a stochastic term. We consider the equations

$$\begin{aligned} V^{t+1} &= \sum_k \sum_q \frac{k\mathcal{P}(k,q)}{\langle k \rangle} f\left(\frac{a\,k}{\langle k \rangle} V^t + \frac{b\,q}{\langle q \rangle} Y^t\right) + \sigma_1^t\,, \\ U^{t+1} &= \sum_k \sum_q \frac{q\mathcal{P}(k,q)}{\langle q \rangle} f\left(\frac{a\,k}{\langle k \rangle} V^t + \frac{b\,q}{\langle q \rangle} Y^t\right) + \sigma_2^t\,, \\ Y^{t+1} &= Y^t f\left(cU^t + d\right) + (1 - Y^t) f(cU^t)\,. \end{aligned} \tag{3.26}$$

In Eqs. (3.26), we draw σ_1^t and σ_2^t uniformly at random from the interval $(0, Q)$ at each time step. These small stochastic perturbations act as a repeated small stimulus to the system. Our decision

to not include a random stimulus to Y^t arises from our observation that the fluctuations in the fraction of hyperedges with opinion 1 is smaller than the fluctuations in the fraction of nodes with opinion 1. This is the case because a hypergraph from the employed random-hypergraph model has many more hyperedges than nodes. There are $N\langle q\rangle/3$ hyperedges in an N-node hypergraph.

In the middle panel of Fig. 3.7b, we show $\mathcal{H}$ from the stochastically perturbed mean-field equations (3.26) with an upper bound of $Q \approx 0.036$ on the stochastic noise. We are not attempting to accurately reproduce the finite-size fluctuations of the stochastic opinion model (3.1)–(3.2). Instead, we seek to demonstrate that the mean-field description (3.19), when augmented with stochastic fluctuations, can produce excitable and oscillatory dynamics that are qualitatively similar to those that we obtain from simulations of the stochastic opinion model.

By simultaneously examining Fig. 3.7a and Fig. 3.7b, we observe that the mean-field approximation [see the bottom panel of Fig. 3.7b] has a region with $\mathcal{H}(V^t,\mathcal{I}) > 0$ of a shape that is qualitatively similar to the oscillatory region in Fig. 3.7a. We expect this similarity because our simulations of the mean-field equations (3.19) in the bottom panel of Fig. 3.7b do not include perturbations or stimuli, and they thus do not exhibit excitable dynamics. We also observe that the region with $\mathcal{H}(V^t,\mathcal{I}) > 0$ in the top and middle panels of Fig. 3.7b is qualitatively similar to the union of the oscillatory region and the lower part of the excitable region in Fig. 3.7a. When we use a larger value of Q in the stochastically perturbed mean-field map (3.26), the region with $\mathcal{H}(V^T,\mathcal{I}) > 0$ more closely resembles the union of the entirety of the excitable and oscillatory regions in Fig. 3.7a.

3.7 Conclusions and discussion

We introduced and analyzed a stochastic model of opinion dynamics in which both nodes and groups of nodes have binary opinions. This opinion model includes novel dynamics that result directly from polyadic interactions. We showed that our model supports a richer repertoire of qualitative dynamics than related models in which only nodes have opinions. In particular, our opinion model has both excitable dynamics (in which brief but strong opinion swings arise from

perturbations of a steady-state solution) and oscillatory dynamics (in which the mean opinions of the nodes and hyperedges have self-sustained oscillations). The excitable dynamics of our system have qualitative similarities with the dynamics of social fads [208]. In particular, opinion changes appear initially in a small number of individuals (or via an external perturbation for our mean-field approximation), experiences a surge that affects the majority of the system, and then quickly dies out. Our opinion model also possesses group–node discordance states, in which nodes and groups have contradictory opinions. Our simulations of the stochastic opinion model and its mean-field approximation both reveal that the excitable and oscillatory dynamics depend significantly on network structure (specifically, on dyadic degrees, polyadic degrees, and the correlation between them).

There are many interesting ways to extend our opinion model. As with all models of opinion dynamics, we greatly simplified human dynamics (or the dynamics between other animals) to formulate a mathematically and computationally tractable model that one can study systematically. For example, we assumed that opinions are binary (instead of allowing more opinion states or continuous-valued opinions), that interactions occur through a known and time-independent hypergraph, and that opinions evolve through precise mathematical rules. It is worth relaxing these assumptions and exploring the consequences of doing so.

One important way to generalize our model is to incorporate various heterogeneities, including in the group sizes, the interaction strengths (e.g., some groups or nodes may be more influential than others), and the shapes of the sigmoidal functions (e.g., some nodes may be more likely than others to change their opinions). For simplicity, we limited our study to groups of size 3. As we illustrated at length, the dynamics that result from considering only groups of size 3 is already very rich. However, it is natural to expect that some phenomena occur only in networks with heterogeneous group sizes. For example, perhaps an opinion can propagate from small groups to large groups (or vice versa). Just as the degree distribution of a graph can significantly influence the qualitative behavior of dynamical processes on it [10, 239], we expect that the hyperedge-size distribution (along with hyperdegree distributions) influences the qualitative behavior of dynamical processes

on a hypergraph. In our study, we also neglected interactions between distinct groups, which are likely to introduce additional interesting dynamics. Another potentially interesting extension of our model is the inclusion of node self-influence, as individuals typically have some conviction in their prior beliefs. Additionally, although our mean-field approximation adequately reproduced the observed dynamics and provided some theoretical insights, it is based on the assumption that the hypergraph that describes the nodes and the groups is generated by a configuration model. It is worthwhile to extend our mean-field approximations to stochastic-block-model hypergraphs with assortative mixing (which can encode homophily) [46] and community structure [47].

Although our opinion model has rich behavior and provides insights into the effects of group opinions on opinion dynamics, it is important to note that we have not validated our model with real-world opinion data. Indeed, such validation efforts are notoriously difficult in the study of opinion dynamics [240, 241], but it can be possible when appropriate data is available [242]. We hope that further studies of opinion dynamics will encourage and guide efforts in data collection, associated data analysis, and model validation.

Chapter 4

Competing Social Contagions with Opinion Dependent Infectivity

4.1 Introduction

In the last few decades, social media has become increasingly ubiquitous in people's lives [61, 62]. Online social media has become a source of news for many individuals, with about half of US adults admitting to receiving news at least "occasionally" through social media [243, 244, 245]. However, the widespread use of social media and other factors such as its low barrier to entry, limited view format, and ideologically segregated social networks make online social media platforms an attractive target for the malicious dissemination of false information (known as disinformation) [135, 246, 247]. The spread of disinformation and misinformation (the unintentional spread of false or inaccurate information) has been labeled a major threat to national security and appears as a concern relating to health security, political instability, and violent societal conflict [60]. These concerns have led to great interest in the study of how disinformation and misinformation spread [248, 249, 250, 135, 251, 37, 252, 253, 135, 254, 255, 249, 256, 257, 258, 259, 260] and in the development of methods to limit the spread of misinformation [261, 262, 263, 264, 265, 266].

Although the spread of disinformation within online social media platforms can be exacerbated by many mechanisms, here we are interested in understanding the effect of individuals' cognitive biases in the spread of disinformation. A cognitive bias is the tendency for human cognition to consistently form beliefs that are systematically distorted from reality [38]. Particularly, we are interested in the effects of the *confirmation bias* and the *illusory truth effect*. Confirmation bias is the tendency of individuals to more readily believe information that aligns better with their own

beliefs [39]. The illusory truth effect is the tendency of individuals to view ideas as more truthful through mere exposure (i.e., exposure to those ideas without additional reinforcement) [267, 37]. Together, these two biases lead to the possibility that individuals may believe a particular piece of information simply from repeated exposure. The effects of repeated exposure promoting the spread of misinformation have been observed in relation to public health misinformation involving COVID-19 [40].

In this chapter we develop an agent-based model to examine how confirmation bias and the illusory truth effect can affect the spreading dynamics of two mutually exclusive beliefs, leading to the predominance of one over the other. In our model, the two competing beliefs are represented as two discrete states, $+1$ and -1. Adopting terminology from the social contagion and epidemic spreading literature, we refer to these states as *contagions*, and the adoption of one of these beliefs as an *infection*. To model confirmation bias and the illusory truth effect, each individual is endowed with an internal, continuous opinion variable, which represents the alignment of the individual's biases towards competing beliefs. This internal opinion is modified by infection attempts, modeling the illusory truth effect, and modifies the infection probabilities, modeling confirmation bias. We study the long-term dynamics of the competing beliefs by means of numerical simulations of the agent-based model and a mean-field description of the dynamics. We find that there is a continuum of disease-free states, each characterized by a different average internal opinion of the population. The average internal opinion determines the stability of the disease-free state. As opposed to traditional spreading processes, the presence of cognitive biases can lead to unexpected dynamics depending on the initial conditions. In some situations, a pair of competing beliefs with numbers of supporters that are initially decaying can rebound, so that one of the beliefs ends up becoming dominant while the other dies. Similarly, a population with an average opinion that initially is biased toward one belief can end up overturning this opinion so that the opposing belief becomes dominant. We also study how the long-term dynamics are modified by external recruitment of spreaders for one of the two beliefs and find that, depending on the initial conditions, this recruitment can lead either to total domination by the promoted belief or coexistence of the two

beliefs.

As discussed in Chapter 2, there are many other studies that have examined the effects of multiple interacting contagions both in the context of biological and social contagions [147, 148, 130, 268]. These have included both competitive and cooperative interactions [147, 148] as well as the simultaneous spread of viral contagions and vaccination-seeking behavior [130]. Some studies have even included many heterogeneous features, such as the work by Kaligotla et al. [268], which developed a threshold-like agent-based model of two competing rumors which included agent reputation, effort of information spreading, and contrarian agents. Although these previous studies examined multiple spreading contagions and their potentially complex interactions, in our study we also highlight the role of individual opinions and cognitive biases in the spread of competing beliefs.

This chapter proceeds as follows. In Sec. 4.2, we introduce our agent-based model. In Sec. 4.3, we formulate a mean-field approximation of our model. In Sec. 4.4, we discuss the possible long-term behaviors of the model and classify their linear stability. In Sec. 4.5, we discuss two of the primary behaviors of the model and how they arise from opinion-dependent stability of the disease-free state. In Sec. 4.6 we study the effect of a heterogeneous distribution of initial opinions. In Sec. 4.7, we modify the model to include external recruitment of spreaders. Finally, in Sec. 4.8, we summarize and discuss our findings. The code for this project is available at `https://github.com/CorbitSampson/Competing_Social_Contagions`.

4.2 Description of the model

We consider a model where individuals can adopt one of two mutually exclusive beliefs or remain neutral, and individuals who have adopted one of the two beliefs try to actively spread their belief to the rest of the population. In order to make contact with existing literature and terminology on social contagion and epidemic processes, we will refer to the two beliefs as "contagions", and label them as $+1$ and -1. We will refer to the neutral state as the "susceptible" state, and label it with a 0. Therefore, each individual has a trinary contagion state, either -1,0, or $+1$. We will also

say that an individual who adopts one of the two beliefs is "infected". In addition to the contagion state, each node has an internal opinion which is used to model the effects of confirmation bias and the illusory truth effect. Confirmation bias is the effect whereby a person is more likely to believe information that already aligns with their current belief [39], and the illusory truth effect is a phenomenon where people are more likely to believe something if they have been repeatedly exposed to it [267, 37]. Below we describe our model in detail.

Our model consists of a network where, at time t, each node i has a discrete contagion state $s_i^t \in \{-1, 0, 1\}$. The contagion states -1 and $+1$ indicate that the individual is infected with one of the two mutually exclusive contagions and can spread this contagion to its network neighbors. The state 0 indicates the individual is susceptible. In addition, each node has a continuous internal opinion $x_i^t \in [-1, 1]$. The opinion x_i^t measures the node's alignment with each of the two contagions. To model the effects of confirmation bias we will assume that, the closer x_i^t is to $+1$ (-1), the more likely it is that node i is infected with opinion $+1$ (-1) when exposed by a neighbor and the less likely it is to recover from it. Furthermore, to model the illusory truth effect, each time a node with contagion s_i attempts to infect a node j, the opinion of node j moves closer to s_i, even if the infection attempt is unsuccessful.

We assume that time evolves in discrete steps, $t = 0$, Δt, $2\Delta t$, $\ldots$. A single time step of the agent-based model is as follows:

(1) M nodes are selected uniformly at random to act as "spreaders".

(2) For each spreader node i:

   (a) if $s_i^t = 0$, nothing is done. Otherwise, one network neighbor j of i is selected uniformly at random to be exposed.

   (b) The opinion of node j is updated to

$$x_j^{t+\Delta t} \;=\; x_j^t + C(s_i^t - x_j^t)\Delta t\,, \tag{4.1}$$

   where $C \in \mathbb{R}^+$ is the rate of opinion shift. If $x_j^{t+\Delta t}$ is larger than $+1$ (less than -1),

$x_j^{t+\Delta t}$ is set to $+1$ (-1).

(c) If $s_j^t = 0$, node j is infected with contagion s_i^t (i.e., $s_j^{t+\Delta t} = s_i^t$) with probability

$$\beta(x_j^t, s_i^t)\Delta t\,. \tag{4.2}$$

(3) Each infected node, d, heals with probability

$$\gamma(x_d^t, s_d^t)\Delta t\,. \tag{4.3}$$

The infection and recovery rates are given, respectively, by

$$\beta(x,s) = \frac{1+sx+\epsilon}{2+\epsilon}\,\beta_{\max}\,, \tag{4.4}$$

$$\gamma(x,s) = \frac{1-sx+\epsilon}{2+\epsilon}\,\gamma_{\max}\,, \tag{4.5}$$

where $\epsilon > 0$ is a parameter that measures the difference between the smallest and largest values of β and γ as shown in Fig. 4.1. The particular choice of β in Eq. (4.4) was made so that the infection rate of a node i with opinion x_i to contagion s is larger if x_i is close to s, to model confirmation bias. Similarly, the form for γ in Eq. (4.5) was selected such that γ is smaller if x_i is close to s, to model the unwillingness to give up an idea that the individual has a strong belief in. In addition, γ increases as x_i gets closer to $-s$, allowing individuals to stop spreading a contagion that is inconsistent with their views.

The parameter ϵ controls the strength of the confirmation bias: for $\epsilon = 0$, the infection and healing rates dependence on the node's internal opinion is the strongest; as $\epsilon \to \infty$, the infection and healing rates become independent of the node's internal opinion.

In simulations of our agent-based model each node is assigned an initial internal opinion and an initial discrete contagion state. To set the initial conditions for the fractions of nodes in the three contagion states, subsets of the n nodes are selected to be infected with the $+1$ contagion, -1 contagion, or left susceptible. These subsets are constructed by drawing N_+ agents uniformly at random from all agents to be infected with the $+1$ contagion. From the remaining agents, an additional N_- are selected uniformly at random to be infected with the -1 contagion. The

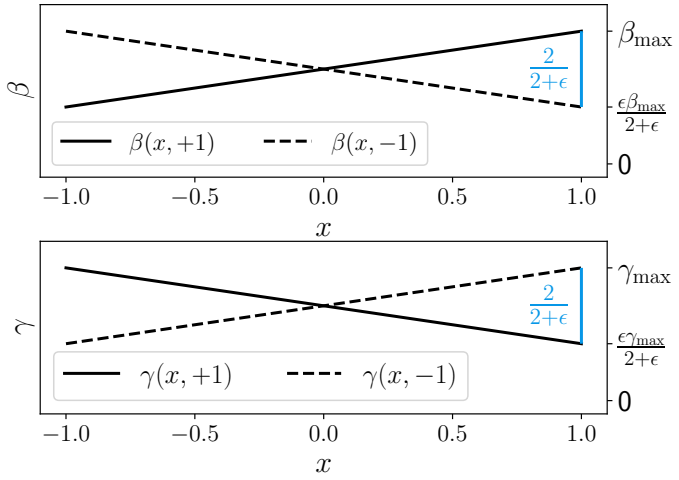

Figure 4.1: Infection and recovery rates $\beta(x, s)$ (top) and $\gamma(x, s)$ (bottom) as functions of the opinion x for parameters $\beta_{\max} = 1$, $\gamma_{\max} = 1$, and $\epsilon = 1.5$, for $s = +1$ (solid lines) and $s = -1$ (dashed lines).

remaining $n - N_+ - N_-$ agents are left susceptible. The initial internal opinions are assigned homogeneously (i.e., all nodes begin with the same internal opinion) in Sections IV and V, while heterogeneous distributions of initial opinions are explored in Section VI.

Fig. 4.2 illustrates our model. Fig. 4.2a shows a network where each node has a contagion state which is either -1 (red), 0 (white), or $+1$ (blue), shown in the inner circle of each node. The opinion of each node is a continuous variable x represented by the color of the outer circle of each node. Fig. 4.2b shows an example of the illusory truth effect and confirmation bias in our model, as a node with contagion $s = +1$ and opinion $x = 0.2$ (left) repeatedly attempts to infect another node (right). With each attempt, the opinion of the node on the right gets closer to $+1$ (illusory truth effect), thus making the node more susceptible to the contagion (confirmation bias).

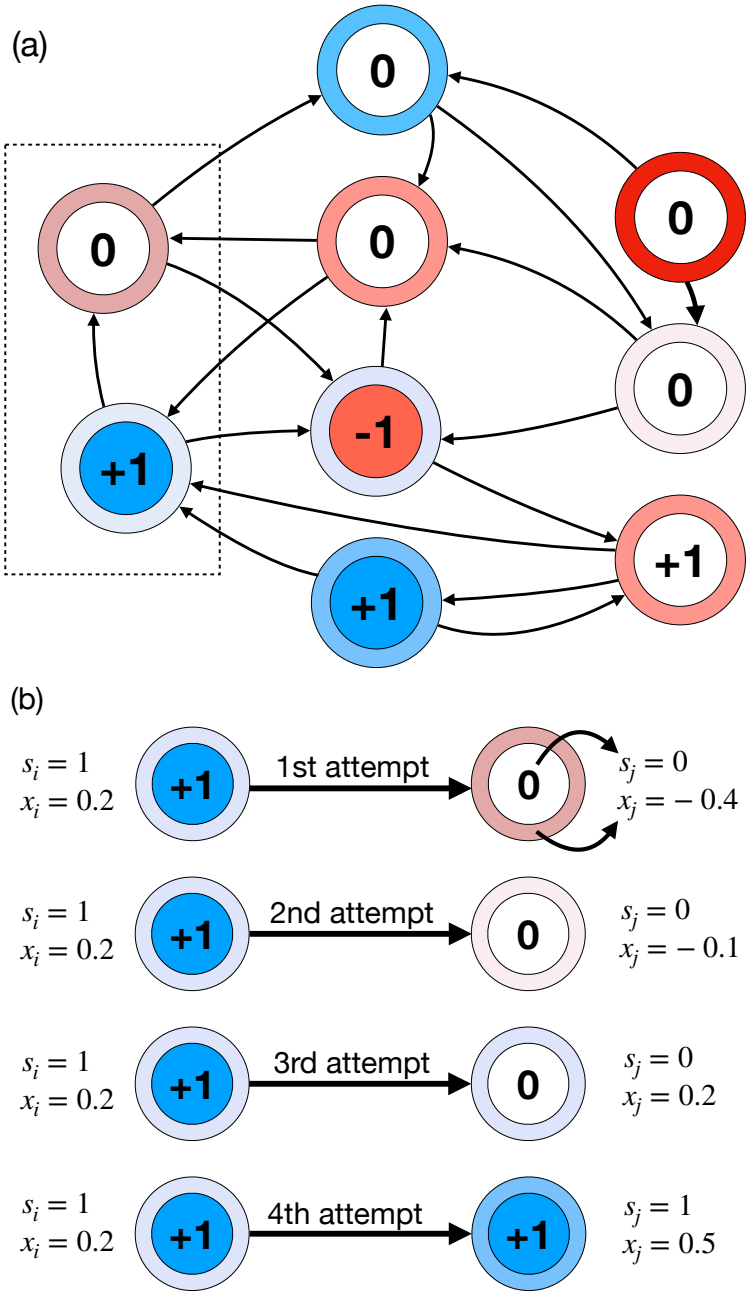

Figure 4.2: (a) A diagram showing an example interaction network for the agent-based model. Each node has a contagion state -1 (red), 0 (white), or $+1$ (blue) (shown as the inner circle). The internal opinion of each node is represented by the color of the outer ring, ranging from -1 (red) to $+1$ (blue). (b) An example of how repeated exposures can change the opinion of node j to align with the contagion of node i and the possible transition of node j from susceptible to infected with the $+1$ contagion.

4.3 Mean-field approximation

To study the dynamics of this model we develop a mean-field approximation for the dynamics of the average opinion and the fraction of nodes with the $+1$ and -1 contagions, given respectively by

$$X = \frac{1}{N}\sum_{i=1}^{N} x_i \,, \tag{4.6}$$

$$S_+ = \frac{1}{N}\sum_{s_i=1} s_i \,, \tag{4.7}$$

$$S_- = \frac{1}{N}\sum_{s_i=-1} |s_i| \,. \tag{4.8}$$

For simplicity, we develop our mean-field approximation only for k-regular networks. The expected fraction of nodes that recover from ± 1 contagion in a small time step of length Δt is approximately

$$\gamma(X, \pm 1) S_\pm \, \Delta t \,. \tag{4.9}$$

Similarly, the expected fraction of nodes that become infected with the ± 1 contagion in a small time step of length Δt is approximately

$$\frac{M}{N} S_\pm \frac{k-1}{k} (1 - S_+ - S_-) \beta(X, \pm 1) \, \Delta t \,, \tag{4.10}$$

where $MS_\pm$ is the expected number of spreader nodes with the ± 1 contagion, $\frac{k-1}{k}(1 - S_+ - S_-)$ is the probability that the randomly chosen neighbor of the spreader node is susceptible, and $\beta(X, \pm 1)\Delta t$ is the probability that the spreader node successfully infects the susceptible neighbor. To understand the need for the factor $(k-1)/k$, note that $(1 - S_+ - S_-)$ would be the expected fraction of susceptible neighbors of the spreader node if these nodes were selected uniformly at random. However, this estimate neglects the fact that neighbors of a spreader node are not chosen uniformly at random, but their choice is conditioned on being neighbors of an already infected node. Since the spreader node must have been infected by one of its neighbor nodes, we remove one node from the count by multiplying by the factor $(k-1)/k$ (this first-order correction neglects the possibility that the node might have healed since it infected the spreader node).

From Eq. (4.1) the average change in opinion over the small time interval Δt due to attempted infections from nodes with the ± 1 contagion is approximately

$$\frac{M}{N} C(\pm 1 - X) S_{\pm} \, \Delta t \, . \tag{4.11}$$

In the limit $\Delta t \to 0$ these approximations result in the following system of differential equations for the three order parameters in Eqs. (4.6)-(4.8):

$$\begin{aligned}
\frac{dS_+}{dt} &= -S_+ \gamma(X, 1) \\
&+ \frac{M}{N} \frac{k-1}{k} (1 - S_+ - S_-) S_+ \beta(X, 1), && (4.12) \\
\frac{dS_-}{dt} &= -S_- \gamma(X, -1) \\
&+ \frac{M}{N} \frac{k-1}{k} (1 - S_+ - S_-) S_- \beta(X, -1), && (4.13) \\
\frac{dX}{dt} &= \frac{M}{N} C \left[(1 - X) S_+ - (1 + X) S_- \right], && (4.14)
\end{aligned}$$

where β and γ are given by Eqs. (4.4) and (4.5). Substituting Eqs. (4.4) and (4.5) and non-dimensionalizing Eqs. (4.12)-(4.14) we arrive at the reduced equations

$$\begin{aligned}
\frac{dS_+}{d\tau} &= -S_+ \left(1 - X + \epsilon \right) \\
&+ r_0 (1 - S_+ - S_-) S_+ \left(1 + X + \epsilon \right), && (4.15) \\
\frac{dS_-}{d\tau} &= -S_- \left(1 + X + \epsilon \right) \\
&+ r_0 (1 - S_+ - S_-) S_- \left(1 - X + \epsilon \right), && (4.16) \\
\frac{dX}{d\tau} &= K \left[(S_+ - S_-) - (S_+ + S_-) X \right], && (4.17)
\end{aligned}$$

where r_0, τ, and K are defined as

$$\begin{aligned}
r_0 &= \frac{M \beta_{\max} (k-1)}{N k \gamma_{\max}}, && (4.18) \\
\tau &= \frac{\gamma_{\max}}{2 + \epsilon}, && (4.19) \\
K &= MC/N \, . && (4.20)
\end{aligned}$$

Note that Eqs. (4.15) and (4.16) correspond to the SIS model for a pair of competing contagions where the healing and infection rates are $[1 - X + \epsilon]$ and $r_0[1 + X + \epsilon]$, respectively, for the $+1$ contagion, and $[1 + X + \epsilon]$ and $r_0[1 - X + \epsilon]$ for the -1 contagion. The healing and infection rates are controlled by the average opinion X, which in turn depends dynamically on the fraction of infected individuals, S_+ and S_-, via Eq. (4.17). In the next section we will study the conditions under which one contagion becomes prevalent while the other disappears. First, however, we discuss some of the assumptions made in developing the model and its mean-field description.

Our mean-field description is based on the assumption of a homogeneous network where each node has degree k. However, our analysis could be extended to networks with heterogeneous degree distributions using the methods of Ref. [269]. We have conducted our numerical simulations of the agent-based model using target k-regular networks constructed via the configuration model and found good agreement with our mean-field approximation even for k as small as 7 (see Fig. 4.4a). The target k-regular networks used in this project were constructed using the complex group interactions (XGI) package for Python [270]. In addition, our mean-field description neglects pair correlations [269].

Other assumptions of our model are the particular functional forms for how the healing and infection rates depend on a node's opinion, and how the opinion changes upon an attempted infection. We chose the forms in Eqs. (4.1), (4.4), and (4.5) for simplicity, and we expect qualitatively similar results for other choices where the infection rates are increasing and decreasing function of the node's opinion for the $+1$ and -1 contagions, respectively, and vice versa for the healing rates.

Our model is based on sequential (rather than simultaneous) updating. The basic update rule in our model is the selection of a random node that, if infected, attempts to spread the contagion. To speed up the numerical simulation of our model, M such updates are carried out every time step. Alternatively, one could consider a simultaneous updating version of our model, where at every time step every infected node attempts to spread its contagion with a certain probability. Although we have not explored this version of our model, it exists as a special case where $M = n$ (i.e., selecting every node at each time step).

When comparing the agent-based model and the mean-field approximation, it is necessary to match their initial conditions. To achieve this, given initial conditions $S_\pm(0)$ for the initial fraction of spreaders in the mean-field model, we compute the initial number of spreaders for each contagion in the agent-based model as $N_\pm = \text{floor}[NS_\pm(0)]$. For the opinions, given a mean opinion $X(0)$ in the mean-field model, we sample their initial opinion from a distribution with mean $X(0)$. In Secs. IV and V we assign all agents in the agent-based model the same opinion $X(0)$. In Sec. VI we allow agents to start with different opinions by sampling their initial opinion from a Gaussian and a bimodal distribution. With these choices, the average opinion of the agents in the agent-based model will be $X(0)$ and the initial fraction of spreaders of the $+1$ and -1 contagions will be approximately $S_+(0)$ and $S_-(0)$, respectively. This allows us to specify the initial conditions of both the agent-based model and mean-field equations as the ordered triplet $(X(0), S_+(0), S_-(0))$. Note that these choices do not allow the initial conditions for opinions and contagion states to be correlated, a potentially important case that will be studied in future work.

4.4 Equilibria and their stability

The mean-field equations (4.15)-(4.17) admit the following equilibrium solutions:

- *Disease-free behavior*: The family $(X, S_+, S_-) = (A, 0, 0)$, where A is an arbitrary constant. This family corresponds to the case where both contagions are absent, but there is an underlying average opinion $X = A$.

- *Endemic behavior*: The two equilibria $(X, S_+, S_-) = (+1, S^*, 0)$ and $(X, S_+, S_-) = (-1, 0, S^*)$, where

$$S^* \;=\; 1 - \frac{\epsilon}{(2+\epsilon)r_0}\,. \tag{4.21}$$

  These two equilibria correspond to the case where one contagion drives the other one to extinction, and the surviving contagion drives the average opinion to consensus (here understood as the state where all nodes hold the same opinion). We refer to these cases, respectively, as *+1 endemic behavior* and *-1 endemic behavior*.

- *Coexistence*: The equilibrium point $(X, S_+, S_-) = (0, \sigma, \sigma)$, where

$$\sigma = \frac{r_0 - 1}{2r_0}. \tag{4.22}$$

This equilibrium point corresponds to a case where the two contagions coexist and the average opinion is zero. However, linear stability analysis shows that this solution is unstable.

The local stability of the disease-free equilibrium solutions $(A, 0, 0)$ depends on the condition that $R_{\rm e}^{\pm}(A) < 1$, where the effective reproduction numbers $R_{\rm e}^{+}(A)$ and $R_{\rm e}^{-}(A)$ are given by

$$R_{\rm e}^{+}(A) = r_0 \left[\frac{1 + A + \epsilon}{1 - A + \epsilon}\right], \tag{4.23}$$

$$R_{\rm e}^{-}(A) = r_0 \left[\frac{1 - A + \epsilon}{1 + A + \epsilon}\right]. \tag{4.24}$$

Similarly, a linear stability analysis about $(+1, S^*, 0)$ and $(-1, 0, S^*)$ results in the conditions $R_{\rm e}^{+}(A) > 1$ and $R_{\rm e}^{-}(A) > 1$, respectively, for these points to be stable.

For a given r_0 and ϵ, the value of the average opinion A that results in instability of the disease-free state towards the $+1$ or -1 contagions (i.e., such that the unstable manifold of the disease-free state is a subset of the basin of attraction of the $+1$ or -1 endemic state) can be found by setting $R_{\rm e}^{+}$ or $R_{\rm e}^{-}$ equal to 1. When $R_{\rm e}^{+} = 1$, Eq. (4.23) gives

$$A^{+} = \max\left\{(1 + \epsilon)\left[\frac{1 - r_0}{1 + r_0}\right], 0\right\}. \tag{4.25}$$

Similarly, setting $R_{\rm e}^{-} = 1$ we get

$$A^{-} = \min\left\{-(1 + \epsilon)\left[\frac{1 - r_0}{1 + r_0}\right], 0\right\}, \tag{4.26}$$

from Eq. (4.24). The inclusion of the $\max(\cdot)$ and $\min(\cdot)$ functions in Eqs. (4.25) and (4.26), respectively, is to ensure that $A^{+} \geq 0$ and $A^{-} \leq 0$ for values of $r_0 > 1$. This is done to emphasize that $+1$ endemic behavior and -1 endemic behavior cannot simultaneously be stable.

The values (4.25) and (4.26) provide bounds on the average opinion for which each of the three equilibria are stable. Particularly, for $A \in (A^{-}, A^{+})$ the equilibrium $(A, 0, 0)$ is stable. For $A > A^{+}$, $(+1, S^*, 0)$ is stable, and for $A < A^{-}$ the equilibrium $(-1, 0, S^*)$ is stable. Notice that for any value of A, there is always exactly one stable equilibrium point.

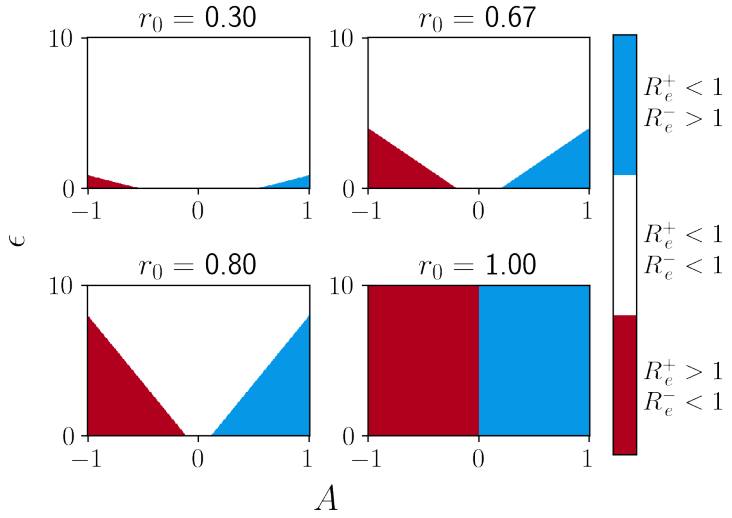

(a) Examples of the stability of the $(A, 0, 0)$ equilibrium state, from Eqs. (4.23) and (4.24), for values of $r_0 \in \{0.30, 0.67, 0.80, 1.00\}$ as a function of A and ϵ. Red represents unstable towards the -1 contagion ($R_e^+ < 1$ and $R_e^- > 1$), blue represents unstable towards the $+1$ contagion ($R_e^+ > 1$ and $R_e^- < 1$), and white represents stable ($R_e^+ < 1$ and $R_e^- < 1$).

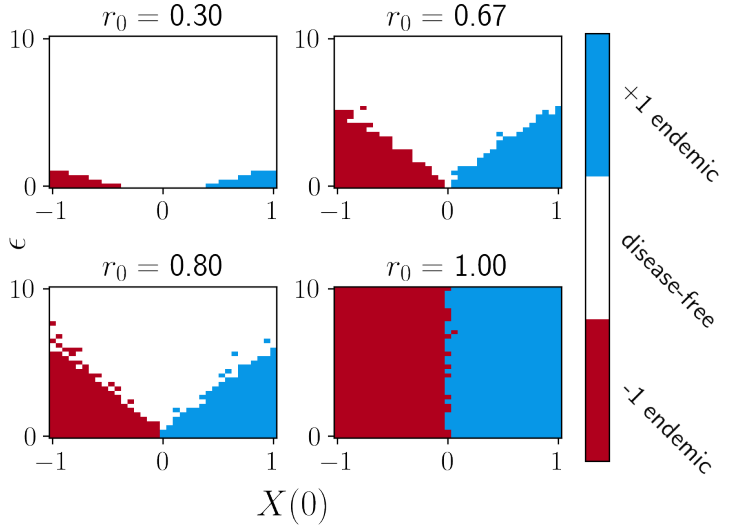

(b) The long-term behavior of the agent-based model for $r_0 \in \{0.30, 0.67, 0.80, 1.00\}$ as a function of $X(0)$ and ϵ. The color of each point represents which contagion was successful more frequently out of 9 independent trails of the agent-based simulation on a 30-regular network of $N = 1000$ nodes. Each simulation ran for 3000 time steps with initial fractions of infected nodes given as $(S_+(0), S_-(0)) \in \{(0.05i/2,\ 0.05j/2) |\ i \in \{0, 1, 2\},\ j \in \{0, 1, 2\}\}$.

Figure 4.3

In Fig. 4.3a we show how the stability of the disease-free equilibrium $(A, 0, 0)$ depends on A and ϵ for values of the reproductive number r_0 given by 0.3 (top left), 0.67 (top right), 0.8 (bottom left), and 1 (bottom right). In each panel, the color white indicates stability of the disease-free state [i.e., $R_{\rm e}^{+}(A) < 1$, $R_{\rm e}^{-}(A) < 1$], red indicates instability towards the -1 contagion [$R_{\rm e}^{-}(A) > 1$, $R_{\rm e}^{+}(A) < 1$], and blue instability towards the $+1$ contagion [$R_{\rm e}^{+}(A) > 1$, $R_{\rm e}^{-}(A) < 1$].

Fig. 4.3b shows the results obtained from numerical simulation of the agent-based model for a target k-regular network with $N = 1000$ and $k = 30$ and the same values of r_0 shown in Fig. 4.3a. For each choice of $(X(0), \epsilon)$, the agent-based model was simulated 9 times with initial fractions of infected nodes $(S_+(0), S_-(0))$ spaced uniformly in the square $[0, 0.05] \times [0, 0.05]$ [i.e., $(S_+(0), S_-(0)) \in \{(0.05i/2,\, 0.05j/2) |\, i \in \{0, 1, 2\},\, j \in \{0, 1, 2\}\}$]. After 3000 time steps the fraction of nodes with each contagion was stored. After the 9 independent simulations for each pair $(X(0), \epsilon)$ the mean final fraction of nodes with each contagion across the 9 simulations was computed. When the mean final fraction of nodes with the $+1$ contagion was larger than the mean final fraction of nodes with the -1 contagion, a 1 was recorded (blue). Conversely, when the mean final fraction of nodes with the -1 contagion was larger than the mean final fraction of nodes with the $+1$, a -1 was recorded (red). Otherwise, a zero was recorded (white). The choice of 3000 time steps allows sufficient time for the system to converge such that the average opinion at 3000 time steps deviates from the mean over the last 200 time steps by less than 0.001. We will use the same number of time steps in the rest of the chapter unless noted. The same condition is fulfilled in the rest of the simulations. Overall, the mean-field approximation and the numerical simulations of the agent-based model agree well for k-regular networks for $k = 30$. We also observe reasonably good agreement for k as small as 7 (cf. Fig. 4.4a).

4.5 Rebound and bias overturning

In the previous section we found that the mean-field version of our model admits disease-free and endemic states, where stability is dependent on the average opinion. Since the average opinion is a dynamic quantity, the transient and long-term behavior of our model depends in a non-trivial

way on the initial conditions. Two examples of the complex dependence of the final state on the initial conditions are the *rebound* and the *bias overturning* behaviors, which we discuss below.

In the rebound, the initial conditions $(X(0), S_+(0), S_-(0))$ are such that $A^- < X < A^+$, so that only the disease-free state with $S_+ = 0 = S_-$ would be stable if X was constant. As S_+ and S_- decay to zero, X changes and moves out of the interval $[A^-, A^+]$, thus bringing the system into the basin of attraction of either the $+1$ endemic or -1 endemic states, depending on whether $X > A^+$ or $X < A^-$, respectively. Fig. 4.4a shows an example of a rebound. Fig. 4.4a (top) shows the average opinion X obtained from the agent-based model (teal solid line) and from the mean-field model (brown dashed line). Fig. 4.4a (bottom) shows S_+ and S_- obtained from the agent-based model (solid lines) and from the mean-field model (dashed lines). As discussed above, while both S_+ and S_- initially decay, X increases, at some point exceeding A^+ (black dot-dashed line). Subsequently, S_+ increases while S_- keeps decaying. This is further illustrated in Fig. 4.4b, which shows the trajectories of (S_+, X) and (S_-, X). After the trajectories enter the region where $X > A^+$ (blue region), they converge to the $+1$ endemic state equilibrium $(S^*, 1)$ and $(0, 1)$ (black circles).

The bias overturning behavior is characterized by the sign of the average opinion in the final state being opposite of that in the initial state. An example is shown in Figs. 4.5a and 4.5b, with the same conventions as those used in Figs. 4.4a and 4.4b. As shown in Fig. 4.5a, the initial value of X is positive. However, there is an excess of spreaders for the -1 contagion which, even as their numbers decay, manage to make X negative, crossing A^- (dot-dashed line), causing the system to converge to the -1 endemic state.

These examples illustrate how the final state of the system depends on the initial values of S_+, S_-, and X. To illustrate this more systematically, in Fig. 4.6 we have plotted the basin of attraction of the $+1$ endemic (blue), -1 endemic (red), and disease-free (white) cases for $S_+(0), S_-(0) \in [0, 0.5]$ and $r_0 \in \{0.3, 0.5, 0.7, 1.0\}$ with an initial opinion bias $X(0) = 0.1$, obtained using numerical solutions of the mean-field equations (4.15)-(4.17) simulated over $t_f = 3000$ time steps. There we see that as r_0 increases the disease-free region becomes smaller until the system transitions directly

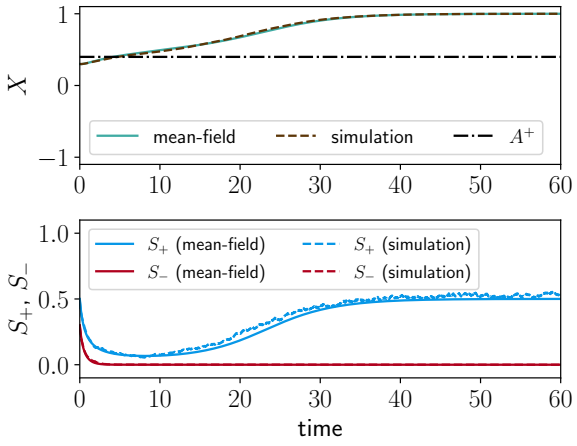

(a) An example of a rebound to the +1 endemic state for a single simulation of the agent-based model and single numerical solution to the mean-field equations (4.15)-(4.17) with parameters $r_0 = 0.66$, $K = 0.4$, and $\tau = 0.07$ on a 7-regular network. The dot-dashed black line indicates the threshold A^+ from Eq. (4.25).

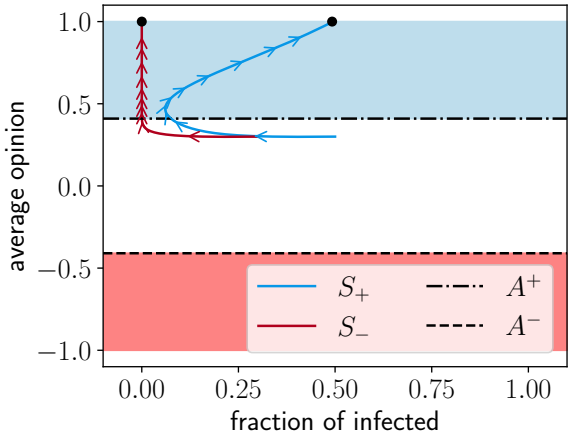

(b) A phase space diagram showing an example of a rebound to the +1 endemic state from a single numerical solution to the mean-field equations (4.15)-(4.17) for $r_0 = 0.66$, $K = 0.4$, and $\tau = 0.07$ on a 7-regular network. The blue and red lines with arrows indicate (S_+, X) and (S_-, X) trajectories, respectively. The black dots indicate the equilibria of the +1 and −1 contagions and the dot-dashed and dashed black lines indicate the thresholds A^+ and A^- from Eqs. (4.25) and (4.26) respectively.

Figure 4.4

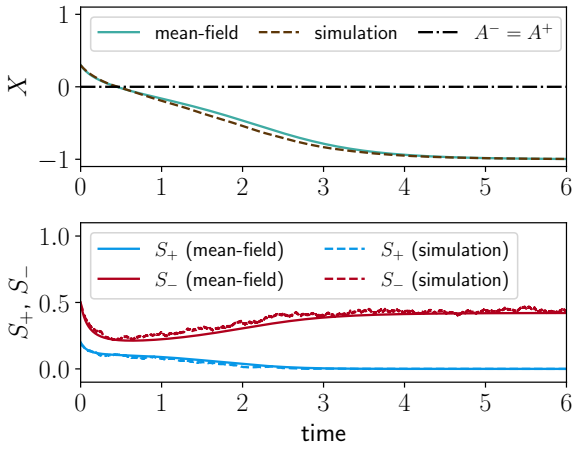

(a) An example bias overturning for a single simulation of the agent-based model and a single numerical solution to the mean-field equations Eqs. (4.15)-(4.17) with parameters $r_0 = 1.44$, $K = 3.20$, and $\tau = 0.017$ on a 10-regular network. The dot-dashed black line indicates the threshold $A^+ = A^-$ from Eqs. (4.25) and (4.26).

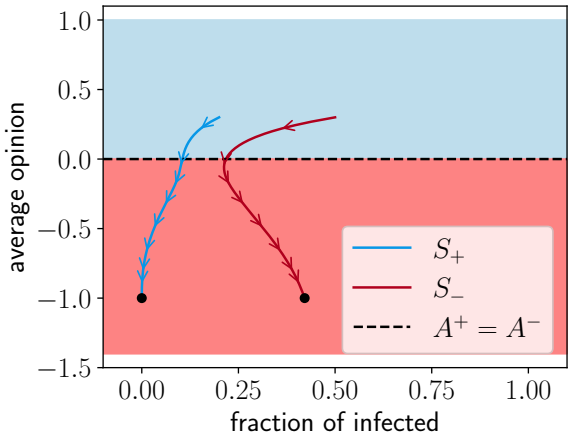

(b) A phase space diagram showing an example bias overturning in the mean-field equations Eqs. (4.15)-(4.17) with parameters $r_0 = 1.44$, $K = 3.20$, and $\tau = 0.017$ on a 10-regular network. The blue and red lines with arrows indicate (S_+, X) and (S_-, X) trajectories, respectively. The black dots indicate the equilibria of the $+1$ and -1 contagions and the dashed black line indicates the threshold $A^+ = A^-$ from Eqs. (4.25) and (4.26).

Figure 4.5

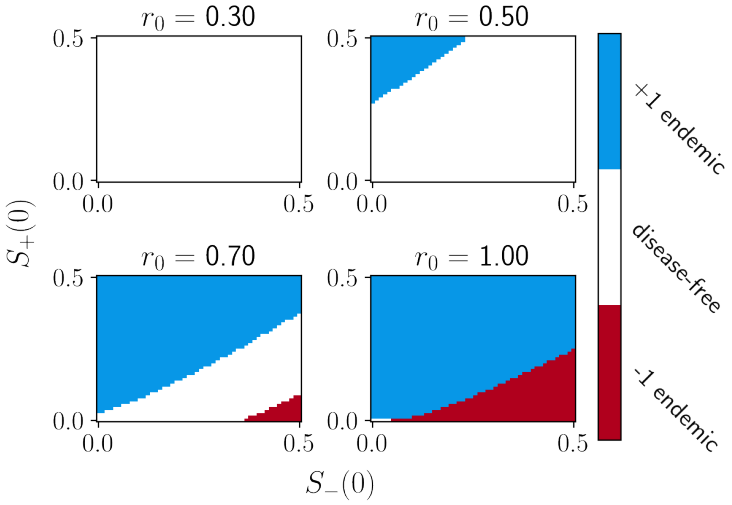

Figure 4.6: Long-term behavior of the mean-field equations (4.15)-(4.17) after 3000 time steps as a function of the initial fraction of infected individuals in states $S_+(0)$ and $S_-(0)$ for $r_0 \in \{0.30, 0.50, 0.70, 1.0\}$, $K = 0.25$, $\tau = 0.1$, $X(0) = 0.1$, and a time step of size $h = 0.25$.

between the $+1$ and -1 endemic cases (lower right panel). Again, since X always changes towards the dominant contagion, if the system is near the transition boundaries (4.25) and (4.26) then a sufficiently large initial portion of the population infected with the opposite contagion can result in the initial bias of the population being overturned. Fig. 4.6 corresponds to an initial mean opinion $X(0) = 0.1$. When a different value of $X(0)$ is used, the basins of attraction for each steady-state grow/shrink in accordance. For example, using a more positive value makes the basins of attraction for the $+1$ endemic state larger, while the basins of attraction for the -1 endemic state and disease-free state become smaller. Additionally, we note that, for the parameters that we have studied, the bias overturning behavior only occurs when the initial bias is small.

When the disease-free region is quite large and bias overturning is impossible (e.g., Fig. 4.6 top right) having a sufficiently large initial population in the state opposite the initial average opinion can still push the system from either the $+1$ or -1 endemic states into the disease-free state. This behavior may have potential consequences for the spread of disinformation, as it suggests that artificially boosting the initial number of spreaders through, for example, social-bot networks may be sufficient to overcome an initial bias towards a belief and potentially sway public opinion.

However, we have also observed that the average initial opinion has a strong effect on the possibility of bias overturning. This suggests that a suitably large initial bias, perhaps through prebunking efforts (the practice of proactively exposing and debunking misinformation before it spreads, see [271]) may provide good protection against bias overturning in the unforced system. We will be considering the effects of external forcing in Sec. 4.7. It should also be noted that this has implications both for protection against misinformation as well as the creation of misinformation, since it shows that if the system becomes initially biased towards a piece of false information, it may be quite difficult to overturn the bias in favor of the truth.

4.6 Heterogeneous initial opinions

Until this point we have made the assumption that all agents begin with the same initial opinion. This assumption is highly unrealistic for any real-world system. In this section we investigate the effects of heterogeneous initial opinions on the behavior of our model and on the accuracy of our mean-field approximation. We consider two cases for the distribution of heterogeneous initial opinions. In the first case, we consider opinions sampled from a normal distribution with mean μ and standard deviation σ truncated to the interval $[-1, 1]$, i.e., values that fall outside of this interval are redrawn from the same distribution until all values are within the given interval. In the second case, we consider an evenly weighted bimodal Dirac delta distribution with mean μ and a distance Δ between the two modes, i.e., a distribution given by $P(X) = [\delta(X-\mu+\Delta/2)+\delta(X-\mu-\Delta/2)]/2$.

Fig. 4.7a shows the results obtained from numerical simulation of the agent-based model for a 30-regular network with $N = 1000$ nodes with $r_0 = 0.67$ for the truncated normal distribution with $\sigma \in \{0.05, 0.1, 0.3, 0.5\}$. For each pair (μ, ϵ) the same procedure is used as in Fig. 4.3b with the same selection of $(S_+(0), S_-(0))$. The panels of Fig. 4.7a should be compared to the top-right panel of Fig. 4.3b ($r_0 = 0.67$). We observe that the general shape of the basins of attraction for the three possible steady-state behaviors is qualitatively similar for smaller values of σ. As σ increases, the similarity decreases; in particular, the basins of attraction of the endemic states become smaller. This shows that while our mean-field results are reasonably accurate with

the inclusion of heterogeneous initial opinions, as the amount of heterogeneity is increased, this accuracy can be lost. Furthermore, we notice that increasing σ causes the basins of attraction of the $+1$ and -1 endemic cases to become smaller, which means that the disease-free state can be stable for smaller values of ϵ. This indicates that when the initial distribution of opinions is more heterogeneous the disease-free state can remain stable even when the infection and healing rates are more strongly affected by an individual's opinion, suggesting that the role of confirmation bias and the illusory truth effect in the spread of information is smaller when the initial opinions are highly heterogeneous.

Fig. 4.7b (middle and bottom) again shows numerical results of our agent-based model for a 30-regular network with $N = 1000$ nodes and $r_0 = 0.67$ for the bimodal Dirac delta distribution for $\mu = 0$ (middle) and $\mu = 0.5$ (bottom) with the same procedure as Figs. 4.3b and 4.7a for each ordered pair (Δ, ϵ). Fig. 4.7b (top) shows an example of the bimodal Dirac delta distribution with mean μ and distance Δ between modes. In Fig. 4.7b (middle) we see that when the average opinion is zero, $\mu = 0$, increasing the distance between the two modes causes a shift from the disease-free state being stable when $\Delta = 0$ to a bistable region between the $+1$ and -1 endemic states when $\Delta > 0$, for sufficiently small values of ϵ. When the distribution is significantly biased to one side, $\mu = 0.5$, (Fig. 4.7b bottom) the difference between the two modes seems to have no effect. However, there is a transition between the $+1$ endemic and the disease-free state as ϵ is increased, mirroring what was found in the case of homogeneous opinions (cf. Fig. 4.3a).

The results of this section show that our model can result in rich behavior that is not captured by our mean field approximation when the initial distribution of opinions is highly heterogeneous. However, we leave an analysis of this case for future research.

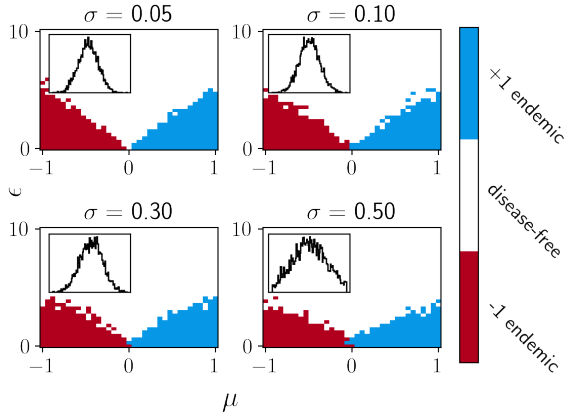

(a) The long-term behavior of the agent-based model for $r_0 = 0.67$ and $\sigma \in \{0.05, 0.10, 0.30, 0.50\}$ as a function of μ and ϵ. The color of each point represents which contagion was successful more frequently out of 9 independent trails of the agent-based simulation on a 30-regular network of $N = 1000$ nodes. Each simulation ran for 3000 time steps with initial fraction of infected nodes given as $(S_+(0), S_-(0)) \in \{(0.05i/2,\ 0.05j/2) | \, i \in \{0, 1, 2\},\ j \in \{0, 1, 2\}\}$. Insert shows a sample truncated Gaussian with mean μ for each value of σ.

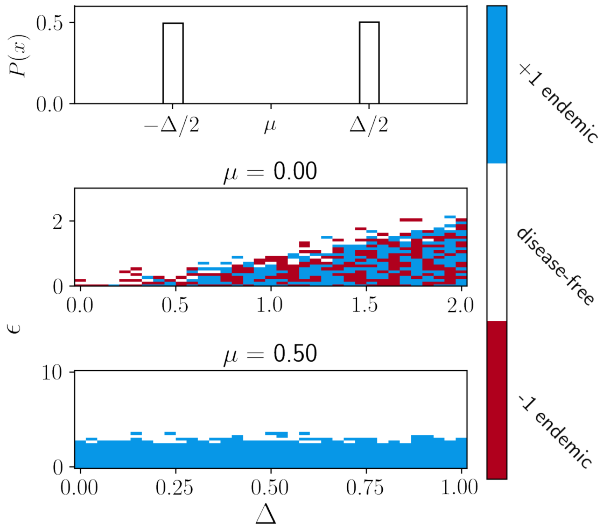

(b) (top) An example of the Dirac delta bimodal distribution with mean μ and distance Δ between modes. (middle) the long-term behavior of the agent-based model for $r_0 = 0.67$ with mean $\mu = 0$ as a function of Δ. (bottom) the long-term behavior of the agent-based model for $r_0 = 0.67$ with mean $\mu = 0.5$ as a function of Δ. The color of each point represents which contagion was successful more frequently out of the 9 independent trails of the agent-based simulation on a 30-regular network of $N = 1000$ nodes. Each simulation ran for 3000 time steps with initial fraction of infected nodes given as $(S_+(0), S_-(0)) \in \{(0.05i/2,\ 0.05j/2) | \, i \in \{0, 1, 2\},\ j \in \{0, 1, 2\}\}$.

Figure 4.7

4.7 External recruitment of spreaders

Now we modify our model to allow for the external recruitment of spreaders. This could model a situation where disinformation is spread by the coordinated actions of malicious external agents. To model this we introduce an additional forcing term to our system which allows for external recruitment of contagion spreaders. Working in the framework of Eqs. (4.15)-(4.17), we modify them as

$$\begin{aligned}
\frac{dS_+}{d\tau} &= -S_+\left[1 - X + \epsilon\right] \\
&+ r_0(1 - S_+ - S_-)S_+\left[1 + X + \epsilon\right] \\
&+ (1 - S_+ - S_-)f_+(t)\,, \qquad (4.27) \\
\frac{dS_-}{d\tau} &= -S_-\left[1 + X + \epsilon\right] \\
&+ r_0(1 - S_+ - S_-)S_-\left[1 - X + \epsilon\right] \\
&+ (1 - S_+ - S_-)f_-(t)\,, \qquad (4.28) \\
\frac{dX}{d\tau} &= K\left[(S_+ - S_-) - (S_+ + S_-)X\right]\,, \qquad (4.29)
\end{aligned}$$

where $f_+(t)$ and $f_-(t)$ represent normalized rates of recruitment of spreaders for the $+1$ and -1 contagions, respectively. Since we are interested in how the spread of disinformation may affect the spread of the "true" information, from this point on we will consider the $+1$ contagion as "true" and the -1 contagion as "false", recognizing that sometimes it is not possible to make such a clear distinction. In addition, for simplicity we will assume that only the "false" contagion will have external recruitment of spreaders, meaning we will consider only the case where $f_+(t) = 0$. For $f_-(t)$ we will consider only the case of constant forcing $f_-(t) = B$, which could represent a constant recruitment of "false" information spreaders due to, for example, an unchanging social-bot network. With the addition of external forcing of the -1 contagion, disease-free behavior is no longer an equilibrium state of the system. Instead, with a constant forcing $f_-(t) = B$ there are now two

steady-state equilibria. The first is of the form $(X, S_+, S_-) = (-1, 0, S_-^*)$ where

$$\begin{aligned} S_-^* &= \frac{-[B+\epsilon-r_0(2+\epsilon)]}{2r_0(2+\epsilon)} \\ &+ \frac{\sqrt{[B+\epsilon-r_0(2+\epsilon)]^2+4r_0(2+\epsilon)B}}{2r_0(2+\epsilon)}\,, \end{aligned} \tag{4.30}$$

which corresponds to the "false" information becoming dominant in the system. The second is of the form $(X, S_+, S_-) = (X^*, S_2^*(X^*), S_1^*(X^*))$ where X^*, S_2^*, and S_1^* are solutions to the non-linear algebraic equations

$$S_1^*(X^*) = \frac{B}{(1+X^*+\epsilon)\left(R_{\rm e}^+(X^*)-R_{\rm e}^-(X^*)\right)}\,, \tag{4.31}$$

$$S_2^*(X^*) = 1-\frac{1}{R_{\rm e}^+(X^*)}-S_1^*(X^*)\,, \tag{4.32}$$

$$X^* = 1-\left[\frac{2R_{\rm e}^+(X^*)}{R_{\rm e}^+(X^*)-1}\right]S_1^*(X^*)\,. \tag{4.33}$$

This second equilibrium corresponds to the $+1$ contagion becoming dominant in the system while the -1 contagion remains sustained by a small fraction of the population, due to the constant external recruitment. We have found numerically that both of these solutions are stable.

Now we discuss how the forcing of the -1 contagion modifies the bias overturning behavior studied in Sec. 4.5. In the absence of forcing, the bias overturning behavior is facilitated by a more infectious contagion: note how, in Fig. 4.6, the red region (corresponding to the initial positive opinion being overturned) increases in size as r_0 increases. In contrast, a more infectious contagion suppresses bias overturning in the presence of constant external forcing. To illustrate this, Fig. 4.8 shows the average opinion after a long period of time ($t_f = 3000$) against the forcing term $f_-(t) = B \in [0,1]$ and $X(0) \in [0,1]$ for $r_0 = 0.3, 0.9$ and $S_+(0) = 0.1, 0.5$ with $S_-(0) = 0$, obtained using the mean-field equations. Since $X(0) > 0$ the system is initially biased towards the true contagion. In Fig. 4.8 we see that as r_0 increases the red region which, again, corresponds to the overturning behavior, becomes smaller. Therefore, in this case, we see that for larger r_0 it is more difficult to overturn the initial bias. Similarly, as $S_+(0)$ increases a larger value of forcing is required to overturn the initial bias.

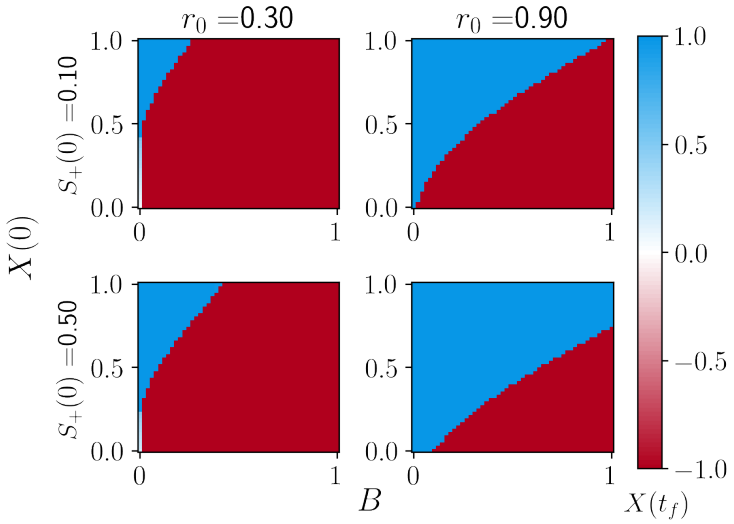

Figure 4.8: Average opinion of the population as a function of $X(0)$ and the constant forcing $f_-(t) = B$ after $t_f = 3000$ time steps with parameters $\tau = 0.1$, $K = 0.25$, $\epsilon = 0.01$, $r_0 \in \{0.3, 0.9\}$, $S_+(0) \in \{0.1, 0.5\}$, and a time step $h = 0.25$.

Although modeling an underlying social-bot network via external forcing terms is a limited approach, we observe within our model that information that spreads with lower values of r_0 is more susceptible to disinformation, as measured by the size of the basis of attraction of the -1 endemic state.

4.8 Discussion

We introduced a hybrid model of a pair of competing beliefs (interpreted as social contagions) coupled with an internal opinion describing the alignment of the individual's biases towards the two beliefs. Modeling cognitive biases, the internal opinion gets modified by infection attempts (modeling the illusory-truth effect) and modifies the infection probabilities (modeling confirmation bias). We found that this model results in an opinion-dependent stability of the disease-free state (i.e., when the two beliefs are not being spread). In addition, we found that the incorporation of cognitive biases in the contagion process can lead to transient dynamical behaviors that are absent in simpler models of social contagions. These behaviors include the rebound, where one of the competing beliefs is revitalized after an initial decay, and the bias overturning, where the initial opinion

of the population switches from one belief to the other. We found that bias overturning is promoted by stronger beliefs, as measured by the effective reproduction number r_0 in Eq. (4.18); however, overturning an initial bias towards one belief when there is external recruitment of spreaders for the opposing belief is more difficult when the effective reproduction number is larger. While examining the role of heterogeneity in initial opinions we found that when the distribution of initial opinions is Gaussian the role of confirmation bias and the illusory truth effect decreases as the variance of the Gaussian increases. Furthermore, we observed that equally weighted bimodal distributions of initial opinions can result in bistability of the ± 1 endemic behavior.

Despite the simplicity of our model, there are a number of results that can be related to the real-world spread of competing beliefs. First, we observe that the initial biasing of the system is highly important in the long-term behavior, both relating to the initial opinions of agents and the initial fraction spreading each belief. This suggests preemptive efforts to combat misinformation through prebunking-type approaches are important in reducing the spread of false information. It also suggests that ignoring the early spread of false information may result in a system that is highly prone to belief in it and may be very resistant to recovery. Second, the formation of the rebound behavior may suggest that the effects of confirmation bias and the illusory-truth effect allow the creation of a type of "reservoir" to the social contagion, similar to the existence of reservoirs in infectious contagions such as avian influenza and bovine tuberculosis [272], allowing the rebound of the belief into a population that initially rejected it. However, confirming such a feature in our model will require further study; particularly, closely examining the role of network and community structures as well as the spatial distribution of opinions within these structures. It should also be noted that the existence of such a rebound behavior and the relevant time scale is difficult to determine as it requires high-quality time-dependent data on the spreading of beliefs in a social network. At this time we have been unable to find sufficient data to confirm or refute this feature of our model in real-world systems and would be an interesting and highly interdisciplinary extension of our study.

Our model is an idealized description of how two competing beliefs may spread in a regular

network where individuals have cognitive biases such as confirmation bias and the illusory truth effect. There are many ways in which the model could be made more realistic. For example, our model doesn't account for potential interactions among more than two contagions, non-binary beliefs, realistic social network structure, fact-checking, or more detailed cognitive bias models. However, even within our highly simplified model there remain many potentially interesting questions. For example, in all analytical results, we assumed that identical initial opinions were assigned to all agents within the agent-based model. An extension of our analysis to the case of initial heterogeneous opinions is left for future work. Other examples include using more heterogeneous networks or real-world social networks instead of a k-regular network.

Chapter 5

The Social Compass Model with Communities and External Sources

5.1 Introduction

Within a society, the ability to reach a state of consensus is paramount to societal function and is an important component in establishing many of the ideas that are foundational to our everyday lives, including the value of money, the meaning of language, and our notions of fairness and equality [56, 57, 58]. However, most social systems rarely exist in a true state of consensus, easily observed in the variety of cultural practices, beliefs, and norms that vary with country, religion, and political ideology, among many other possible divisions [273]. Instead, many social systems exist in a state of local consensus such that there are groups of individuals that share the same or a similar opinion. Such a state is sometimes referred to as fragmentation in models of opinion dynamics [71]. In some cases, these fragmented states can become more extreme resulting in two (or sometimes more) groups with opposite and extreme opinions, a state known as opinion polarization. However, it should be noted that this definition is used to place this work in alignment with the terminology used in [1] and that polarization can refer to a large number of related concepts. For an in-depth discussion on definitions and types of polarization see Ref. [274]. Opinion polarization is a social phenomenon that has been observed across a wide range of topics including religious and political ideologies [275, 59], race [276], and climate change [277]. Although some opinion models suggest that a certain amount of polarization may promote consensus [278], typically the existence of opinion polarization in a population is associated with negative societal outcomes such as reduced democratic stability [59], increased political division [279], slower resolution of

societal challenges [280], and may promote the spread of conspiracy theories and misinformation [281]. Additionally, the formation of opinion polarization is often associated with homophily (i.e., the tendency for individuals to form connections with similar individuals) [282, 283], tribalism (a tendency for individuals to form an "us versus them" mentality), and increased social tensions [59]. There has been some work that has shown that a tendency toward homophily can result in the formation of communities in an adaptive bounded-confidence model of opinion dynamics [113]. Furthermore, a major 2021 study by Cinelli et al. found that homophilic communities in online social media tend to dominate online interactions and act as echo-chambers (i.e., groups of like-minded individuals reinforcing a shared narrative) [284]. These echo chambers may play an important role in the formation of opinion polarization [285]. These results suggest that the role of communities, specifically those that exhibit homophily, is an important component in the formation of an opinion-polarized system. In addition to communities, the formation of extreme opinions, and possible opinion polarization, may be influenced by external actors that publicly broadcast their opinions; we will refer to such entities as opinion leaders (e.g., politicians, news and entertainment, celebrities, and online personalities) [286, 287, 288, 289]. One study found evidence that an opinion-polarized social network, with the presence of opinion leaders, tended to also have homophilic communities [287]. While this finding doesn't imply that these communities have formed as a consequence of the opinion leaders, it demonstrates that opinion leaders and homophilic communities can coexist. Thus, it is worthwhile to study the interactions between community structure and external sources of opinions.

Unsurprisingly, there is a great interest in studying the mechanisms that underlie the formation of an opinion-polarized system and how polarization can be reduced. Many of the current models for studying the formation of polarization focus on the formation of a polarized state in regards to a single topic [1, 290, 291]. However, it is common for individuals to carry correlated opinions on different topics (known as opinion alignment), allowing polarization to occur along an axis defined by two topics [1, 292, 293, 294]. Ojer et al. noted that many models that have multi-dimensional opinion spaces have failed to reproduce opinion polarization and often neglect

opinion alignment [1]. However, there are a small number of studies that do include or produce opinion alignment. The particular example that we discuss here is Schweighofer et al.'s highly comprehensive model of opinion dynamics, which is based on cognitive dissonance and structural balance theories from psychology. In particular, Schweighofer et al. propose an agent-based model that exhibits opinion alignment and polarization as emergent phenomena in a multi-dimensional opinion space [295]. However, as this is a rather complex agent-based model, Schweighofer et al. developed no major analytical results.

The lack of analytically tractable models of polarization that include or produce opinion alignment led Ojer et al. to propose the *social compass model*, which is a model of opinion consensus and polarization where individuals hold opinions on two different, but possibly interdependent topics [1]. In the social compass model, the opinion space is represented in the polar plane, where the opinion orientation of a pair of opinions (x, y) is represented as the angle $\theta = \text{atan2}(y, x)$ and individuals' conviction (i.e., how strongly individuals hold onto their initial stance) is represented as the radius $\rho = \sqrt{x^2 + y^2}$. It is assumed that the opinions x and y are continuous, real-valued opinions measured on the open interval $(-\infty, \infty)$. Furthermore, the social compass model allows one to study how correlation between the two opinions x and y (i.e., opinion alignment) affects the onset of consensus. To illustrate how opinion alignment is modeled, one can consider the following examples. First, suppose that topic X is abortion rights and topic Y is pineapple on pizza, with each topic measured on $[-1, 1]$, for simplicity, with -1 representing against and 1 representing begin in favor. One would not expect to find individuals' stances on these topics to be correlated. Therefore, one would expect 4 extreme opinions: $(-1, -1)$, $(-1, 1)$, $(1, -1)$, and $(1, 1)$. Alternatively, consider an example where topic X is abortion rights and topic Y is now gun control, again measured on $[-1, 1]$ with the same convention. Anecdotally, these topics tend to be correlated, which suggests that, in this case, there are only 2 extreme opinions: $(-1, -1)$ and $(1, 1)$. In each case, if one assumes that the population begins in a polarized state, then the distribution of initial opinion orientations for the first example should be quadrimodal, corresponding to the 4 possible extreme opinions, [see Fig. 5.1(right)] while the distribution of initial opinion orientations in the second

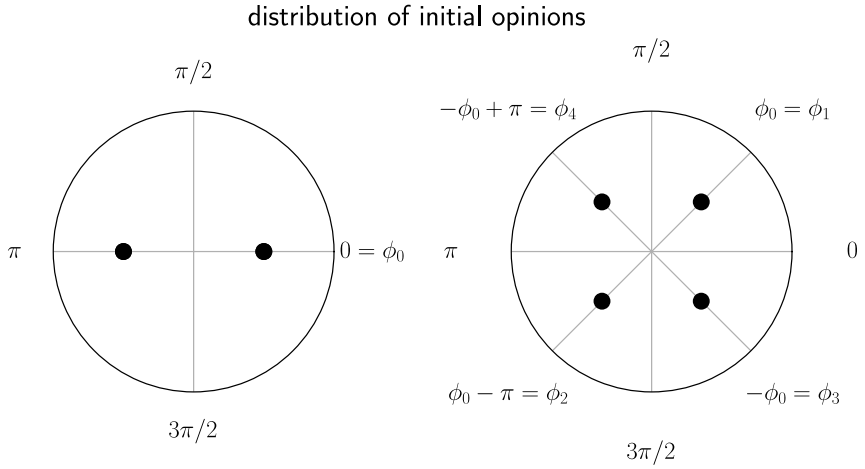

Figure 5.1: A schematic representation of the distribution of initial opinion orientations for correlated initial opinions (left) and uncorrelated initial opinions (right). The black dots mark the location of of initial opinion orientations.

example should be bimodal, as there are only 2 extreme opinions [see Fig. 5.1(left)].

To date, Ojer et al. has shown that the social compass model exhibits a phase transition from a state of initially polarized opinions to one of consensus that is strongly dependent on the initial correlation of opinions. Particularly, they found that when initial opinions were uncorrelated the social compass model exhibited a first-order transition to consensus (i.e., one which is discontinuous), while for correlated initial opinions they observed a continuous transition to consensus [1]. Additionally, in a follow-up study, Ojer et al. showed that when coupling among individuals occurs along a network structure, then the critical coupling strength, marking the transition between polarization and consensus, depends strongly on the network topology. Furthermore, Ojer et al. showed that the threshold for the transition vanishes in networks with highly heterogeneous degree distributions in the limit $N \to \infty$, suggesting that network degree heterogeneity may mitigate polarization [4].

Although the social compass model provides an interesting way of encoding opinion alignment into an analytically tractable model of opinion dynamics, there are a number of assumptions made in [1] that result in several limitations, which we discuss now. First, by defining an individual's conviction ρ as the magnitude of their opinions represented in polar coordinates and treating

conviction as a fixed value they implicitly assume that an individual's opinion on the two topics X and Y are coupled. As a result, when an individual's opinion orientation changes, they necessarily decrease their stance on one topic in favor of the other. While this may be appropriate for some topics, it is not a behavior one would expect to observe in general. Furthermore, the assumption that an individual's conviction is constant also introduces the implicit assumption that individuals with particularly high values of ρ are simply highly affected by their own opinion regardless of their belief. This suggests that an individual who holds an extreme opinion initially and therefore has a strong conviction is difficult to sway from any stance regardless if this is their initial stance or one adopted through further social interaction. However, while it is important to explicitly discuss these assumptions, they allow for a particularly simple model that can be easily studied via analytical approaches.

The social compass model exhibits a structural similarity with the Kuramoto model, due to the form of the term that describes interactions between individuals. The techniques used by Ojer et al., particularly the construction and expansion of a self-consistent equation in the thermodynamic limit (or continuum limit), are similar to the early approaches used to study the Kuramoto model [7]. However, they do not allow for the analytical study of some important generalizations, such as the existence of external forcing or community structure [181] or the study of the time evolution of macroscopic model variables. Within the study of Kuramoto models, these limitations led to the proposal of the Ott-Antonsen ansatz [181, 184, 186, 185], which allows the high-dimensional Kuramoto model to be reduced to a single integro-differential equation or a small system of coupled ordinary differential equations (depending on the underlying distribution of natural frequencies) [181]. Inspired by Ojer et al.'s social compass model, we seek to exploit the similarity between the social compass model and the Kuramoto model and use the Ott-Antonsen ansatz to develop a reduced representation of the dynamics of the social compass model. We find that this method is successful at capturing the global dynamics of the social compass model. Furthermore, we use our alternative approach to generalize Ojer et al.'s results to consider continuous distributions of initial opinions and convictions. Lastly, we extend the social compass model to include external

forces and community structure and apply the Ott-Antonsen ansatz to this generalization as well.

The organization of this chapter is as follows. In Sec. 5.2 we introduce the social compass model proposed in [1] that will be studied in the rest of the chapter. In Sec. 5.3 we apply the Ott-Antonsen ansatz to the social compass model to derive a reduced description of the dynamics, the equilibrium solution, and the resulting self-consistent equation. In Subsections 5.3.1 and 5.3.2, we use our approach to recover one of the self-consistent equations used by Ojer et al. and generalize their results to continuous distributions of initial opinions and convictions, respectively. In Sec. 5.4 we introduce a generalization of the social compass model that includes community structure and external forcing. We also apply the Ott-Antonsen ansatz to our generalization to again find a reduced description of the dynamics. Finally, in Sec. 5.6 we discuss our findings and planned future work.

5.2 The social compass model

The social compass model from Ref. [1] is a consensus model of N interacting agents of the form

$$\dot{\theta}_i = \rho_i \sin(\phi_i - \theta_i) + \frac{K}{N} \sum_{j=1}^{N} \sin(\theta_j - \theta_i), \tag{5.1}$$

for $i = 1, 2, 3, \ldots, N$. Here, ρ_i is the conviction of agent i, which measures how strongly agent i holds their original opinion and is randomly drawn for each agent from a distribution $P(\rho)$. The phase θ_i represents the opinion orientation of node i, as measured by an $\theta_i = \text{atan2}(y_i, x_i)$, where $y_i, x_i \in \mathbb{R}$ are agents i's opinions on topics Y and X, each of which is a continuous opinion defined on the interval $(-\infty, \infty)$. The phase ϕ_i represents the initial opinion orientation of node i and is drawn randomly from a distribution $Q(\phi)$. Lastly, K is the coupling strength between agents. This model assumes that each agent's opinion orientation is pulled towards its initial value, ϕ_i, which can represent a bias, and towards other agents' opinion orientations.

Since consensus in this model is modeled as alignment of the phases θ_j of each agent, we can

measure consensus as the magnitude of the complex-valued order parameter

$$z = re^{i\psi} = \frac{1}{N}\sum_{j=1}^{N} e^{i\theta_j}. \tag{5.2}$$

We refer to the magnitude r of this complex order parameter as the degree of consensus. This order parameter can be understood by representing the opinion orientation of each agent as a complex number with phase θ_j on the complex unit circle (i.e., $e^{i\theta_j}$) and then taking the mean of these complex numbers. When the opinion orientations of the agents are distributed approximately uniformly around the unit circle then r is small. When the agents are near consensus, their phases will be concentrated around a single phase and $r \approx 1$. In terms of the order parameter in Eq. (5.2) and the complex number representation of the initial state of each agent $a_i = \rho_i e^{\phi_i}$, we can express the system of ODEs in Eq. (5.1) as

$$\dot{\theta}_i = \mathrm{Im}\{(a_i + Kz)e^{-i\theta_i}\}. \tag{5.3}$$

It is also convenient to define the constant $H_i = a_i + Kz$, which can be thought of as the combined pull of the agent's own initial opinion (a_i), and the other agents in the system (Kz). Then the behavior of each agent i is described by the system

$$\dot{\theta}_i = \mathrm{Im}\{H_i e^{-i\theta_i}\}, \quad i = 1, 2, \ldots N. \tag{5.4}$$

The form of the social compass model shown in Eq. (5.4) is particularly useful as it will allow us to derive a reduced description of the social compass model and a general self-consistent equation using the Ott-Antonsen ansatz using Eq. (5.4), and then choose particular forms of H to include additional features to the model, such as external sources and community structure without the need to rederive the reduced system for each variation of the model.

The method used in [1] is to solve for the fixed points of Eq. (5.3) and consider the thermodynamic limit ($N \to \infty$) of the order parameter. This results in a self-consistent equation that can be used to study the behavior of the steady states of the system's order parameter and the transition from a polarized (incoherent) state to a consensus (synchronized) state.

However, as for the original Kuramoto model, the method of self-consistent equations is ill-suited for certain types of problems, such as stability analysis or determining the dynamics of the order parameter [181]. In the remainder of this chapter, we will employ the Ott-Antonsen ansatz introduced in [181] to study a generalization of the social compass model. This will allow us to provide an alternative method for recovering the self-consistent equations of [1] while providing a reduced description of the dynamics. We then incorporate the effects of community structure and external forcing into the social compass models.

5.3 Dimensionality reduction of the social compass model

In this section we use the Ott-Antonsen ansatz (see [181]) to derive a set of reduced equations for the generalized form of the social compass model [see Eq. (5.4)] that we will then use to study special cases in the subsequent sections. We begin by following the approach by Ott and Antonsen [181] and summarized in Chapter 2, expressing the system's order parameter in integral form by taking the continuum limit,

$$z = \int_0^\infty \int_0^{2\pi} \int_0^{2\pi} f(t,\theta,\rho,\phi) e^{i\theta} d\theta d\phi d\rho, \tag{5.5}$$

where $f(t,\theta,\phi,\rho)$ is the density of agents with opinion orientation θ, conviction ρ, and initial opinion orientation ϕ at time t. We then require that f satisfies the continuity equation (since agents are assumed to be conserved)

$$\frac{\partial f}{\partial t} + \frac{\partial}{\partial \theta}\left[\mathrm{Im}\{H_i e^{-i\theta_i}\} f\right] = 0, \tag{5.6}$$

and expand the density f in Fourier series in θ. We then make the Ott-Antonsen ansatz, $\alpha_n = \alpha^n$, to get

$$f(t,\theta,\rho,\phi) = \frac{P(\rho)Q(\phi)}{2\pi}\left[1 + \sum_{n=1}^{\infty} \alpha^n(t,\rho,\phi) e^{in\theta} + \text{C.C.}\right]. \tag{5.7}$$

Inserting Eq. (5.7) into the continuity equation [Eq. (5.6)] and collecting like terms results in the same ODE for every n,

$$\dot{\alpha}(t,\rho,\phi) + \frac{H}{2}\alpha^2(t,\rho,\phi) - \frac{\overline{H}}{2} = 0, \tag{5.8}$$

where the bar indicates complex conjugation. Finally, inserting Eq. (5.7) into Eq. (5.5) reduces the order parameter to

$$z = \int_0^\infty \int_0^{2\pi} \overline{\alpha}(t, \rho, \phi) P(\rho) Q(\phi) d\phi d\rho. \tag{5.9}$$

The integro-differential equation described by Eqs. (5.8) and (5.9), together with $H = \rho e^{i\phi} + Kz$, describes the dynamics of the original system in reduced form.

Unlike the Kuramoto model, the social compass model is a model of consensus, and therefore we expect the steady-state behavior to approach a constant value (note that the intrinsic frequency of each oscillator is zero). Setting $\dot{\alpha} = 0$ in Eq. (5.8) we find that there is an equilibrium solution given by

$$\alpha = \frac{\overline{H}}{|\overline{H}|}. \tag{5.10}$$

Inserting this in Eq. (5.9) we find a self-consistent equation for the steady state behavior as

$$z = \int_0^\infty \int_0^{2\pi} P(\rho) Q(\phi) \frac{H}{|H|} d\phi d\rho. \tag{5.11}$$

At this point, we use our results from Eqs. (5.8) and (5.9) to reproduce some of the results in Ref. [1]. In addition, we use the reduced dimensional description to develop further insights into the dynamics of the model. This will be the topic of subsection 5.3.1. We then will consider the case of a continuous distribution of initial opinions $Q(\phi)$ in subsection 5.3.2.

5.3.1 Recovery of the results of Ref. [1]

In this Section we will consider one of the two cases considered in [1]. In particular, we consider the case where

$$P(\rho) = \delta(\rho - \rho_{\max}), \tag{5.12}$$

and

$$Q(\phi) = \frac{1}{4} \left[\delta(\phi - \phi_0) + \delta(\phi - \phi_0 + \pi) + \delta(\phi + \phi_0) + \delta(\phi + \phi_0 - \pi) \right]. \tag{5.13}$$

where $\phi_0 \in [0, \pi/4]$ parameterizes the transition from correlated initial opinions (at $\phi_0 = 0$) to uncorrelated initial opinions (for $\phi_0 > 0$). The distribution $Q(\phi)$ is shown schematically in Fig. 5.1.

There are two goals of this Section. First, we will consider the utility of developing a reduced description of the dynamics and gain further insight into the social compass model. Second, using Eqs. (5.8) and (5.9), we will reproduce the self-consistent equation of Ojer et al., from which all of their results can be recovered.

To begin with our first goal, we will apply our choices of $P(\rho)$ and $Q(\phi)$ to Eqs. (5.8) and (5.9), resulting in a collection of ordinary differential equations for the dynamics of $\alpha(t, \rho, \phi)$, coupled by the global order parameter z. With these choices, Eqs. (5.8) and (5.9) become

$$\dot{\alpha_i} + \frac{a_i + Kz}{2}\alpha_i^2 - \frac{\overline{a_i} + K\overline{z}}{2} = 0, \quad i = 1, 2, 3, 4, \tag{5.14}$$

and

$$z = \frac{1}{4}\sum_{j=1}^{4} \overline{\alpha_j}, \tag{5.15}$$

respectively, where $\alpha_j(t) = \alpha(t, \rho_{\max}, \phi_j)$, $a_j = \rho_{\max} e^{i\phi_j}$, $\phi_1 = \phi_0$, $\phi_2 = \phi_0 - \pi$, $\phi_3 = -\phi_0$, and $\phi_4 = -\phi_0 + \pi$. Next, to better understand Eq. (5.14) we will take $\alpha_j = r_j e^{i\theta_j}$ and split Eq. (5.14) into its real and imaginary parts. This results in

$$\dot{r_j} + i r_j \dot{\theta_j} + \frac{(a_j + Kz)e^{i\theta_j}}{2} r_j^2 + \frac{\overline{(a_j + Kz)e^{i\theta_j}}}{2} = 0, \tag{5.16}$$

or

$$\dot{r_j} = -\frac{1}{2}(r_j^2 - 1)\left[\rho_{\max}\cos(\phi_j + \theta_j) + Kr\cos(\psi + \theta_j)\right], \tag{5.17}$$

$$r_j\dot{\theta_j} = -\frac{1}{2}(r_j^2 + 1)\left[\rho_{\max}\sin(\phi_j + \theta_j) + Kr\sin(\psi + \theta_j)\right], \tag{5.18}$$

$$j = 1, 2, 3, 4,$$

where $z = re^{i\psi}$. From here, note that $\dot{r_j} = 0$ whenever $r_j = 1$, which is observed numerically to be stable. On the invariant surface where $r_j = 1$ for $j = 1, 2, 3, 4$, the dynamics of the phases reduce to

$$\dot{\theta_j} = \rho_{\max}\sin(-\phi_j - \theta_j) + Kr\sin(-\psi - \theta_j), \quad j = 1, 2, 3, 4. \tag{5.19}$$

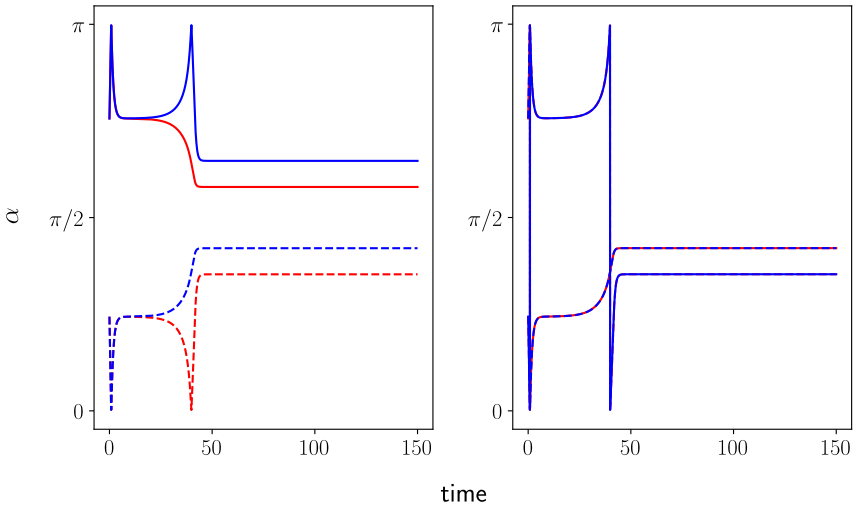

Figure 5.2: The phases θ_j shown in the top half of the unit circle from numerical solutions of Eq. (5.19) (left). The phase θ_j shown in the top half of the unit circle from numerical solutions of Eq. (5.19) after applying the mappings in Eqs. (5.20) and (5.21).

In the following, we will search for stationary solutions on this invariant surface.

Next, we will make use of the symmetry about the imaginary axis in the distribution $Q(\phi)$ to further reduce the system in Eq. (5.19). Note that

$$\theta_2(0) = \phi_2 = \pi - \theta_3(0), \tag{5.20}$$

$$\theta_4(0) = \phi_4 = \pi - \theta_1(0), \tag{5.21}$$

and that therefore, from Eq. (5.15), $\psi(0) = \pm\frac{\pi}{2}$. One can check that $\theta_2 + \theta_3$ and $\theta_1 + \theta_4$ are conserved by Eqs. (5.19) as long as $\psi = \pm\frac{\pi}{2}$, and so we can assume that $\theta_2 + \theta_3 = -\pi$, $\theta_1 + \theta_4 = \pi$, $\psi = \pm\frac{\pi}{2}$ and reduce the dimension of the system. Additionally, Fig. 5.2 shows the effect of applying the transformations $\theta_2 = -\pi - \theta_3$, $\theta_4 = \pi - \theta_1$ to a numerical solution of Eq. (5.19). Making the substitutions $\theta_2 = -\pi - \theta_3$, $\theta_4 = \pi - \theta_1$ in Eq. (5.15), we obtain

$$\begin{aligned} z &= \frac{1}{4}\left[e^{-i\theta_1} + e^{-i(\pi-\theta_3)} + e^{-i\theta_3} + e^{-i(\pi-\theta_1)}\right] \\ &= -\frac{i}{2}\left[\sin(\theta_1) + \sin(\theta_3)\right]. \end{aligned} \tag{5.22}$$

Thus the order parameter exists purely on the imaginary line, meaning that $\psi = \pm\pi/2$, as assumed

above. Enforcing this on Eq. (5.19) we find that

$$\dot{\theta_j} = \rho_{\max} \sin(-\phi_j - \theta_j) \pm Kr\cos(\theta_j), \quad j = 1, 2, 3, 4. \tag{5.23}$$

Lastly, we apply the transformation in Eqs. (5.20) and (5.21) to get

$$\dot{\theta_1} = \rho_{\max} \sin(-\phi_0 - \theta_1) \pm Kr\cos(\theta_1), \tag{5.24}$$

$$\dot{\theta_3} = \rho_{\max} \sin(\phi_0 - \theta_3) \pm Kr\cos(\theta_3), \tag{5.25}$$

with the order parameter z defined by Eq. (5.22). Eqs. (5.24) and (5.25), together with Eq. (5.22), capture the dynamics of the original high-dimensional system.

Next, we want to use this result to recover the key results of Ojer et al. To do this, we solve Eqs. (5.24) and (5.25) for the constant valued solutions θ_1^*, θ_3^*, corresponding to $\dot{\theta_1} = 0$ and $\dot{\theta_3} = 0$. These are

$$\theta_1^* = \arctan\left[-\tan(\phi_0) \pm \frac{Kr}{\rho_{\max}}\sec(\phi)\right], \tag{5.26}$$

$$\theta_3^* = \arctan\left[\tan(\phi_0) \pm \frac{Kr}{\rho_{\max}}\sec(\phi)\right]. \tag{5.27}$$

Then, substituting these into $r = \frac{1}{2}\left[\sin(\theta_1^*) + \sin(\theta_3^*)\right]$ and simplifying, we get

$$\begin{aligned} r = &\frac{-\rho_{\max}\sin(\phi_0) \pm Kr}{2\sqrt{\rho_{\max}^2 + (Kr)^2 - Kr\rho_{\max}\sin(\phi_0)}} \\ &+ \frac{\rho_{\max}\sin(\phi_0) \pm Kr}{2\sqrt{\rho_{\max}^2 + (Kr)^2 + Kr\rho_{\max}\sin(\phi_0)}}. \end{aligned} \tag{5.28}$$

the right-hand side of Eq. (5.28) is identical to equation (31) from the supplement of [1], meaning that additional results, such as the onset of bistability and the critical coupling strength can be recovered using the same techniques from this point on.

5.3.2 Generalized distributions of opinion orientation and conviction

In this section, we use our alternative approach to study the effects of symmetric continuous distributions $Q(\phi)$ and arbitrary continuous distributions $P(\rho)$. In real-world opinion distributions, it is common for there to be some level of deviation in individuals' opinions, as opposed to the

population being split into a discrete number of opinions. By studying continuous distributions of initial opinion orientations, we can maintain the comparison between correlated and uncorrelated initial opinions, as in Ref. [1], which are not simply drawn from a discrete number of choices. Throughout this section we will be considering distributions $Q(\phi)$ such that

$$\int_0^{2\pi} e^{i\phi} Q(\phi) d\phi = 0, \tag{5.29}$$

and that $Q(\phi)$ is symmetric about the imaginary axis. These conditions can be understood as generalizations of the symmetries that were exploited in the previous section. We begin by showing that $\alpha^* = \overline{H}/|\overline{H}|$ is still an equilibrium solution to our system when $z = 0$

$$\begin{aligned}
z &= \int_0^{\infty} \int_0^{2\pi} \overline{\alpha^*} Q(\phi) P(\rho) d\phi d\rho \\
0 &= \int_0^{\infty} P(\rho) \int_0^{2\pi} \frac{H}{|H|} Q(\phi) d\phi d\rho \\
&= \int_0^{\infty} P(\rho) \int_0^{2\pi} \frac{\rho e^{i\phi} + Kz}{|\rho e^{i\phi} + Kz|} Q(\phi) d\phi d\rho \\
&= \int_0^{\infty} P(\rho) \int_0^{2\pi} \frac{\rho e^{i\phi}}{|\rho e^{i\phi}|} Q(\phi) d\phi d\rho, \quad \text{since } z = 0, \\
&= \int_0^{\infty} P(\rho) d\rho \int_0^{2\pi} e^{i\phi} Q(\phi) d\phi \\
&= 0.
\end{aligned}$$

Where the last line of this equality comes from our assumption about the symmetry of $Q(\phi)$. Therefore $\alpha^* = \overline{H}/|\overline{H}|$ is an equilibrium solution to Eq. (5.14) when $z = 0$. Now we study the linear stability of this solution by studying the evolution of small perturbations

$$\delta\alpha = \alpha - \alpha^*, \tag{5.30}$$

and [see Eq. (5.9)]

$$\delta z = \int_0^{\infty} P(\rho) \int_0^{2\pi} Q(\phi) \overline{\delta\alpha}\, d\phi d\rho. \tag{5.31}$$

Linearizing Eq. (5.14) we get

$$\frac{\delta\dot{\alpha}}{\rho} + \delta\alpha + \frac{K}{2}\left[\frac{(\alpha^*)^2}{\rho}\delta z - \frac{1}{\rho}\overline{\delta z}\right] = 0. \tag{5.32}$$

We are interested in the critical coupling strength, marked by the transition from decreasing to increasing $\delta\alpha$. Taking $\delta\dot{\alpha} = 0$ we get

$$\delta\alpha + \frac{K_c}{2}\left[\frac{(\alpha^*)^2}{\rho}\delta z - \frac{1}{\rho}\overline{\delta z}\right] = 0. \tag{5.33}$$

Next, we multiply Eq. (5.33) by $P(\rho)Q(\phi)$ and integrate on $[0, 2\pi] \times [0, \infty)$, obtaining

$$\overline{\delta z} + \frac{K_c}{2}\left(E_\phi\left[e^{2i\phi}\right] E_\rho\left[1/\rho\right] \delta z - E_\rho\left[1/\rho\right] \overline{\delta z}\right) = 0, \tag{5.34}$$

where

$$E_\phi[e^{2i\phi}] = \int_0^{2\pi} e^{2i\phi} Q(\phi) d\phi, \tag{5.35}$$

and

$$E_\rho[1/\rho] = \int_0^{\infty} \frac{P(\rho)}{\rho} d\rho. \tag{5.36}$$

Next, due to the symmetry in $Q(\phi)$, δz is purely imaginary and Eq. (5.34) reduces to

$$-1 + \frac{K_c}{2}\left(E_\phi\left[e^{2i\phi}\right] E_\rho\left[1/\rho\right] + E_\rho\left[1/\rho\right]\right) = 0. \tag{5.37}$$

Solving for K_c we get

$$K_c = \frac{2\left(E_\rho[1/\rho]\right)^{-1}}{1 + E_\phi[e^{2i\phi}]}, \tag{5.38}$$

as the critical coupling strength.

Next, we test 2 example distributions for ϕ and 3 example distributions for ρ to make comparisons with simulations of the agent-based model of Eq. (5.1) with $N = 2000$ agents. For the distributions of individuals' convictions, we consider a Dirac delta distribution [see Eq. (5.12)], an inverse power-law distribution with the limiting form $P(\rho) \sim \rho^{-\gamma}$ above a minimum possible conviction $\rho_{\min}$, and a truncated power-law distribution with the limiting form $P(\rho) \sim \rho^{\gamma}$ below a maximum possible conviction $\rho_{\max}$. We use the power-law exponent $\gamma = 3$ in both of the latter cases. Note that we select the minimum conviction $\rho_{\min}$, the maximum conviction $\rho_{\max}$, and the

constant conviction of Eq. (5.12) to ensure the same mean value of the distributions. For the distributions of initial opinion orientations $Q(\phi)$, we consider the quadrimodal case as in Eq. (5.13) with $\phi_0 = \pi/6$ and a bimodal Cauchy distribution wrapped onto the unit circle with a probability density function of the form

$$Q(\phi) = \frac{1-c^2}{4\pi}\left(\frac{1}{1+c^2-2c\cos(\phi-\mu_1)} + \frac{1}{1+c^2-2c\cos(\phi-\mu_2)}\right), \tag{5.39}$$

where $c = 1/1.5$ is the shape parameter and $\mu_1 = 0$ and $\mu_2 = \pi$ are the centers of the two modes. For the examples with the Dirac quadrimodal distribution of initial opinion orientations, we use a mean value of the conviction $\langle\rho\rangle = 1$, while for the bimodal Cauchy distribution we use $\langle\rho\rangle = 3$. Fig. 5.3 shows the degree of consensus r plotted against the coupling strength K with a vertical line marking the critical coupling strength K_c [see Eq. (5.38)]. The degree of consensus r is calculated using Eq. (5.2) from the results of a single numerical solution of the social compass mode [see Eq. (5.1)] for each value of K using $N = 2000$ agents. Numerical solutions are produced using Euler's method with a step size $h = 0.05$ for the time interval $[0, 50]$. Initial conditions for $K = 0$ are drawn for each agent randomly from the distribution $Q(\phi)$ and the initial conditions for subsequent values of K are selected as the end conditions at $t = 50$ from the previous value of K. The predictions of the critical coupling strength calculated from Eq. (5.38) are marked by black vertical lines. We observe good agreement between the predicted critical coupling strength and the numerical simulations of the agent-based model [Eq. (5.1)] for all three cases. However, it should be noted that the process described above only provides a prediction of the critical coupling strength when the polarized state becomes unstable and cannot be used to predict the onset of bistability and the resulting discontinuous transitions to consensus.

5.4 Community structure and external forcing

In the previous sections we demonstrated an alternative approach for studying the social compass model based on an application of the Ott-Antonsen ansatz. From this approach we have derived a collection of reduced equations describing the dynamics of the original agent-based model,

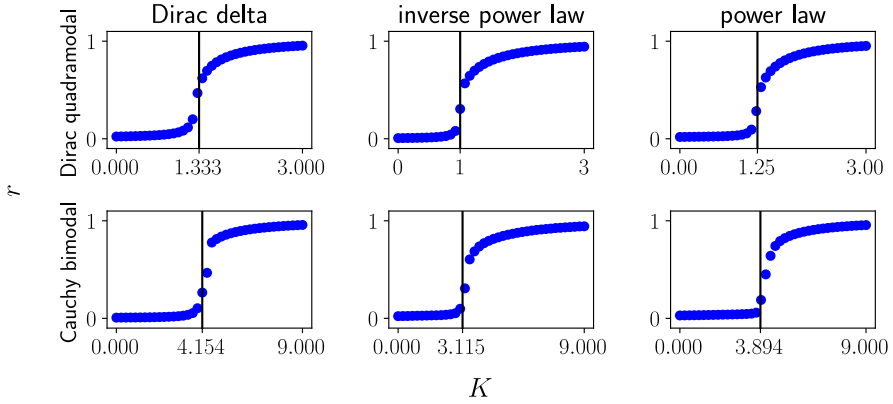

Figure 5.3: Forward continuation of the degree of consensus r plotted against the coupling strength K for an initial distribution of opinion orientations $Q(\phi)$ that are quadrimodal Dirac delta distributions [as in Eq. (5.13) with $\phi_0 = \pi/6$] (top row) and Cauchy bimodal distributions [Eq. (5.39)] (bottom row). distributions of individuals' conviction $P(\rho)$ are Dirac delta distributions [Eq. (5.12)] (first column), inverse power-law distribution [i.e., $P(\rho) \sim \rho^{-\gamma}$], and power-law distribution [i.e., $P(\rho) \sim \rho^{\gamma}$] (third column).

rederived Ojer et al.'s self-consistent equation, and derived an alternative expression of the critical coupling strength for distributions of ϕ with the symmetry property in Eq. (5.29). Now, we want to extend the social compass model to include the effects of community structure and external forcing.

Community structure often plays an important role in social interactions as it is often a network structure that partially (or fully) isolates individuals from different groups. Community structure is usually defined in terms of the number of connections between individuals within a community relative to the number of connections out of the community [296]. Here we will consider a somewhat similar approach where the network is all-to-all, but intracommunity coupling is stronger than intercommunity coupling. Furthermore, there are a number of different social interactions that can be well modeled as external sources, such as, different news sources may broadcast information that changes on a substantially slower time scale than the opinions of individuals, spreaders of disinformation may spread claims that mostly don't change, and some influential individuals may post content that is biased towards their opinions. All of these cases can be thought of as an external source that holds a single opinion state broadcast into the system with a specific strength or intensity.

Inspired by these ideas we consider a generalization of the social compass model where there are two communities, 1 and 2, of sizes $N/2$. The model is described by the following equation:

$$\begin{aligned}\frac{d\theta_i^\sigma}{dt} &= \rho_i^\sigma \sin(\phi_i^\sigma - \theta_i^\sigma) + \frac{K^{\sigma\sigma}}{N}\sum_{j=1}^{N/2}\sin(\theta_j^\sigma - \theta_i^\sigma) \\ &+ \frac{K^{\sigma\sigma'}}{N}\sum_{j=1}^{N/2}\sin(\theta_j^{\sigma'} - \theta_i^\sigma) \\ &+ \sum_{m=1}^{M} F_m \sin(\beta_m - \theta_i^\sigma), \quad \sigma \neq \sigma'. \end{aligned} \tag{5.40}$$

In Eq. (5.40), θ_i^σ and ρ_i^σ are the opinion orientation and conviction, respectively, of node i in community σ. $K^{\sigma\sigma}$ is the intracommunity coupling, $K^{\sigma\sigma'}$ is the intercommunity coupling, M is the number of external sources, β_m is the opinion orientation of source m, and F_m is the intensity with which source m broadcasts its opinion.

As in the previous case, without forcing and community structure [See Eq. (5.1)], we can define an order parameter to measure the amount of consensus in each community. We define

$$z_\sigma = \frac{2}{N}\sum_{j=1}^{N/2} e^{i\theta_j^\sigma}, \tag{5.41}$$

as the local order parameter for community σ. Then the global order parameter is given by

$$z = \frac{1}{2}\left(z_\sigma + z_{\sigma'}\right). \tag{5.42}$$

With the definition of the local order parameter in Eq. (5.41), we can express the generalized social compass model in Eq. (5.40) as

$$\frac{d\theta_j^\sigma}{dt} = \mathrm{Im}\left\{H_\sigma e^{-i\theta_j^\sigma}\right\}, \tag{5.43}$$

where

$$H_\sigma = \rho_j^\sigma e^{i\phi_j^\sigma} + \frac{1}{2}K^{\sigma\sigma} z_\sigma + \frac{1}{2}K^{\sigma\sigma'} z_{\sigma'} + \sum_{m=1}^{M} F_m e^{i\beta_m}, \quad \sigma \neq \sigma'. \tag{5.44}$$

Now, applying the Ott-Antonsen ansatz, as in Sec. 5.3, we arrive at the reduced description of the system dynamics given by

$$\frac{d\alpha_\sigma}{dt} = \frac{1}{2}\overline{H_\sigma} - \frac{1}{2}H_\sigma \alpha_\sigma^2, \tag{5.45}$$

for each community σ and

$$z_\sigma = \int_0^\infty \int_0^{2\pi} \overline{\alpha_\sigma}(t,\rho,\phi) P_\sigma(\rho) Q_\sigma(\phi) d\phi d\rho, \tag{5.46}$$

where $P_\sigma(\rho)$ is the distribution of convictions and $Q_\sigma(\phi)$ is the distribution of initial opinion orientations of individuals in community σ, respectively. Lastly, we can write down a self-consistent equation for the equilibrium solutions of the generalized social compass model. The equilibrium solution to Eq. (5.45) is

$$\alpha_\sigma = \frac{\overline{H_\sigma}}{|\overline{H_\sigma}|}. \tag{5.47}$$

Substituting the equilibrium solution into Eq. (5.46) we get

$$z_\sigma = \int_0^\infty \int_0^{2\pi} \frac{H_\sigma}{|H_\sigma|}(t,\rho,\phi) P_\sigma(\rho) Q_\sigma(\phi) d\phi d\rho. \tag{5.48}$$

Finally, using Eq. (5.42) we have

$$z = \frac{1}{2} \int_0^\infty \int_0^{2\pi} \left[\frac{H_\sigma}{|H_\sigma|}(t,\rho,\phi) P_\sigma(\rho) Q_\sigma(\phi) + \frac{H_{\sigma'}}{|H_{\sigma'}|}(t,\rho,\phi) P_{\sigma'}(\rho) Q_{\sigma'}(\phi) \right] d\phi d\rho, \tag{5.49}$$

together with Eq. (5.44), as a self-consistent equation for the global order parameter at equilibrium.

5.5 Results

At this point, it is helpful to consider specific cases of interest. Particularly, we will be considering the effects of only community structure (subsection 5.5.1) and only external forcing (subsection 5.5.2).

5.5.1 Community structure

To begin our study of the social compass model with communities, we let the number of external sources be zero (i.e., $M = 0$) and select the distributions of initial opinion orientations for communities 1 and 2, respectively, as

$$Q_1(\phi) = \frac{1}{2} \left[\delta(\phi - \phi_0) + \delta(\phi + \phi_0) \right], \tag{5.50}$$

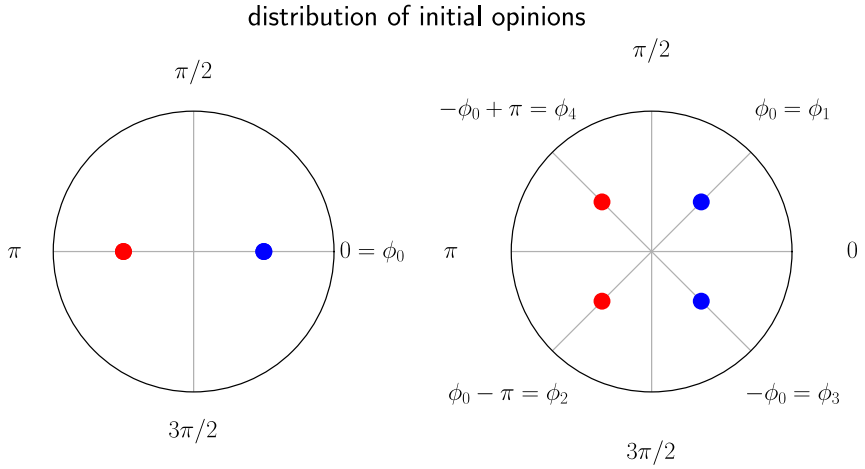

Figure 5.4: A schematic representation of the distribution of initial opinion orientations for correlated initial opinions (left) and uncorrelated initial opinions (right). The blue dots mark the location of initial opinion orientations for community 1 while the red dots mark the locations of the initial opinion orientations for community 2.

and

$$Q_2(\phi) = \frac{1}{2}\left[\delta(\phi - \phi_0 + \pi) + \delta(\phi + \phi_0 - \pi)\right]. \tag{5.51}$$

In Fig. 5.4 we include a schematic representation of these distributions with the modes associated with community 1 in blue and the modes associated with community 2 in red. This choice is made to ensure that initially correlated opinions ($\phi_0 = 0$) are held in distinct communities. We also make the choice that the intercommunity coupling ($K^{\sigma\sigma'}$ with $\sigma' \neq \sigma$) has the form $K^{\sigma\sigma'} = \mu K^{\sigma\sigma}$ with $0 \leq \mu \leq 1$ and we also assume $K^{11} = K^{22}$. The choice $\mu = 0$ corresponds to completely disconnected communities, while $\mu = 1$ corresponds to no community structure. Fig. 5.5 shows a bifurcation diagram for the transitions between a polarized state ($r = 0$), a consensus state ($r \approx 1$), and a bistable state versus $K^{\sigma\sigma}$ and μ for the agent-based model [right, Eq. (5.40)] and reduced description of the dynamics [left, Eq. (5.45)]. We see that as the amount of intercommunity coupling decreases, reaching consensus requires larger intracommunity coupling and the region of bistablity becomes more narrow. Within the range that we have considered (i.e., $K^{\sigma\sigma} \in [0, 3]$), reaching consensus becomes impossible for μ less than about 0.4, although it is unclear if consensus could still be reached for sufficiently large values of intracommunity coupling outside the range

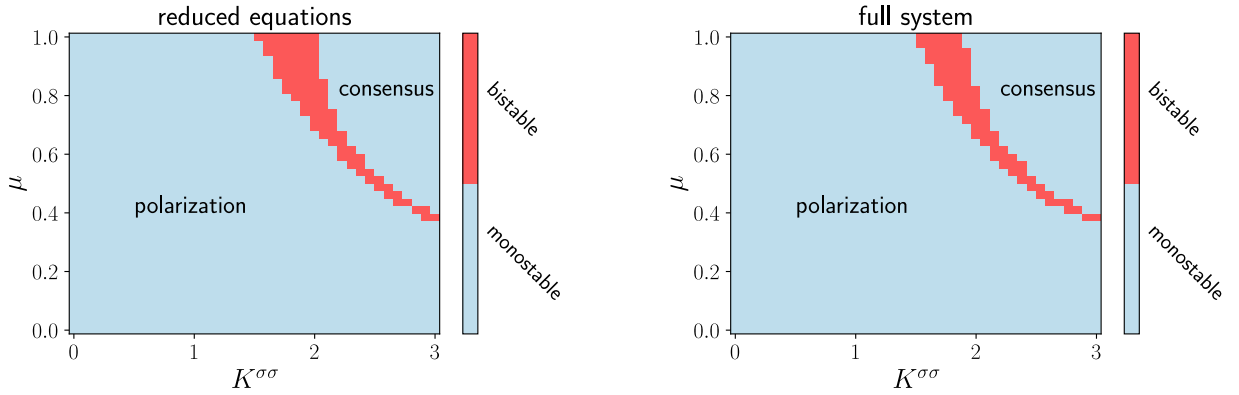

Figure 5.5: (left) A bifurcation diagram of the steady-state behavior of Eq. (5.45) in the region $\mu \in [0, 1]$ and $K^{\sigma\sigma} \in [0, 3]$ for 2 communities with initial opinion distributions as in Eqs. (5.50) and (5.51) with $\phi_0 = \pi/4$ and convictions all equal to 1 [i.e., as in Eq. (5.12) with $\rho_{\max} = 1$]. (right) A bifurcation diagram of the agent-based model [i.e., Eq. (5.40)] with $N = 1500$ of the steady-state behavior in the region $\mu \in [0, 1]$ and $K^{\sigma\sigma} \in [0, 3]$ for the same conventions as in the reduced equations [i.e., Eq. (5.45)].

that we have considered. Additionally, comparing the left and right panels of Fig. 5.4, we see good qualitative agreement between the reduced dimensional description of the dynamics [Eq. (5.45)] and the agent-based model [Eq. (5.40)].

5.5.2 External forcing

Now we will consider the effect of including a single external source ($M = 1$) that broadcasts opinion orientation β with strength F to every agent. This could model, for example, a single news station watched by all agents. For this example, we will return to considering only a single community with the quadrimodal distribution of initial opinion orientations [Eq. (5.13)] and a Dirac delta distribution of convictions [Eq. (5.12)] with $\rho_{\max} = 1$. Fig. 5.6, shows a bifurcation diagram in the number of stable equilibrium solutions of r versus K and F for an external source with opinion orientation $\beta = \pi/6$. We see that the bistable region vanishes for a non-zero value of the external forcing. Furthermore, Fig. 5.7 shows a plot of r versus K and F, with the same conventions. Here we see that, as in the unforced model, consensus is reached above a critical value K_C of the coupling strength. However, we also see an increase in r, blurring the transition from polarization

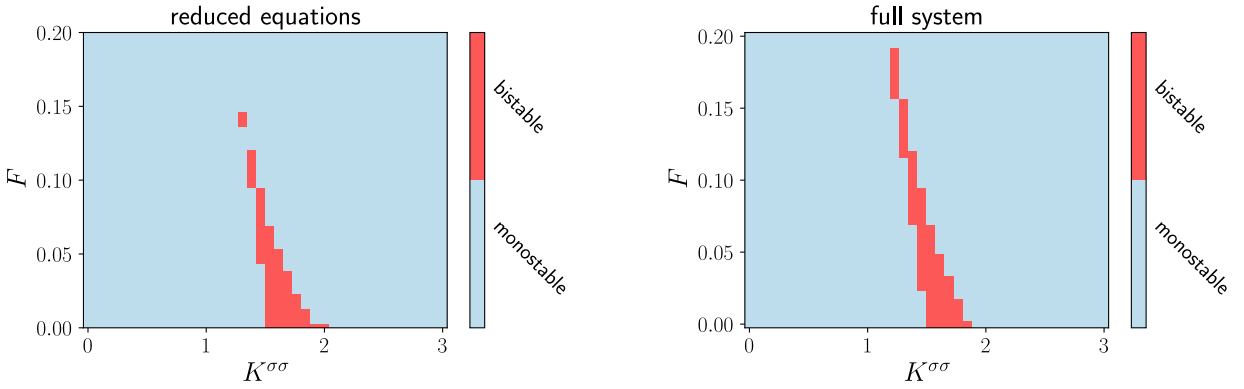

Figure 5.6: (left) A bifurcation diagram of the steady-state behavior of Eq. (5.45) in the region $F \in [0, 0.2]$ and $K^{\sigma\sigma} \in [0, 3]$ with external forcing of opinion orientation $\beta = \pi/6$ and initial opinion distributions as in Eq. (5.13) with $\phi_0 = \pi/4$ and convictions all equal to 1 [i.e., as in Eq. (5.12) with $\rho_{\max} = 1$]. (right) A bifurcation diagram of the agent-based model [i.e., Eq. (5.40)] with $N = 1500$ of the steady-state behavior in the region $F \in [0, 0.2]$ and $K^{\sigma\sigma} \in [0, 3]$ for the same conventions as in the reduced equations [i.e., Eq. (5.45)].

to consensus, for sufficiently large external forcing. As in the case of two communities, we also observe good qualitative agreement between the reduced description of the dynamics [Eq. (5.45)] and the agent-based model [Eq. (5.40)].

5.6 Discussion and future work

The work presented in this chapter is currently ongoing and we are still working on developing some of our key results. Despite this, we have shown that, like the Kuramoto model, the dynamics of the social compass model can be represented with a low-dimensional dynamical system by application of the Ott-Antonsen ansatz. This method provides an alternative approach to study the social compass model, which allows for the study of its dynamics in addition to its equilibria. We have also shown that a generalization of the social compass model that includes communities and external forces can also be represented as a reduced dimensional system using the Ott-Antonsen ansatz, in the limit $N \to \infty$, showing that the agent-based model and reduced description of the dynamics have reasonable qualitative agreement.

Using our generalized version of the social compass model, we have examined the role of

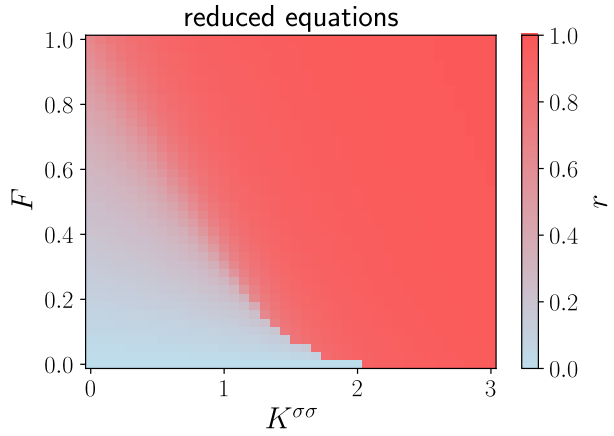

Figure 5.7: A plot of the degree of consensus r versus F and K generated from the reduced description of the dynamics [Eq. (5.45)] without communities, a single external force with opinion orientation $\beta = \pi/6$, and initial opinion and conviction distributions as in Eqs. (5.13) and (5.12), respectively.

communities on a system's ability to reach consensus from polarization. Particularly, we find that the balance of intracommunity coupling, $K^{\sigma\sigma}$, and intercommunity coupling, $K^{\sigma\sigma'}$, affects the onset of consensus, with less intercommunity coupling resulting in more difficulty reaching consensus (i.e., requiring larger coupling strength) and a smaller region of bistability. We have also found that the inclusion of external forcing results in a non-trivial transition from a region of bistability between polarization and consensus, to a continuous transition between the two. We have observed that a sufficiently strong external force can increase the degree of consensus, r, even when the coupling strength is insufficient on its own, and lowers the necessary critical coupling. However, it should be noted that this doesn't account for additional behaviors such as rejection of certain opinions or other contrarian-like behaviors.

While it is difficult to provide an in-depth interpretation of the role of bistability in a model of opinion consensus, some features of this transition that are worth noting are as follows. First, the existence of bistability, as appears in the social compass model, allows the system to transition from a state of polarization to one of consensus as a discontinuous transition. This suggests that the transition to consensus can occur in a more widespread manner very quickly. Additionally, as this type of bistability introduces hysteresis into the system, when the system is already in

consensus it is more difficult to bring it into a polarized state by decreasing the coupling strength. One interpretation of this is that a bistable region, as in this model, may make a social system in consensus more robust to a decreasing coupling strength and helps the system remain in a state of consensus, and is therefore desirable. In the context of our findings, this suggests that the separation of a population into 2 communities, with weaker coupling strength between members of opposite communities, makes the system more vulnerable to becoming polarized since it decreases the size of the bistable region and requires a larger intracommunity coupling to reach consensus. Furthermore, the introduction of an external force can remove the region of bistability altogether, possibly making the system less robust to polarization, but can promote the formation of consensus for sufficiently large values of F and seems to decrease the critical coupling strength.

As this is an ongoing project, there are still a number of advancements that we are currently working towards. First, we will be continuing the work presented in Sec. 5.3.2 to find an expression describing the transition from a continuous to a discontinuous bifurcation in the steady-state behavior for the class of distributions considered in that section. We then are planning to extend these results to the version of the social compass model with communities to find analytical expressions of the critical coupling strength and formation of bistability. We also plan to extend these techniques to the social compass model with external forcing to develop an understanding of how forcing can reduce bistability and the behavior of the model with more external sources.

Bibliography

[1] Jaume Ojer, Michele Starnini, and Romualdo Pastor-Satorras. Modeling explosive opinion depolarization in interdependent topics. Physical review letters, 130(20):207401, 2023.

[2] Corbit R Sampson, Mason A Porter, and Juan G Restrepo. Oscillatory and excitable dynamics in an opinion model with group opinions. arXiv preprint arXiv:2408.13336, 2024.

[3] Corbit R. Sampson and Juan G. Restrepo. Competing social contagions with opinion-dependent infectivity. Phys. Rev. E, 111:024313, Feb 2025.

[4] Jaume Ojer, Michele Starnini, and Romualdo Pastor-Satorras. Social network heterogeneity promotes depolarization of multidimensional correlated opinions. Physical Review Research, 7(1):013207, 2025.

[5] Mark EJ Newman. Complex systems: A survey. arXiv preprint arXiv:1112.1440, 2011.

[6] James Ladyman, James Lambert, and Karoline Wiesner. What is a complex system? European Journal for Philosophy of Science, 3:33–67, 2013.

[7] Yoshiki Kuramoto. International symposium on mathematical problems in theoretical physics. Lecture notes in Physics, 30:420, 1975.

[8] Morris H DeGroot. Reaching a consensus. Journal of the American Statistical association, 69(345):118–121, 1974.

[9] Sebastien Motsch and Eitan Tadmor. Heterophilious dynamics enhances consensus. SIAM review, 56(4):577–621, 2014.

[10] Mark Newman. Networks. Oxford university press, 2018.

[11] Ana P. Millán, Joaquín J. Torres, and Ginestra Bianconi. Explosive higher-order Kuramoto dynamics on simplicial complexes. Physical Review Letters, 124(21):218301, 2020.

[12] Reza Ghorbanchian, Juan G Restrepo, Joaquín J. Torres, and Ginestra Bianconi. Higher-order simplicial synchronization of coupled topological signals. Communications Physics, 4(1):120, 2021.

[13] Timoteo Carletti, Lorenzo Giambagli, and Ginestra Bianconi. Global topological synchronization on simplicial and cell complexes. Physical Review Lettets, 130:187401, 2023.

[14] Graphs with prescribed degree of vertices. Mat. Lapok., 11:264–274, 1960.

[15] William Aiello, Fan Chung, and Linyuan Lu. A random graph model for power law graphs. Experimental mathematics, 10(1):53–66, 2001.

[16] Fan Chung and Linyuan Lu. The average distances in random graphs with given expected degrees. Proceedings of the National Academy of Sciences, 99(25):15879–15882, 2002.

[17] Fan Chung and Linyuan Lu. Connected components in random graphs with given expected degree sequences. Annals of combinatorics, 6(2):125–145, 2002.

[18] Marián Boguná and Romualdo Pastor-Satorras. Epidemic spreading in correlated complex networks. Physical Review E, 66(4):047104, 2002.

[19] Marián Boguná, Romualdo Pastor-Satorras, and Alessandro Vespignani. Absence of epidemic threshold in scale-free networks with degree correlations. Physical review letters, 90(2):028701, 2003.

[20] Claudio Castellano and Romualdo Pastor-Satorras. Thresholds for epidemic spreading in networks. Physical review letters, 105(21):218701, 2010.

[21] Takashi Ichinomiya. Frequency synchronization in a random oscillator network. Physical Review E—Statistical, Nonlinear, and Soft Matter Physics, 70(2):026116, 2004.

[22] Deok-Sun Lee. Synchronization transition in scale-free networks: Clusters of synchrony. Physical Review E—Statistical, Nonlinear, and Soft Matter Physics, 72(2):026208, 2005.

[23] Louis M Pecora and Thomas L Carroll. Master stability functions for synchronized coupled systems. Physical review letters, 80(10):2109, 1998.

[24] Robin Cowan and Nicolas Jonard. Network structure and the diffusion of knowledge. Journal of economic Dynamics and Control, 28(8):1557–1575, 2004.

[25] Hanool Choi, Sang-Hoon Kim, and Jeho Lee. Role of network structure and network effects in diffusion of innovations. Industrial marketing management, 39(1):170–177, 2010.

[26] Federico Battiston, Enrico Amico, Alain Barrat, Ginestra Bianconi, Guilherme Ferraz de Arruda, Benedetta Franceschiello, Iacopo Iacopini, Sonia Kéfi, Vito Latora, Yamir Moreno, et al. The physics of higher-order interactions in complex systems. Nature Physics, 17(10):1093–1098, 2021.

[27] Federico Battiston, Giulia Cencetti, Iacopo Iacopini, Vito Latora, Maxime Lucas, Alice Patania, Jean-Gabriel Young, and Giovanni Petri. Networks beyond pairwise interactions: structure and dynamics. Physics Reports, 874:1–92, 2020.

[28] Abigail Hickok, Yacoub Kureh, Heather Z Brooks, Michelle Feng, and Mason A Porter. A bounded-confidence model of opinion dynamics on hypergraphs. SIAM Journal on Applied Dynamical Systems, 21(1):1–32, 2022.

[29] Margaret M Mayfield and Daniel B Stouffer. Higher-order interactions capture unexplained complexity in diverse communities. Nature ecology & evolution, 1(3):0062, 2017.

[30] Eyal Bairey, Eric D Kelsic, and Roy Kishony. High-order species interactions shape ecosystem diversity. Nature communications, 7(1):12285, 2016.

[31] Anna Ritz, Allison N Tegge, Hyunju Kim, Christopher L Poirel, and TM Murali. Signaling hypergraphs. Trends in biotechnology, 32(7):356–362, 2014.

[32] Elad Schneidman, Michael J Berry, Ronen Segev, and William Bialek. Weak pairwise correlations imply strongly correlated network states in a neural population. Nature, 440(7087):1007–1012, 2006.

[33] Shan Yu, Hongdian Yang, Hiroyuki Nakahara, Gustavo S Santos, Danko Nikolić, and Dietmar Plenz. Higher-order interactions characterized in cortical activity. Journal of neuroscience, 31(48):17514–17526, 2011.

[34] Chad Giusti, Eva Pastalkova, Carina Curto, and Vladimir Itskov. Clique topology reveals intrinsic geometric structure in neural correlations. Proceedings of the National Academy of Sciences, 112(44):13455–13460, 2015.

[35] Lina Merchan and Ilya Nemenman. On the sufficiency of pairwise interactions in maximum entropy models of networks. Journal of Statistical Physics, 162:1294–1308, 2016.

[36] Elad Ganmor, Ronen Segev, and Elad Schneidman. Sparse low-order interaction network underlies a highly correlated and learnable neural population code. Proceedings of the National Academy of sciences, 108(23):9679–9684, 2011.

[37] Gordon Pennycook, Tyrone D Cannon, and David G Rand. Prior exposure increases perceived accuracy of fake news. Journal of experimental psychology: general, 147(12):1865, 2018.

[38] FOC BIAS. The evolution of cognitive bias. The Handbook of Evolutionary Psychology, 2, 2015.

[39] William Hart, Dolores Albarracín, Alice H Eagly, Inge Brechan, Matthew J Lindberg, and Lisa Merrill. Feeling validated versus being correct: a meta-analysis of selective exposure to information. Psychological bulletin, 135(4):555, 2009.

[40] Olivia Weng, Kimberly J Johnson, and Matthew W Kreuter. Repeated exposure to covid-19 misinformation: A longitudinal analysis of prevalence and predictors in a community sample. Journal of Public Health Management and Practice, 30(5):E211–E214, 2024.

[41] Damon Centola and Michael Macy. Complex contagions and the weakness of long ties. American journal of Sociology, 113(3):702–734, 2007.

[42] Doug McAdam and Ronnelle Paulsen. Specifying the relationship between social ties and activism. American journal of sociology, 99(3):640–667, 1993.

[43] Iacopo Iacopini, Giovanni Petri, Alain Barrat, and Vito Latora. Simplicial models of social contagion. Nature communications, 10(1):1–9, 2019.

[44] Emilio Ferrara, Onur Varol, Clayton Davis, Filippo Menczer, and Alessandro Flammini. The rise of social bots. Communications of the ACM, 59(7):96–104, 2016.

[45] Nicholas W Landry and Juan G Restrepo. The effect of heterogeneity on hypergraph contagion models. Chaos: An Interdisciplinary Journal of Nonlinear Science, 30(10):103117, 2020.

[46] Nicholas W Landry and Juan G Restrepo. Hypergraph assortativity: A dynamical systems perspective. Chaos: An Interdisciplinary Journal of Nonlinear Science, 32(5), 2022.

[47] Nicholas W Landry and Juan G Restrepo. Opinion disparity in hypergraphs with community structure. Physical Review E, 108(3):034311, 2023.

[48] Daniel Hernández Serrano, Javier Villarroel, Juan Hernández-Serrano, and Ángel Tocino. Stochastic simplicial contagion model. Chaos, Solitons & Fractals, 167:113008, 2023.

[49] Pedro Cisneros-Velarde and Francesco Bullo. Multi-group sis epidemics with simplicial and higher-order interactions. IEEE Transactions on Control of Network Systems, 2021.

[50] Sabina Adhikari, Juan G Restrepo, and Per Sebastian Skardal. Synchronization of phase oscillators on complex hypergraphs. Chaos: An Interdisciplinary Journal of Nonlinear Science, 33(3):033116, 2023.

[51] Sabina Adhikari. Synchronization of Coupled Phase Oscillators on Hypergraphs. PhD thesis, University of Colorado at Boulder, 2024.

[52] Per Sebastian Skardal, Sabina Adhikari, and Juan G Restrepo. Multistability in coupled oscillator systems with higher-order interactions and community structure. Chaos: An Interdisciplinary Journal of Nonlinear Science, 33(2), 2023.

[53] Xavier Ouvrard. Hypergraphs: an introduction and review. arXiv preprint arXiv:2002.05014, 2020.

[54] Qionghai Dai and Yue Gao. Mathematical foundations of hypergraph. In Hypergraph Computation, pages 19–40. Springer, 2023.

[55] Giorgio Gallo, Giustino Longo, Stefano Pallottino, and Sang Nguyen. Directed hypergraphs and applications. Discrete applied mathematics, 42(2-3):177–201, 1993.

[56] David Lewis. Convention: A philosophical study. John Wiley & Sons, 2008.

[57] Michael Hechter and Christine Horne. Theories of social order: a reader. Stanford University Press, 2009.

[58] Andrea Baronchelli. The emergence of consensus: a primer. Royal Society open science, 5(2):172189, 2018.

[59] Jennifer McCoy, Tahmina Rahman, and Murat Somer. Polarization and the global crisis of democracy: Common patterns, dynamics, and pernicious consequences for democratic polities. American Behavioral Scientist, 62(1):16–42, 2018.

[60] Annual threat assessment of the us intelligence community. Technical report, Office of the Director of National Intelligence Washington, DC, 2023.

[61] Simeon Edosomwan, Sitalaskshmi Kalangot Prakasan, Doriane Kouame, Jonelle Watson, and Tom Seymour. The history of social media and its impact on business. Journal of Applied Management and entrepreneurship, 16(3):79, 2011.

[62] Karin Sajithra and Rajindra Patil. Social media–history and components. Journal of Business and Management, 7(1):69–74, 2013.

[63] Ivan V. Kozitsin. Opinion dynamics of online social network users: A micro-level analysis. The Journal of Mathematical Sociology, 47(1):1–41, 2023.

[64] Juan Fernández-Gracia, Krzysztof Suchecki, José J Ramasco, Maxi San Miguel, and Víctor M Eguíluz. Is the voter model a model for voters? Physical review letters, 112(15):158701, 2014.

[65] Leonhard Horstmeyer and Christian Kuehn. Adaptive voter model on simplicial complexes. Physical Review E, 101(2):022305, 2020.

[66] Guillaume Deffuant, David Neau, Frederic Amblard, and Gérard Weisbuch. Mixing beliefs among interacting agents. Advances in Complex Systems, 3(01n04):87–98, 2000.

[67] Leonie Neuhäuser, Andrew Mellor, and Renaud Lambiotte. Multibody interactions and nonlinear consensus dynamics on networked systems. Physical Review E, 101(3):032310, 2020.

[68] Quanbo Zha, Gang Kou, Hengjie Zhang, Haiming Liang, Xia Chen, Cong-Cong Li, and Yucheng Dong. Opinion dynamics in finance and business: a literature review and research opportunities. Financial Innovation, 6(1):1–22, 2020.

[69] David A Siegel. Social networks and collective action. American journal of political science, 53(1):122–138, 2009.

[70] Henrik Olsson and Mirta Galesic. Analogies for modeling belief dynamics. Trends in Cognitive Sciences, 28(10):907–923, 2024.

[71] Rainer Hegselmann and Ulrich Krause. Consensus and fragmentation of opinions with a focus on bounded confidence. The American Mathematical Monthly, 126(8):700–716, 2019.

[72] Lin Li, Anna Scaglione, Ananthram Swami, and Qing Zhao. Consensus, polarization and clustering of opinions in social networks. IEEE Journal on Selected Areas in Communications, 31(6):1072–1083, 2013.

[73] Craig W Reynolds. Flocks, herds and schools: A distributed behavioral model. In Proceedings of the 14th annual conference on Computer graphics and interactive techniques, pages 25–34, 1987.

[74] Tamás Vicsek, András Czirók, Eshel Ben-Jacob, Inon Cohen, and Ofer Shochet. Novel type of phase transition in a system of self-driven particles. Physical review letters, 75(6):1226, 1995.

[75] Bruce Stephen, Cathy Dwyer, Jimmy Hyslop, Matthew Bell, David Ross, Kae Hsiang Kwong, Craig Michie, and Ivan Andonovic. Statistical interaction modeling of bovine herd behaviors. IEEE Transactions on Systems, Man, and Cybernetics, Part C (Applications and Reviews), 41(6):820–829, 2010.

[76] Peter Clifford and Aidan Sudbury. A model for spatial conflict. Biometrika, 60(3):581–588, 1973.

[77] Iain D Couzin, Jens Krause, Richard James, Graeme D Ruxton, and Nigel R Franks. Collective memory and spatial sorting in animal groups. Journal of theoretical biology, 218(1):1–11, 2002.

[78] Felipe Cucker and Steve Smale. Emergent behavior in flocks. IEEE Transactions on automatic control, 52(5):852–862, 2007.

[79] Michele Ballerini, Nicola Cabibbo, Raphael Candelier, Andrea Cavagna, Evaristo Cisbani, Irene Giardina, Vivien Lecomte, Alberto Orlandi, Giorgio Parisi, Andrea Procaccini, et al. Interaction ruling animal collective behavior depends on topological rather than metric distance: Evidence from a field study. Proceedings of the national academy of sciences, 105(4):1232–1237, 2008.

[80] Denys Grushchak, Jenna Kline, Danilo Pianini, and Nicolas Farabegoli. An agent-based model of directional multi-herds. In 2024 IEEE International Conference on Autonomic Computing and Self-Organizing Systems Companion (ACSOS-C), pages 15–20. IEEE, 2024.

[81] Reza Olfati-Saber. Flocking for multi-agent dynamic systems: Algorithms and theory. IEEE Transactions on automatic control, 51(3):401–420, 2006.

[82] Douglas H Kelley and Nicholas T Ouellette. Emergent dynamics of laboratory insect swarms. Scientific reports, 3(1):1073, 2013.

[83] Eitan Tadmor. On the mathematics of swarming: emergent behavior in alignment dynamics. arXiv preprint arXiv:2102.09134, 2021.

[84] Reza Olfati-Saber and Richard M Murray. Consensus problems in networks of agents with switching topology and time-delays. IEEE Transactions on automatic control, 49(9):1520–1533, 2004.

[85] Bao Huynh, Haimonti Dutta, and Dane Taylor. Impact of community structure on consensus machine learning. arXiv preprint arXiv:2011.01334, 2020.

[86] Richard A Holley and Thomas M Liggett. Ergodic theorems for weakly interacting infinite systems and the voter model. The annals of probability, pages 643–663, 1975.

[87] Mason A Porter and James P Gleeson. Dynamical systems on networks. Frontiers in Applied Dynamical Systems: Reviews and Tutorials, 4:29, 2016.

[88] J Theodore Cox and David Griffeath. Diffusive clustering in the two dimensional voter model. The Annals of Probability, pages 347–370, 1986.

[89] Vishal Sood and Sidney Redner. Voter model on heterogeneous graphs. Physical review letters, 94(17):178701, 2005.

[90] Vishal Sood, Tibor Antal, and Sidney Redner. Voter models on heterogeneous networks. Physical Review E, 77(4):041121, 2008.

[91] Renaud Lambiotte and Sidney Redner. Dynamics of vacillating voters. Journal of Statistical Mechanics: Theory and Experiment, 2007(10):L10001, 2007.

[92] Renaud Lambiotte and Sidney Redner. Dynamics of non-conservative voters. Europhysics Letters, 82(1):18007, 2008.

[93] JT Cox and Richard Durrett. Nonlinear voter models. Springer, 1991.

[94] Thomas M Liggett. Coexistence in threshold voter models. The Annals of Probability, 22(2):764–802, 1994.

[95] Enrique D Andjel, Thomas M Liggett, and Thomas Mountford. Clustering in one-dimensional threshold voter models. Stochastic processes and their applications, 42(1):73–90, 1992.

[96] Duncan J Watts. A simple model of global cascades on random networks. Proceedings of the National Academy of Sciences, 99(9):5766–5771, 2002.

[97] Serge Galam. Minority opinion spreading in random geometry. The European Physical Journal B-Condensed Matter and Complex Systems, 25:403–406, 2002.

[98] Nicolas Lanchier and Jared Neufer. Stochastic dynamics on hypergraphs and the spatial majority rule model. Journal of Statistical Physics, 151(1-2):21–45, 2013.

[99] U Krause. A discrete nonlinear and non-autonomous model of consensus. In Communications in Difference Equations: Proceedings of the Fourth International Conference on Difference Equations, page 227. CRC Press, 2000.

[100] Meng Ji and Magnus Egerstedt. Distributed coordination control of multiagent systems while preserving connectedness. IEEE Transactions on Robotics, 23(4):693–703, 2007.

[101] Christian Ringhofer. Traffic flow models and service rules for complex production systems. Decision Policies for Production Networks, pages 209–233, 2012.

[102] Michael M Zavlanos and George J Pappas. Potential fields for maintaining connectivity of mobile networks. IEEE Transactions on robotics, 23(4):812–816, 2007.

[103] Roger L Berger. A necessary and sufficient condition for reaching a consensus using degroot's method. Journal of the American Statistical Association, 76(374):415–418, 1981.

[104] Noah E Friedkin and Eugene C Johnsen. Social influence and opinions. Journal of mathematical sociology, 15(3-4):193–206, 1990.

[105] Zhaogang Ding, Xia Chen, Yucheng Dong, and Francisco Herrera. Consensus reaching in social network degroot model: The roles of the self-confidence and node degree. Information Sciences, 486:62–72, 2019.

[106] Yucheng Dong, Zhaogang Ding, Luis Martínez, and Francisco Herrera. Managing consensus based on leadership in opinion dynamics. Information Sciences, 397:187–205, 2017.

[107] Guillaume Deffuant, Frédéric Amblard, and Gérard Weisbuch. Modelling group opinion shift to extreme: the smooth bounded confidence model. arXiv preprint cond-mat/0410199, 2004.

[108] Sylvie Huet, Guillaume Deffuant, and Wander Jager. A rejection mechanism in 2d bounded confidence provides more conformity. Advances in Complex Systems, 11(04):529–549, 2008.

[109] Javier Gómez-Serrano, Carl Graham, and Jean-Yves Le Boudec. The bounded confidence model of opinion dynamics. Mathematical Models and Methods in Applied Sciences, 22(02):1150007, 2012.

[110] Grace J Li, Jiajie Luo, and Mason A Porter. Bounded-confidence models of opinion dynamics with adaptive confidence bounds. arXiv preprint arXiv:2303.07563, 2023.

[111] Gerard Weisbuch. Bounded confidence and social networks. The European Physical Journal B, 38:339–343, 2004.

[112] X Flora Meng, Robert A Van Gorder, and Mason A Porter. Opinion formation and distribution in a bounded-confidence model on various networks. Physical Review E, 97(2):022312, 2018.

[113] Unchitta Kan, Michelle Feng, and Mason A Porter. An adaptive bounded-confidence model of opinion dynamics on networks. Journal of Complex Networks, 11(1):415–444, 2023.

[114] Hegselmann Rainer and Ulrich Krause. Opinion dynamics and bounded confidence: Models, analysis and simulation. Journal of Artificial Societies and Social Simulation, 5(3), 2002.

[115] Igor Douven and Rainer Hegselmann. Network effects in a bounded confidence model. Studies in History and Philosophy of Science, 94:56–71, 2022.

[116] Takasumi Kurahashi-Nakamura, Michael Mäs, and Jan Lorenz. Robust clustering in generalized bounded confidence models. Journal of Artificial Societies and Social Simulation, 19(4), 2016.

[117] Hendrik Schawe, Sylvain Fontaine, and Laura Hernández. When network bridges foster consensus. bounded confidence models in networked societies. Physical Review Research, 3(2):023208, 2021.

[118] Ronald E. Riggio and Clara R. Riggio. Social contagion. In Howard S. Friedman and Charlotte H. Markey, editors, Encyclopedia of Mental Health (Third Edition), pages 270–273. Academic Press, Oxford, third edition edition, 2023.

[119] Gustave Le Bon. The crowd. Routledge, 2017.

[120] David A Levy and Paul R Nail. Contagion: a theoretical and empirical review and reconceptualization. Genetic, social, and general psychology monographs, 119(2):233–284, 1993.

[121] Nicholas A Christakis and James H Fowler. Social contagion theory: examining dynamic social networks and human behavior. Statistics in medicine, 32(4):556–577, 2013.

[122] Aaron Lynch. Thought contagion: How belief spreads through society: The new science of memes. Basic Books, 2008.

[123] Christian Bauckhage. Insights into internet memes. In Proceedings of the International AAAI Conference on Web and Social Media, volume 5, pages 42–49, 2011.

[124] Rosanna E Guadagno, Daniel M Rempala, Shannon Murphy, and Bradley M Okdie. What makes a video go viral? an analysis of emotional contagion and internet memes. Computers in human behavior, 29(6):2312–2319, 2013.

[125] Geah Pressgrove, Brooke Weberling McKeever, and S Mo Jang. What is contagious? exploring why content goes viral on twitter: A case study of the als ice bucket challenge. International Journal of Nonprofit and Voluntary Sector Marketing, 23(1):e1586, 2018.

[126] Shannon Ward, Tara M Dumas, Ankur Srivastava, Jordan P Davis, and Wendy Ellis. Uploading risk: Examining the social profile of young adults most susceptible to engagement in risky social media challenges. Cyberpsychology, Behavior, and Social Networking, 24(12):846–850, 2021.

[127] Prashant Bordia and Nicholas DiFonzo. Problem solving in social interactions on the internet: Rumor as social cognition. Social Psychology Quarterly, 67(1):33–49, 2004.

[128] Adrien Friggeri, Lada Adamic, Dean Eckles, and Justin Cheng. Rumor cascades. In proceedings of the international AAAI conference on web and social media, volume 8, pages 101–110, 2014.

[129] Ellsworth Campbell and Marcel Salathé. Complex social contagion makes networks more vulnerable to disease outbreaks. Scientific reports, 3(1):1905, 2013.

[130] Feng Fu, Nicholas A Christakis, and James H Fowler. Dueling biological and social contagions. Scientific reports, 7(1):43634, 2017.

[131] Maxime Lucas, Iacopo Iacopini, Thomas Robiglio, Alain Barrat, and Giovanni Petri. Simplicially driven simple contagion. Physical Review Research, 5(1):013201, 2023.

[132] Chrysanthos Dellarocas. The digitization of word of mouth: Promise and challenges of online feedback mechanisms. Management science, 49(10):1407–1424, 2003.

[133] Paul Dwyer. Measuring the value of electronic word of mouth and its impact in consumer communities. Journal of Interactive marketing, 21(2):63–79, 2007.

[134] Jo Brown, Amanda J Broderick, and Nick Lee. Word of mouth communication within online communities: Conceptualizing the online social network. Journal of interactive marketing, 21(3):2–20, 2007.

[135] Hunt Allcott and Matthew Gentzkow. Social media and fake news in the 2016 election. Journal of economic perspectives, 31(2):211–236, 2017.

[136] Douglas Guilbeault, Joshua Becker, and Damon Centola. Complex contagions: A decade in review. Complex spreading phenomena in social systems: Influence and contagion in real-world social networks, pages 3–25, 2018.

[137] Julie C Blackwood and Lauren M Childs. An introduction to compartmental modeling for the budding infectious disease modeler. Letters in Biomathematics, 5(1):195–221, 2018.

[138] Matt J Keeling and Ken TD Eames. Networks and epidemic models. Journal of the royal society interface, 2(4):295–307, 2005.

[139] Vittoria Colizza, Alain Barrat, Marc Barthélemy, and Alessandro Vespignani. The role of the airline transportation network in the prediction and predictability of global epidemics. Proceedings of the National Academy of Sciences, 103(7):2015–2020, 2006.

[140] Sune Lehmann and Yong-Yeol Ahn. Complex spreading phenomena in social systems. Computational Social Sciences, 10:978–3, 2018.

[141] Odo Diekmann, Johan Andre Peter Heesterbeek, and Johan Anton Jacob Metz. On the definition and the computation of the basic reproduction ratio r 0 in models for infectious diseases in heterogeneous populations. Journal of mathematical biology, 28:365–382, 1990.

[142] Fred Brauer. Compartmental models in epidemiology. Mathematical epidemiology, pages 19–79, 2008.

[143] Mark S Granovetter. The strength of weak ties. American journal of sociology, 78(6):1360–1380, 1973.

[144] Duncan J Watts and Steven H Strogatz. Collective dynamics of 'small-world'networks. nature, 393(6684):440–442, 1998.

[145] Daniel Trpevski, Wallace KS Tang, and Ljupco Kocarev. Model for rumor spreading over networks. Physical Review E—Statistical, Nonlinear, and Soft Matter Physics, 81(5):056102, 2010.

[146] Alex Beutel, B Aditya Prakash, Roni Rosenfeld, and Christos Faloutsos. Interacting viruses in networks: can both survive? In Proceedings of the 18th ACM SIGKDD international conference on Knowledge discovery and data mining, pages 426–434, 2012.

[147] Yun-Bei Zhuang, JJ Chen, and Zhi-hong Li. Modeling the cooperative and competitive contagions in online social networks. Physica A: Statistical Mechanics and its Applications, 484:141–151, 2017.

[148] Seth A Myers and Jure Leskovec. Clash of the contagions: Cooperation and competition in information diffusion. In 2012 IEEE 12th international conference on data mining, pages 539–548. IEEE, 2012.

[149] Guilherme Ferraz de Arruda, Giovanni Petri, and Yamir Moreno. Social contagion models on hypergraphs. Physical Review Research, 2(2):023032, 2020.

[150] Joseph L Waner. Mixed viral infections: detection and management. Clinical microbiology reviews, 7(2):143–151, 1994.

[151] Milton Untiveros, Segundo Fuentes, and Luis F Salazar. Synergistic interaction of sweet potato chlorotic stunt virus (crinivirus) with carla-, cucumo-, ipomo-, and potyviruses infecting sweet potato. Plant disease, 91(6):669–676, 2007.

[152] JT Guidry and RS Scott. The interaction between human papillomavirus and other viruses. Virus research, 231:139–147, 2017.

[153] Lubna Pinky and Hana M Dobrovolny. Epidemiological consequences of viral interference: a mathematical modeling study of two interacting viruses. Frontiers in microbiology, 13:830423, 2022.

[154] Telma DaPalma, Bently P Doonan, Nicole M Trager, and Laura M Kasman. A systematic approach to virus–virus interactions. Virus research, 149(1):1–9, 2010.

[155] Jerzy Syller. Facilitative and antagonistic interactions between plant viruses in mixed infections. Molecular plant pathology, 13(2):204–216, 2012.

[156] Luca Di Stefano and Omar Inverso. Emerging synchrony in applauding audiences: formal analysis and specification. In International Symposium on Leveraging Applications of Formal Methods, pages 253–270. Springer, 2024.

[157] John Buck and Elisabeth Buck. Biology of synchronous flashing of fireflies. Nature, 211:562–564, 1966.

[158] Raphaël Sarfati, Julie C Hayes, Élie Sarfati, and Orit Peleg. Spatio-temporal reconstruction of emergent flash synchronization in firefly swarms via stereoscopic 360-degree cameras. Journal of The Royal Society Interface, 17(170):20200179, 2020.

[159] James Pantaleone. Synchronization of metronomes. American Journal of Physics, 70(10):992–1000, 2002.

[160] Pat Dallard, Tony Fitzpatrick, Anthony Flint, Angus Low, Roger Ridsdill Smith, Michael Willford, and Mark Roche. London millennium bridge: pedestrian-induced lateral vibration. Journal of bridge Engineering, 6(6):412–417, 2001.

[161] Steven H Strogatz, Daniel M Abrams, Allan McRobie, Bruno Eckhardt, and Edward Ott. Crowd synchrony on the millennium bridge. Nature, 438(7064):43–44, 2005.

[162] Bruno Eckhardt, Edward Ott, Steven H Strogatz, Daniel M Abrams, and Allan McRobie. Modeling walker synchronization on the millennium bridge. Physical Review E—Statistical, Nonlinear, and Soft Matter Physics, 75(2):021110, 2007.

[163] Bihui Zhu, Johannes Schachenmayer, Minghui Xu, F Herrera, Juan G Restrepo, Murray J Holland, and Ana Maria Rey. Synchronization of interacting quantum dipoles. New Journal of Physics, 17(8):083063, 2015.

[164] Florian Dörfler, Michael Chertkov, and Francesco Bullo. Synchronization in complex oscillator networks and smart grids. Proceedings of the National Academy of Sciences, 110(6):2005–2010, 2013.

[165] Martin Rohden, Andreas Sorge, Marc Timme, and Dirk Witthaut. Self-organized synchronization in decentralized power grids. Physical review letters, 109(6):064101, 2012.

[166] Jesús Pastor, Rafael García de Sola, and Guillermo J Ortega. Hyper-synchronization, de-synchronization, synchronization and seizures, volume 6. Chapter, 2012.

[167] MD Prokhorov, VI Ponomarenko, VI Gridnev, MB Bodrov, and AB Bespyatov. Synchronization between main rhythmic processes in the human cardiovascular system. Physical Review E, 68(4):041913, 2003.

[168] L Henk van der Tweel, FL Meijler, and FJ van Capelle. Synchronization of the heart. Journal of Applied Physiology, 34(2):283–287, 1973.

[169] Guillaume Dumas, Jacqueline Nadel, Robert Soussignan, Jacques Martinerie, and Line Garnero. Inter-brain synchronization during social interaction. PloS one, 5(8):e12166, 2010.

[170] Guy Bloch, Erik D Herzog, Joel D Levine, and William J Schwartz. Socially synchronized circadian oscillators. Proceedings of the Royal Society B: Biological Sciences, 280(1765):20130035, 2013.

[171] Laura Astolfi, Jlenia Toppi, Fabrizio De Vico Fallani, Giovanni Vecchiato, Serenella Salinari, Donatella Mattia, Febo Cincotti, and Fabio Babiloni. Neuroelectrical hyperscanning measures simultaneous brain activity in humans. Brain topography, 23:243–256, 2010.

[172] Marleen B Schippers, Alard Roebroeck, Remco Renken, Luca Nanetti, and Christian Keysers. Mapping the information flow from one brain to another during gestural communication. Proceedings of the National Academy of Sciences, 107(20):9388–9393, 2010.

[173] Silke Anders, Jakob Heinzle, Nikolaus Weiskopf, Thomas Ethofer, and John-Dylan Haynes. Flow of affective information between communicating brains. Neuroimage, 54(1):439–446, 2011.

[174] Per Sebastian Skardal and Alex Arenas. Control of coupled oscillator networks with application to microgrid technologies. Science advances, 1(7):e1500339, 2015.

[175] Alex Arenas. Control of coupled oscillator networks with application to microgrid technologies. In APS March Meeting Abstracts, volume 2017, pages F40–004, 2017.

[176] Bharat Monga and Jeff Moehlis. Phase distribution control of a population of oscillators. Physica D: Nonlinear Phenomena, 398:115–129, 2019.

[177] Thomas G Sugar, Andrew Bates, Matthew Holgate, Jason Kerestes, Marc Mignolet, Philip New, Ragesh K Ramachandran, Sangram Redkar, and Chase Wheeler. Limit cycles to enhance human performance based on phase oscillators. Journal of Mechanisms and Robotics, 7(1):011001, 2015.

[178] Hyunsuk Hong and Steven H Strogatz. Conformists and contrarians in a kuramoto model with identical natural frequencies. Physical Review E—Statistical, Nonlinear, and Soft Matter Physics, 84(4):046202, 2011.

[179] Alessandro Pluchino, Vito Latora, and Andrea Rapisarda. Compromise and synchronization in opinion dynamics. The European Physical Journal B-Condensed Matter and Complex Systems, 50:169–176, 2006.

[180] Ziqiao Zhang, Said Al-Abri, and Fumin Zhang. A generalized kuramoto model for opinion dynamics on the unit sphere. Automatica, 171:111957, 2025.

[181] Edward Ott and Thomas M Antonsen. Low dimensional behavior of large systems of globally coupled oscillators. Chaos: An Interdisciplinary Journal of Nonlinear Science, 18(3), 2008.

[182] Yoshiki Kuramoto. Chemical Oscillations, Waves, and Turbulence. Springer, Berlin, Heidelberg, 1984.

[183] Juan A Acebrón, Luis L Bonilla, Conrad J Pérez Vicente, Félix Ritort, and Renato Spigler. The kuramoto model: A simple paradigm for synchronization phenomena. Reviews of modern physics, 77(1):137–185, 2005.

[184] Lauren M Childs and Steven H Strogatz. Stability diagram for the forced kuramoto model. Chaos: An Interdisciplinary Journal of Nonlinear Science, 18(4), 2008.

[185] Per Sebastian Skardal and Alex Arenas. Abrupt desynchronization and extensive multistability in globally coupled oscillator simplexes. Physical review letters, 122(24):248301, 2019.

[186] Erik Andreas Martens, Ernest Barreto, Steven H Strogatz, Edward Ott, Paul So, and Thomas M Antonsen. Exact results for the kuramoto model with a bimodal frequency distribution. Physical Review E—Statistical, Nonlinear, and Soft Matter Physics, 79(2):026204, 2009.

[187] Ajitesh Srivastava, Charalampos Chelmis, and Viktor K Prasanna. Computing competing cascades on signed networks. Social Network Analysis and Mining, 6(1):1–14, 2016.

[188] Cecilia Toccaceli, Letizia Milli, and Giulio Rossetti. Opinion dynamic modeling of fake news perception. In International Conference on Complex Networks and Their Applications, pages 370–381. Springer, 2020.

[189] Slobodan Maletić and Milan Rajković. Consensus formation on a simplicial complex of opinions. Physica A: Statistical Mechanics and its Applications, 397:111–120, 2014.

[190] Rohit Sahasrabuddhe, Leonie Neuhäuser, and Renaud Lambiotte. Modelling non-linear consensus dynamics on hypergraphs. Journal of Physics: Complexity, 2(2):025006, 2021.

[191] Fabian Baumann, Philipp Lorenz-Spreen, Igor M Sokolov, and Michele Starnini. Modeling echo chambers and polarization dynamics in social networks. Physical Review Letters, 124(4):048301, 2020.

[192] Heather Z. Brooks, Philip S. Chodrow, and Mason A. Porter. Emergence of polarization in a sigmoidal bounded-confidence model of opinion dynamics. SIAM Journal on Applied Dynamical Systems, 23(2):1442–1470, 2024.

[193] Alina Sîrbu, Vittorio Loreto, Vito D. P. Servedio, and Francesca Tria. Opinion dynamics: Models, extensions and external effects. In Vittorio Loreto, Muki Haklay, Andreas Hotho, Vito D.P. Servedio, Gerd Stumme, Jan Theunis, and Francesca Tria, editors, Participatory Sensing, Opinions and Collective Awareness, pages 363–401, Cham, Switzerland, 2017. Springer International Publishing.

[194] Hossein Noorazar, Kevin R Vixie, Arghavan Talebanpour, and Yunfeng Hu. From classical to modern opinion dynamics. International Journal of Modern Physics C, 31(07):2050101, 2020.

[195] Ziping Xie, Xiao Song, and Qiyuan Li. A review of opinion dynamics. In Theory, Methodology, Tools and Applications for Modeling and Simulation of Complex Systems: 16th Asia Simulation Conference and SCS Autumn Simulation Multi-Conference, AsiaSim/SCS AutumnSim 2016, Beijing, China, October 8–11, 2016, Proceedings, Part IV 16, pages 349–357, Heidelberg, Germany, 2016. Springer-Verlag.

[196] Sidney Redner. Reality-inspired voter models: A mini-review. Comptes Rendus Physique, 20:275–292, 2019.

[197] Serge Galam. Minority opinion spreading in random geometry. The European Physical Journal B, 25:403–406, 2002.

[198] Carmela Bernardo, Claudio Altafini, Anton Proskurnikov, and Francesco Vasca. Bounded confidence opinion dynamics: A survey. Automatica, 159, 2024.

[199] Ronald L. Breiger. The duality of persons and groups. Social forces, 53(2):181–190, 1974.

[200] Caroline Burningham and Michael A West. Individual, climate, and group interaction processes as predictors of work team innovation. Small Group Research, 26(1):106–117, 1995.

[201] Gary Alan Fine. The hinge: Civil society, group culture, and the interaction order. Social Psychology Quarterly, 77(1):5–26, 2014.

[202] Meike Eilert and Abigail Nappier Cherup. The activist company: Examining a company's pursuit of societal change through corporate activism using an institutional theoretical lens. Journal of Public Policy & Marketing, 39(4):461–476, 2020.

[203] Ryan C Black, Ryan J Owens, Justin Wedeking, and Patrick C Wohlfarth. US Supreme Court Opinions and Their Audiences. Cambridge University Press, Cambridge, UK, 2016.

[204] Robert B Cialdini and Noah J Goldstein. Social influence: Compliance and conformity. Annual review of psychology, 55(1):591–621, 2004.

[205] Vladas Griskevicius, Noah J Goldstein, Chad R Mortensen, Robert B Cialdini, and Douglas T Kenrick. Going along versus going alone: when fundamental motives facilitate strategic (non) conformity. Journal of personality and social psychology, 91(2):281, 2006.

[206] Rodolphe Sepulchre, Guillaume Drion, and Alessio Franci. Excitable behaviors. In Emerging Applications of Control and Systems Theory: A Festschrift in Honor of Mathukumalli Vidyasagar, pages 269–280, Heidelberg, Germany, 2018. Springer-Verlag.

[207] Eugene M. Izhikevich. Dynamical Systems in Neuroscience. MIT Press, Cambridge, MA, USA, 2007.

[208] Joel Best. Flavor of the Month: Why Smart People Fall for Fads. University of California Press, Oakland, CA, USA, 2006.

[209] B. E. Aguirre, E. L. Quarantelli, and Jorge L. Mendoza. The collective behavior of fads: The characteristics, effects, and career of streaking. American Sociological Review, 53(4):569, 1988.

[210] Federico Battiston, Enrico Amico, Alain Barrat, Ginestra Bianconi, Guilherme Ferraz de Arruda, Benedetta Franceschiello, Iacopo Iacopini, Sonia Kéfi, Vito Latora, Yamir Moreno, Micah M. Murray, Tiago P. Peixoto, Francesco Vaccarino, and Giovanni Petri. The physics of higher-order interactions in complex systems. Nature Physics, 17:1093–1098, 2021.

[211] Christian Bick, Elizabeth Gross, Heather A. Harrington, and Michael T. Schaub. What are higher-order networks? SIAM Review, 65(3):686–731, 2023.

[212] Z Gao, D Ghosh, H. A. Harrington, J. G. Restrepo, and D. Taylor. Dynamics on networks with higher-order interactions. Chaos: An Interdisciplinary Journal of Nonlinear Science, 33:040401, 2023.

[213] Ronald H. Atkin. Combinatorial Connectivities in Social Systems: An Application of Simplicial Complex Structures to the Study of Large Organizations. Springer-Verlag, Heidelberg, Germany, 1977.

[214] Peter A. Abrams. Arguments in favor of higher order interactions. The American Naturalist, 121(6):887–891, 1983.

[215] Henry M. Wilbur and John E. Fauth. Experimental aquatic food webs: Interactions between two predators and two prey. The American Naturalist, 135(2):176–204, 1990.

[216] HR Schaffer and Christine Liddell. Adult–child interaction under dyadic and polyadic conditions. British Journal of Developmental Psychology, 2(1):33–42, 1984.

[217] Leonie Neuhäuser, Michael T Schaub, Andrew Mellor, and Renaud Lambiotte. Opinion dynamics with multi-body interactions. In International Conference on Network Games, Control and Optimization, pages 261–271. Springer, 2021.

[218] Giulia Cencetti, Federico Battiston, Bruno Lepri, and Márton Karsai. Temporal properties of higher-order interactions in social networks. Scientific Reports, 11(1):7028, 2021.

[219] James Noonan and Renaud Lambiotte. Dynamics of majority rule on hypergraphs. Physical Review E, 104(2):024316, 2021.

[220] J. Kim, D.-S. Lee, B. Min, M. A. Porter, M. San Miguel, and K.-I. Goh. Competition between group interactions and nonlinearity in voter dynamics on hypergraphs. arXiv preprint arXiv:2407.11261, 2024.

[221] Laurent Hébert-Dufresne, Timothy M. Waring, Guillaume St-Onge, Meredith T. Niles, Laura Kati Corlew, Matthew P. Dube, Stephanie J. Miller, Nicholas J. Gotelli, and Brian J. McGill. Source-sink behavioural dynamics limit institutional evolution in a group-structured society. Royal Society Open Science, 9(3):211743, 2022.

[222] Guillaume St-Onge, Laurent Hébert-Dufresne, and Antoine Allard. Nonlinear bias toward complex contagion in uncertain transmission settings. Proceedings of the National Academy of Sciences of the United States of America, 121(1):e2312202121, 2024.

[223] Jonathan St-Onge, Giulio Burgio, Samuel F. Rosenblatt, Timothy M. Waring, and Laurent Hébert-Dufresne. Paradoxes in the coevolution of contagions and institutions. Proceedings of the Royal Society B: Biological Sciences, 291(2028):20241117, 2024.

[224] Ana P. Millán, Hanlin Sun, Lorenzo Giambagli, Riccardo Muolo, Timoteo Carletti, Joaquín J. Torres, Filippo Radicchi, Jürgen Kurths, and Ginestra Bianconi. Topology shapes dynamics of higher-order networks. Nature Physics, 2025. available at `https://doi.org/10.1038/s41567-024-02757-w`.

[225] Per Sebastian Skardal and Alex Arenas. Higher order interactions in complex networks of phase oscillators promote abrupt synchronization switching. Communications Physics, 3(1):218, 2020.

[226] Deborah A. Prentice and Dale T. Miller. Pluralistic ignorance and the perpetuation of social norms by unwitting actors. Advances in Experimental Social Psychology, 28:161–209, 1996.

[227] Dale T Miller and Cathy McFarland. Pluralistic ignorance: When similarity is interpreted as dissimilarity. Journal of Personality and Social Psychology, 53(2):298, 1987.

[228] Irving L. Janis. Groupthink. Psychology Today, 5(6):43–46, 74–76, 1971.

[229] Y. H. Kureh and M. A. Porter. Fitting in and breaking up: A nonlinear version of coevolving voter models. Physical Review E, 101:062303, 2020.

[230] Cristina Bicchieri and Hugo Mercier. Norms and beliefs: How change occurs. In The Complexity of Social Norms, pages 37–54, Heidelberg, Germany, 2014. Springer-Verlag.

[231] Kyurkchiev Nikolay and Markov Svetoslav. Sigmoid Functions: Some Approximation and Modelling Aspects. Lambert Academic Publishing, London, UK, 2015.

[232] Anastasia Bizyaeva, Alessio Franci, and Naomi Ehrich Leonard. Nonlinear opinion dynamics with tunable sensitivity. IEEE Transactions on Automatic Control, 68(3):1415–1430, 2023.

[233] Istvan Z. Kiss, Joel C. Miller, and Pëter L. Simon. Mathematics of Epidemics on Networks: From Exact to Approximate Models. Springer International Publishing, Cham, Switzerland, 2017.

[234] Guilherme Ferraz de Arruda, Alberto Aleta, and Yamir Moreno. Contagion dynamics on higher-order networks. Nature Reviews Physics, 6:468–482, 2024.

[235] Philip S. Chodrow. Configuration models of random hypergraphs. Journal of Complex Networks, 8(3):cnaa018, 2020.

[236] Sergey Melnik, Mason A. Porter, Peter J. Mucha, and James P. Gleeson. Dynamics on modular networks with heterogeneous correlations. Chaos: An Interdisciplinary Journal of Nonlinear Science, 24(2):023106, 2014.

[237] Roberto Barrio, Stephen Coombes, Mathieu Desroches, Flavio Fenton, Stefan Luther, and Esther Pueyo. Excitable dynamics in neural and cardiac systems. Communications in Nonlinear Science and Numerical Simulation, 86:105275, 2020.

[238] John D'Errico. Adaptive Robust Numerical Differentiation. Version 1.6, available at `https://www.mathworks.com/matlabcentral/fileexchange/13490-adaptive-robust-numerical-differentiation` (last accessed 22 February 2025), 2014.

[239] Mason A. Porter and James P. Gleeson. Dynamical Systems on Networks: A Tutorial, volume 4. Springer International Publishing, Cham, Switzerland, 2016. Frontiers in Applied Dynamical Systems: Reviews and Tutorials.

[240] Michael Mäs. Challenges to simulation validation in the social sciences. A critical rationalist perspective. In Claus Beisbart and Nicole J. Saam, editors, Computer Simulation Validation: Fundamental Concepts, Methodological Frameworks, and Philosophical Perspectives, pages 857–879. Springer International Publishing, Cham, Switzerland, 2019.

[241] Joseph B. Bak-Coleman, Mark Alfano, Wolfram Barfuss, Carl T. Bergstrom, Miguel A. Centeno, Iain D. Couzin, Jonathan F. Donges, Mirta Galesic, Andrew S. Gersick, Jennifer Jacquet, Albert B. Kao, Rachel E. Moran, Pawel Romanczuk, Daniel I. Rubenstein, Kaia J. Tombak, Jay J. Van Bavel, and Elke U. Weber. Stewardship of global collective behavior. Proc. Natl. Acad. Sci. USA, 118(27), 2021.

[242] Iacopo Iacopini, Márton Karsai, and Alain Barrat. The temporal dynamics of group interactions in higher-order social networks. Nature Communications, 15:7391, 2024.

[243] Elisa Shearer and Katerina Matsa. News use across social media platforms in 2018. Technical report, Pew Research Center, 2018.

[244] Andrew Chadwick and Cristian Vaccari. News sharing on uk social media: Misinformation, disinformation, and correction. Technical report, Loughborough University, 2019.

[245] Liedke and Wang. Social media and news fact sheet. Technical report, Pew Research Center, 2023.

[246] Eytan Bakshy, Solomon Messing, and Lada A Adamic. Exposure to ideologically diverse news and opinion on facebook. Science, 348(6239):1130–1132, 2015.

[247] Giandomenico Di Domenico, Jason Sit, Alessio Ishizaka, and Daniel Nunan. Fake news, social media and marketing: A systematic review. Journal of Business Research, 124:329–341, 2021.

[248] Axel Gelfert. Fake news: A definition. Informal logic, 38(1):84–117, 2018.

[249] Pierre R Berthon and Leyland F Pitt. Brands, truthiness and post-fact: managing brands in a post-rational world. Journal of Macromarketing, 38(2):218–227, 2018.

[250] Regina Rini. Fake news and partisan epistemology. Kennedy Institute of Ethics Journal, 27(2):E–43, 2017.

[251] David MJ Lazer, Matthew A Baum, Yochai Benkler, Adam J Berinsky, Kelly M Greenhill, Filippo Menczer, Miriam J Metzger, Brendan Nyhan, Gordon Pennycook, David Rothschild, et al. The science of fake news. Science, 359(6380):1094–1096, 2018.

[252] Michael V Bronstein, Gordon Pennycook, Adam Bear, David G Rand, and Tyrone D Cannon. Belief in fake news is associated with delusionality, dogmatism, religious fundamentalism, and reduced analytic thinking. Journal of applied research in memory and cognition, 8(1):108–117, 2019.

[253] Rose McDermott. Psychological underpinnings of post-truth in political beliefs. PS: Political Science & Politics, 52(2):218–222, 2019.

[254] Michela Del Vicario, Walter Quattrociocchi, Antonio Scala, and Fabiana Zollo. Polarization and fake news: Early warning of potential misinformation targets. ACM Transactions on the Web (TWEB), 13(2):1–22, 2019.

[255] Edson C Tandoc Jr, Richard Ling, Oscar Westlund, Andrew Duffy, Debbie Goh, and Lim Zheng Wei. Audiences' acts of authentication in the age of fake news: A conceptual framework. New media & society, 20(8):2745–2763, 2018.

[256] Yang Cheng and Zifei Fay Chen. The influence of presumed fake news influence: Examining public support for corporate corrective response, media literacy interventions, and governmental regulation. In What IS News?, pages 103–127. Routledge, 2021.

[257] Zifei Fay Chen and Yang Cheng. Consumer response to fake news about brands on social media: the effects of self-efficacy, media trust, and persuasion knowledge on brand trust. Journal of Product & Brand Management, 29(2):188–198, 2020.

[258] Michail Vafeiadis, Denise S Bortree, Christen Buckley, Pratiti Diddi, and Anli Xiao. Refuting fake news on social media: nonprofits, crisis response strategies and issue involvement. Journal of Product & Brand Management, 29(2):209–222, 2020.

[259] Jonathan Franceschi and Lorenzo Pareschi. Spreading of fake news, competence and learning: kinetic modelling and numerical approximation. Philosophical Transactions of the Royal Society A, 380(2224):20210159, 2022.

[260] Taichi Murayama, Shoko Wakamiya, Eiji Aramaki, and Ryota Kobayashi. Modeling the spread of fake news on twitter. Plos one, 16(4):e0250419, 2021.

[261] Nicholas Rabb, Lenore Cowen, Jan P de Ruiter, and Matthias Scheutz. Cognitive cascades: How to model (and potentially counter) the spread of fake news. Plos one, 17(1):e0261811, 2022.

[262] Marcella Tambuscio, Giancarlo Ruffo, Alessandro Flammini, and Filippo Menczer. Fact-checking effect on viral hoaxes: A model of misinformation spread in social networks. In Proceedings of the 24th international conference on World Wide Web, pages 977–982, 2015.

[263] Ceren Budak, Divyakant Agrawal, and Amr El Abbadi. Limiting the spread of misinformation in social networks. In Proceedings of the 20th international conference on World wide web, pages 665–674, 2011.

[264] Ahmad Zareie and Rizos Sakellariou. Minimizing the spread of misinformation in online social networks: A survey. Journal of Network and Computer Applications, 186:103094, 2021.

[265] Sander Van Der Linden. Misinformation: susceptibility, spread, and interventions to immunize the public. Nature Medicine, 28(3):460–467, 2022.

[266] John Cook, Ullrich Ecker, and Stephan Lewandowsky. Misinformation and how to correct it. Emerging trends in the social and behavioral sciences: An interdisciplinary, searchable, and linkable resource, pages 1–17, 2015.

[267] Lynn Hasher, David Goldstein, and Thomas Toppino. Frequency and the conference of referential validity. Journal of verbal learning and verbal behavior, 16(1):107–112, 1977.

[268] Chaitanya Kaligotla, Enver Yücesan, and Stephen E. Chick. An agent based model of spread of competing rumors through online interactions on social media. In 2015 Winter Simulation Conference (WSC), pages 3985–3996, 2015.

[269] István Z.. Kiss, Joel S.. Miller, and Péter Simon. Mathematics of Epidemics on Networks: From Exact to Approximate Models. Springer International Publishing, 2017.

[270] Nicholas W. Landry, Maxime Lucas, Iacopo Iacopini, Giovanni Petri, Alice Schwarze, Alice Patania, and Leo Torres. XGI: A Python package for higher-order interaction networks. Journal of Open Source Software, 8(85):5162, May 2023.

[271] Stephan Lewandowsky and Sander Van Der Linden. Countering misinformation and fake news through inoculation and prebunking. European Review of Social Psychology, 32(2):348–384, 2021.

[272] VR Simpson. Wild animals as reservoirs of infectious diseases in the uk. The Veterinary Journal, 163(2):128–146, 2002.

[273] Ronald F Inglehart, Miguel Basanez, and Alejandro Moreno. Human values and beliefs: A cross-cultural sourcebook. University of Michigan Press, 1998.

[274] Aaron Bramson, Patrick Grim, Daniel J Singer, Steven Fisher, William Berger, Graham Sack, and Carissa Flocken. Disambiguation of social polarization concepts and measures. The Journal of Mathematical Sociology, 40(2):80–111, 2016.

[275] Samuel L Perry. American religion in the era of increasing polarization. Annual Review of Sociology, 48(1):87–107, 2022.

[276] José G Montalvo and Marta Reynal-Querol. Ethnic polarization, potential conflict, and civil wars. American economic review, 95(3):796–816, 2005.

[277] Aaron M McCright and Riley E Dunlap. The politicization of climate change and polarization in the american public's views of global warming, 2001–2010. The sociological quarterly, 52(2):155–194, 2011.

[278] Floriana Gargiulo and Yerali Gandica. The role of homophily in the emergence of opinion controversies. arXiv preprint arXiv:1612.05483, 2016.

[279] Shanto Iyengar, Gaurav Sood, and Yphtach Lelkes. Affect, not ideology: A social identity perspective on polarization. Public opinion quarterly, 76(3):405–431, 2012.

[280] Zhen Wang, Marko Jusup, Hao Guo, Lei Shi, Sunčana Geček, Madhur Anand, Matjaž Perc, Chris T Bauch, Jürgen Kurths, Stefano Boccaletti, et al. Communicating sentiment and outlook reverses inaction against collective risks. Proceedings of the National Academy of Sciences, 117(30):17650–17655, 2020.

[281] George Michael. The rise of the alt-right and the politics of polarization in america. Skeptic (Altadena, CA), 22(2):9–18, 2017.

[282] Marc Esteve-Del-Valle. Homophily and polarization in twitter political networks: A cross-country analysis. Media and Communication, 10(2):81–92, 2022.

[283] Pranav Dandekar, Ashish Goel, and David T Lee. Biased assimilation, homophily, and the dynamics of polarization. Proceedings of the National Academy of Sciences, 110(15):5791–5796, 2013.

[284] Matteo Cinelli, Gianmarco De Francisci Morales, Alessandro Galeazzi, Walter Quattrociocchi, and Michele Starnini. The echo chamber effect on social media. Proceedings of the national academy of sciences, 118(9):e2023301118, 2021.

[285] Sara B Hobolt, Katharina Lawall, and James Tilley. The polarizing effect of partisan echo chambers. American Political Science Review, 118(3):1464–1479, 2024.

[286] Gregory J Martin and Ali Yurukoglu. Bias in cable news: Persuasion and polarization. American Economic Review, 107(9):2565–2599, 2017.

[287] Felipe Bonow Soares, Raquel Recuero, and Gabriela Zago. Influencers in polarized political networks on twitter. In Proceedings of the 9th international conference on social media and society, pages 168–177, 2018.

[288] Alfredo Jose Morales, Javier Borondo, Juan Carlos Losada, and Rosa M Benito. Measuring political polarization: Twitter shows the two sides of venezuela. Chaos: An Interdisciplinary Journal of Nonlinear Science, 25(3), 2015.

[289] Amit Kumar Kushwaha, Arpan Kumar Kar, Sanjit Kumar Roy, and P Vigneswara Ilavarasan. Capricious opinions: A study of polarization of social media groups. Government Information Quarterly, 39(3):101709, 2022.

[290] Wander Jager and Frédéric Amblard. Uniformity, bipolarization and pluriformity captured as generic stylized behavior with an agent-based simulation model of attitude change. Computational & Mathematical Organization Theory, 10:295–303, 2005.

[291] HF Chau, CY Wong, FK Chow, and Chi-Hang Fred Fung. Social judgment theory based model on opinion formation, polarization and evolution. Physica A: Statistical Mechanics and its Applications, 415:133–140, 2014.

[292] Kenneth Benoit and Michael Laver. The dimensionality of political space: Epistemological and methodological considerations. European Union Politics, 13(2):194–218, 2012.

[293] Delia Baldassarri and Andrew Gelman. Partisans without constraint: Political polarization and trends in american public opinion. American Journal of Sociology, 114(2):408–446, 2008.

[294] Paul DiMaggio, John Evans, and Bethany Bryson. Have american's social attitudes become more polarized? American journal of Sociology, 102(3):690–755, 1996.

[295] Simon Schweighofer, David Garcia, and Frank Schweitzer. An agent-based model of multi-dimensional opinion dynamics and opinion alignment. Chaos: An Interdisciplinary Journal of Nonlinear Science, 30(9), 2020.

[296] Mark EJ Newman. Modularity and community structure in networks. Proceedings of the national academy of sciences, 103(23):8577–8582, 2006.

[297] Leo Torres, Ann S. Blevins, Danielle Bassett, and Tina Eliassi-Rad. The why, how, and when of representations for complex systems. SIAM Review, 63(3):435–485, 2021.

[298] Bailey K. Fosdick, Daniel B. Larremore, Joel Nishimura, and Johan Ugander. Configuring random graph models with fixed degree sequences. Siam Review, 60(2):315–355, 2018.

[299] Mark E. J. Newman. Random graphs with clustering. Physical Review Letters, 103:058701, 2009.

[300] Joel C. Miller. Percolation and epidemics in random clustered networks. Physical Review E, 80:020901, 2009.

Appendix A

Supporting Work for Chapter 3

A.1 Hypergraphs and the random-hypergraph model

As we stated in Sec. 3.3, it is convenient to use hypergraphs to describe our networks, which consist of nodes and groups of nodes. A hypergraph is a generalization of a graph that includes both ordinary edges (i.e., dyadic adjacencies) and hyperedges with more than two nodes (i.e., polyadic adjacencies) [10, 211]. Following standard convention, we use the term "hyperedge" for any of these adjacencies. Mathematically, a hypergraph $\mathcal{H}_{\mathcal{G}} = (\mathcal{V}, \mathcal{E})$ consists of a set $\mathcal{V}$ of nodes and a set $\mathcal{E}$ of hyperedges. Each hyperedge is a nonempty subset of $\mathcal{V}$; the number of nodes in this subset is the "size" of the hyperedge. In an ordinary graph, each node $i \in \mathcal{V}$ has an associated degree k_i, which indicates the number of edges that are attached (i.e., "incident") to it. The "hyperdegree" of node i is the vector $\mathbf{k}_i = [k_i^{(2)}, k_i^{(3)}, \ldots, k_i^{(L)}]$, where L is the size of its largest hyperedge and the lth-order degree $k_i^{(l)}$ is the number of size-l hyperedges that are incident to node i. Each hypergraph has a hyperdegree distribution $\mathcal{P}(\mathbf{k})$, which encodes the probabilities that a uniformly-randomly-chosen node has hyperdegree $\mathbf{k}$ for each $\mathbf{k}$.

Just as one can describe a hypergraph using a bipartite network [10], it is also possible to formulate our opinion model by considering dynamics on an ordinary graph with two types of nodes. In this formulation, the agents constitute one type of node and the groups constitute a second type of node. An agent can have adjacencies both with groups and with other agents, and a group is adjacent to each agent that participates in it. We view the group language as much more natural than bipartite-network language, just as the language of hypergraphs and simplicial complexes is

natural for studying polyadic interactions [211, 297].

We now describe the particular random-hypergraph model that we employ. Consider a set of nodes $i \in \{1, 2, 3, \ldots, N\}$ with hyperdegrees $\mathbf{k}_i$, where $k_i^{(l)}$ is the number of loose ends (i.e., "stubs") of size-l hyperedges that are attached to i. We form a size-l hyperedge by uniformly randomly selecting l stubs for the hyperedge. We repeat this stub-selection process until all stubs are assigned to a hyperedge. If $\langle k^{(l)} \rangle$ is finite, the probability that there is a size-l hyperedge that connects nodes $\{i_1, i_2, \ldots, i_l\}$ in the limit $N \to \infty$ is

$$f_l(\mathbf{k}_{i_1}, \mathbf{k}_{i_2}, \ldots, \mathbf{k}_{i_l}) = \frac{(l-1)!\, k_{i_1}^{(l)} k_{i_2}^{(l)} \times \cdots \times k_{i_l}^{(l)}}{\left(N \langle k^{(l)} \rangle\right)^{l-1}} \,. \tag{A.1}$$

This expression is a generalization of an associated expression for ordinary configuration-model graphs [298, 10].

The above random-hypergraph model is a special case of the stub-labeled hypergraph configuration model in [235] in which we allow only hyperedges of sizes 2 and 3. Constructing a hypergraph with a configuration model yields a small number of self-hyperedges (i.e., hyperedges in which a single node participates two or more times) and multi-hyperedges (i.e., redundant hyperedges, which are hyperedges that occur two or more times) (See Sec. 12.1 of Ref. [10] for a relevant discussion in the context of graphs.) Because we assume that nodes do not influence themselves, we remove these self-hyperedges when constructing a hypergraph. For example, in a calculation of means using a single sample of 20 instantiations of a 2500-node hypergraph with $\gamma = 4$ and $\langle k \rangle = \langle q \rangle = 20$, we remove approximately 0.05% of the edges and approximately 0.15% of the triangles. However, we retain multi-hyperedges. From the same sample of 20 instantiations of a 2500-node hypergraph with $\gamma = 4$ and $\langle k \rangle = \langle q \rangle = 20$, we find that about 0.33% of all edges and about 0.0003% of all triangles are multi-hyperedges.

Our random-hypergraph model is reminiscent of the closely related random-graph models with clustering that were proposed independently by Newman [299] and Miller [300]. In a Newman–Miller model, nodes have specified dyadic and triadic (i.e., triangle) degree sequences, which one uses independently in a stub-matching procedure. However, a "triangle" in the Newman–Miller

model corresponds to three dyadic interactions, rather than to a single size-3 hyperedge.

A.2 Detailed derivation of the mean-field approximation (3.19)

In this appendix, we give a detailed derivation of our mean-field equations (3.19). As we discussed in Sec. 3.4, we consider the time evolution of the three order parameters V^t, U^t, and Y^t.

We begin by expressing V^t and U^t in terms of $x^t_{\mathbf{k}}$, which is the fraction of nodes at time t with hyperdegree $\mathbf{k} = [k, q]$ that have opinion 1. The total numbers of edges is $N\langle k\rangle/2$, and the total number of triangles is $N\langle q\rangle/3$. The expected fraction of opinion-1 nodes in a uniformly randomly selected edge is thus

$$V^t = \sum_{\mathbf{k}}\sum_{\mathbf{k}'} \frac{N\mathcal{P}(\mathbf{k})N\mathcal{P}(\mathbf{k}')}{2!}\left(\frac{kk'}{N\langle k\rangle}\right)\left(\frac{x^t_{\mathbf{k}}+x^t_{\mathbf{k}'}}{2}\right)\Big/\left(\frac{N\langle k\rangle}{2}\right) = \sum_{\mathbf{k}}\frac{k\mathcal{P}(\mathbf{k})x^t_{\mathbf{k}}}{\langle k\rangle}\,, \tag{A.2}$$

where $NP(\mathbf{k})NP(\mathbf{k}')/2!$ is the expected number of pairs of nodes with hyperdegrees $\mathbf{k}$ and $\mathbf{k}'$, the quantity $kk'/(N\langle k\rangle)$ is the expected fraction of these pairs that are connected by an edge [see Eq. (A.1) with $l = 2$], and $(x^t_{\mathbf{k}} + x^t_{\mathbf{k}'})/2$ is the expected fraction of opinion-1 nodes that are attached to an edge that connects uniformly-randomly-selected nodes with hyperdegrees $\mathbf{k}$ and $\mathbf{k}'$. Analogously, the expected fraction of opinion-1 nodes in a uniformly randomly selected triangle is

$$U^t = \sum_{\mathbf{k}}\sum_{\mathbf{k}'}\sum_{\mathbf{k}''} \frac{N\mathcal{P}(\mathbf{k})\,N\mathcal{P}(\mathbf{k}')\,N\mathcal{P}(\mathbf{k}'')}{3!}\left(\frac{2q\,q'\,q''}{(N\langle q\rangle)^2}\right)\left(\frac{x^t_{\mathbf{k}}+x^t_{\mathbf{k}'}+x^t_{\mathbf{k}''}}{3}\right)\Big/\left(\frac{N\langle q\rangle}{3}\right) = \sum_{\mathbf{k}}\frac{q\mathcal{P}(\mathbf{k})x^t_{\mathbf{k}}}{\langle q\rangle}\,. \tag{A.3}$$

Because we generate hypergraphs using a configuration model, the probability that there is a hyperedge that connects a group of nodes depends only on the hyperdegrees of those nodes. We can thus use a hyperdegree-based compartmental model to obtain mean-field equations. Consider the probability [see Eq. (3.1)] that a node i with hyperdegree $\mathbf{k} = [k, q]$ has opinion 1 at time $t+1$. Assuming that all nodes with the same hyperdegree behave in the same way (i.e., the probability that node j has opinion 1 is $x^t_{\mathbf{k}}$ for all nodes j with hyperdegree $\mathbf{k}_j = \mathbf{k}$), we approximate the

normalized number $\bar{x}_i^t$ of neighbors of node i that have opinion 1 [see Eq. (3.4)] by

$$\begin{aligned}\bar{x}_i^t &= \frac{1}{\langle k\rangle}\sum_{j=1}^{N} A_{ij}x_j^t \\ &\approx \frac{1}{\langle k\rangle}\sum_{\mathbf{k}'} N\mathcal{P}(k',q')\left(\frac{kk'}{N\langle k\rangle}\right)x_{\mathbf{k}'}^t \\ &= \frac{k}{\langle k\rangle}\sum_{\mathbf{k}'}\frac{k'\mathcal{P}(k',q')x_{\mathbf{k}'}^t}{\langle k\rangle} \\ &= kV^t/\langle k\rangle\,, \end{aligned} \tag{A.4}$$

where the approximation in the second line replaces the number of opinion-1 neighbors of node i with its expected value. The term $\bar{y}_i^t$, which is the normalized number of triangles that are attached to node i and have opinion 1 [see Eq. (3.7)], is approximately

$$\bar{y}_i^t \approx qY^t/\langle q\rangle \tag{A.5}$$

because node i is attached to q triangles and Y^t is the expected fraction of triangles that have opinion 1. We insert the approximations (A.4) and (A.5) into Eqs. (3.1)–(3.3) to obtain

$$\begin{aligned}x_{\mathbf{k}}^{t+1} &= \frac{1}{N\mathcal{P}(\mathbf{k})}\sum_{\mathbf{k}_i=\mathbf{k}}\mathbb{E}[x_i^{t+1}] \\ &= \frac{1}{N\mathcal{P}(\mathbf{k})}\sum_{\mathbf{k}_i=\mathbf{k}} f\left(a\bar{x}_i^t + b\bar{y}_i^t\right) \\ &\approx \frac{1}{N\mathcal{P}(\mathbf{k})}\sum_{\mathbf{k}_i=\mathbf{k}} f\left(\frac{ak}{\langle k\rangle}V^t + \frac{bq}{\langle q\rangle}Y^t\right) \\ &= f\left(\frac{ak}{\langle k\rangle}V^t + \frac{bq}{\langle q\rangle}Y^t\right)\,, \end{aligned} \tag{A.6}$$

where $\mathbb{E}[\cdot]$ denotes the expectation. The time evolution of the expected fraction Y^t of triangles with opinion 1 satisfies

$$\begin{aligned}Y^{t+1} &= \mathbb{E}\left[\frac{1}{S}\sum_{j=1}^{S} y_j^{t+1}\right] = \frac{1}{S}\sum_{j=1}^{S}\mathbb{E}\left[y_j^{t+1}\right] \\ &= \frac{1}{S}\sum_{j=1}^{S}\Big\{\mathbb{E}[y_j^{t+1}|y_j^t=1]P(y_j^t=1) \\ &\qquad + \mathbb{E}[y_j^{t+1}|y_j^t=0]P(y_j^t=0)\Big\}\,. \end{aligned} \tag{A.7}$$

Making the mean-field assumption that all triangles behave in the same way (i.e., $y_j^t = y^t$ and $\bar{z}^t = \bar{z}_j^t$ for all j) yields

$$\begin{aligned} Y^{t+1} &= \mathbb{E}[y^{t+1}|y^t = 1]P(y^t = 1) \\ &\quad + \mathbb{E}[y^{t+1}|y^t = 0]P(y^t = 0)\,. \end{aligned} \tag{A.8}$$

We then use Eq. (3.6) for the expected values and the relation $P(y^t = 1) = Y^t$ to obtain

$$Y^{t+1} = f(c\bar{z}^t + d)Y^t + f(c\bar{z}^t)(1 - Y^t)\,. \tag{A.9}$$

Finally, similarly to our approximation of $\bar{y}_i^t$ in Eq. (3.14), we approximate $\bar{z}^t$ (i.e., the fraction of nodes with opinion 1 in a triangle that we select uniformly at random) by

$$\bar{z}^t \approx U^t\,, \tag{A.10}$$

which is the expected fraction of opinion-1 nodes at time t in a triangle that we select uniformly at random. Substituting Eq. (A.10) into Eq. (A.9) yields

$$Y^{t+1} = Y^t f\left(cU^t + d\right) + (1 - Y^t)f(cU^t)\,. \tag{A.11}$$

Inserting Eq. (A.6) into Eqs. (A.2)–(A.3) yields the closed map (3.19) for the time evolution of the three order parameters:

$$\begin{aligned} V^{t+1} &= \sum_k \sum_q \frac{k\mathcal{P}(k,q)}{\langle k\rangle} f\left(\frac{a\,k}{\langle k\rangle}V^t + \frac{b\,q}{\langle q\rangle}Y^t\right)\,, \\ U^{t+1} &= \sum_k \sum_q \frac{q\mathcal{P}(k,q)}{\langle q\rangle} f\left(\frac{a\,k}{\langle k\rangle}V^t + \frac{b\,q}{\langle q\rangle}Y^t\right)\,, \\ Y^{t+1} &= Y^t f\left(cU^t + d\right) + (1 - Y^t)f(cU^t)\,. \end{aligned} \tag{A.12}$$

A.3 Selection of initial conditions

In this appendix, we discuss how we select initial conditions for our simulations of the stochastic opinion model (3.1)–(3.2), the deterministic mean-field approximation (3.19), and the stochastically perturbed mean-field approximation (3.26). In most of our simulations, we perform parameter

sweeps using W^2 evenly spaced initial conditions in the unit square. For each initial condition, we perform a single simulation of the stochastic opinion model (3.1)–(3.2), the deterministic mean-field map (3.19), or the stochastically perturbed mean-field map (3.26).

For the stochastic opinion model (3.1)–(3.2), we use the W^2 evenly spaced probabilities (u_1, u_2) (which we described in Sec. 3.2) in the set $\{(i/(W-1),\, j/(W-1))|\ i, j \in \{0, 1, \ldots, W-1\}\}$ for our parameter sweeps. For the mean-field equations (3.19) and (3.26), we need to select initial values for the three order parameters (V^0, U^0, Y^0). As we described in Sec. 3.4, we employ initial conditions with $V^0 = U^0$ so that our initial conditions resemble our initial conditions for the stochastic opinion model as closely as possible. Therefore, we use the W^2 evenly spaced initial conditions (V^0, U^0, Y^0) in the set $\{(i/(W-1)),\, i/(W-1)),\, j/(W-1)))|\ i, j \in \{0, 1, \ldots, W-1\}\}$ for our parameter sweeps.